ICE CLOUDS OVER FAIRBANKS, ALASKA

By

Vinay Kumar Kayetha

RECOMMENDED:

Dr. Nicole Mölders

Dr. Richard Collins

Dr. Kenneth Sassen
Advisory Committee Chair

Dr. Uma Bhatt
Chair, Department of Atmospheric Sciences

APPROVED:

Dr. Paul Layer
Dean, College of Natural Science and Mathematics

Dr. John Eichelberger
Dean of Graduate School

Date

ICE CLOUDS OVER FAIRBANKS, ALASKA

A

THESIS

Presented to the Faculty
of the University of Alaska Fairbanks

in Partial Fulfillment of the Requirements
for the Degree of

MASTER OF SCIENCE

By

Vinay Kumar Kayetha, M.TECH, B.TECH

Fairbanks, Alaska

May 2014

ABSTRACT

Arctic clouds have been recognized long ago as one of the key elements modulating the global climate system. They have gained much interest in recent years because the availability of new continuous datasets is opening doors to explore cloud and aerosol properties as never before. This is particularly important in the light of current climate change studies that predict changing weather scenarios around the world. This research investigates the occurrence and properties of a few types of ice clouds over the Arctic region with datasets available through the *Arctic Facility for Atmospheric Remote Sensing* (AFARS; 64.86^{o} N, 147.84^{o} W). This study exclusively focuses on ice clouds that form in the upper (cirrus clouds) and midlevels of the troposphere, and that are transparent to laser pulses (visible optical depth, $\tau < 3.0 - 4.0$). Cirrus clouds are ice-dominated clouds that are formed in the upper levels of the troposphere and are relatively thin such that their visual appearances range from bluish to gray in color. Mid-level ice clouds are those clouds primarily composed of ice crystals forming in the midlevels of the troposphere. It is hypothesized that unlike the basic midlevel cloud type (altostratus), other varieties of midlevel ice clouds exist at times over the Arctic region. The midlevel ice clouds studied here are also transparent to laser pulses and sometimes appear as a family of cirrus clouds to a surface observer. Because of their intermediate heights of occurrence in the troposphere, these could have microphysical properties and radiative effects that are distinct from those associated with upper level ice clouds in the troposphere. A ground-based lidar dataset with visual observations for identifying cloud types collected at AFARS over eight years is used to investigate this hypothesis. Cloud types over AFARS have been identified by a surface observer (Professor Kenneth Sassen) using established characteristics traits. Essential macrophysical properties of the clouds are derived from the lidar data, which serves as a climatological representation for the visually identified cirrus and mid-level ice clouds over a typical sub-Arctic location. Synoptic-scale weather patterns conducive for such cloud type formations are derived using a clustering technique applied to a re-analysis dataset. The cloud properties derived

from ground-based lidar over AFARS are used to assess the cloud observations from the CALIPSO satellite.

TABLE OF CONTENTS

LIST OF FIGURES

LIST OF TABLES

ACKNOWLEDGEMENTS

First of all, I would like to thank my advisor Professor Kenneth Sassen for giving me an opportunity to work with him. My sincere thanks to Dr. Sassen for training me in several aspects of conducting research that also helped me with visual observations of identifying cloud types and occasional hands-on experience in lidar–radar operations at the AFARS station. I am also greatly indebted to my other committee members Dr. Nicole Mölders and Dr. Richard Collins for helping me in this journey towards my goal and want to extend my heartful thanks to all.

I would like to thank my research group members Dr. Jiang Zhu and Mr. Colin Triplett for their help whenever needed, especially Jiang Zhu for his help with IDL programs. I also want thank Dr. Xiangdong Zhang, Dr. Peter Bieniek, and Mr. Soumik for ideas of analysis and discussions in understanding weather patterns. Thanks to the entire team of faculty and fellow students associated with the Department of Atmospheric Sciences for their enthusiasm and Barbara Day for assistance with all deadlines and paper work. Thanks to Dave Covey of the Geophysical Institute for his help with computer hardware problems whenever they arise.

I would like to thank my parents for their support and patience, which never let me down. Also my thanks all my friends here who has been my surrogate family and made my life peaceful.

This research is supported by National Science Foundation (NSF) to AFARS for Remote Sensing Education and research in the Arctic, NSF grant ATM-0645644 and CALIPSO–CloudSat Science team through contracts, NASA grant NNX0A056G, and JPL contract NAS-7-1407.

Chapter 1

Introduction

For centuries, humans have been fascinated by the beauty of clouds in the atmosphere through their wide variety of appearance (*size, shape, color, texture*) and occurrence [*WMO*, 1987]. Clouds typically form when a buoyant force lifts water vapor in an airmass up, cools to reach its saturation, and thereby condenses on particles (acting as nuclei) existing in the atmosphere. The interaction of clouds with both solar shortwave and terrestrial longwave radiation regulates the amount of energy reaching the Earth's surface and leaving the atmosphere, thereby forming our weather. Thus, undoubtedly clouds comprise an important component of our weather and cloud processes need to be better understood to accurately parameterize and represent them in models to obtain reliable predictions.

In general, clouds consist of water droplets, ice particles, or mixed-phase water and ice particles, depending on the altitude in the atmosphere where they are formed and exist. Those clouds formed high in the troposphere are ice-dominated because of the sufficiently low temperatures, and generally pose a net warming effect (*greenhouse effect*) to the Earth's climate by trapping the outgoing terrestrial longwave radiation. Whereas clouds formed at the low levels in the troposphere are water-dominated and pose a net cooling effect (*albedo effect*) to the Earth's climate by reflecting shortwave radiation back to space. Clouds formed in the intermediate heights of the troposphere exist in the mixed-phase, or with the dominance of either water or ice phase particles, depending on the ambient conditions, and pose a net cooling or warming or negligible

effect to the Earth's climate. Radiative effects of various types of clouds to the climate system are distinct and entirely dependent on their basic macrophysical [*Minnis et al.*, 1990] and microphysical (*phase, size, particle concentration*) properties [*Hartmann and Doelling*, 1991; *Fu and Liou*, 1992; *Hartmann et al.*, 1992]. Changes to such cloud properties as well as their geographical occurrence can have a profound effect on the climate system. The magnitudes of the cloud-climate feedbacks are known to have great variability among the present climate models due to the poor representation of *cloud types* [*Senior and Mitchell*, 1993; *Stainforth et al.*, 2005; *Zhang et al.*, 2005]. Our limited understanding of the cloud dynamical processes and their radiative effects has been identified by the Intergovernmental Panel for Climate Change (IPCC) as one of the major uncertainties in assessing the present and projected climate [*Solomon et al.*, 2007].

1.1 Ice clouds

Ice clouds cover about 30% of the earth's atmosphere and play a pivotal role in the atmospheric radiation budget [*Liou*, 1986]. The formation and existence of ice in the troposphere serves as one of the important mechanisms to initiate precipitation and regulate the global water cycle. Ice cloud properties are known for their complexity to understand the underlying processes for several reasons, such as due to a variety of ice particle shapes/habits, size distributions, the difficulty to obtain in-situ measurements, etc. Formation of ice particles in clouds can occur through either homogeneous or heterogeneous nucleation of tiny particles composed of solid particles or aqueous solutions at sub-freezing temperatures [*Pruppacher and Klett*, 1997]. Heterogeneous nucleation refers to the process where the presence of a particle (ice nuclei) acts as a catalyst for freezing of water vapor. Whereas homogeneous nucleation is the process where water droplets freeze spontaneously at sufficiently low temperatures (i.e., -38^{o} C and below). Experimental studies show that homogeneous freezing of water droplets with 100 μm equivalent diameter occurs at -35^{o} C and freezing of water droplets of 1 μm equivalent diameter occurs at -41^{o} C [*Mason*, 1971].

At any given temperature from 0^{o} to -38^{o} C with ice-supersaturated relative humidity, formation of ice depends on the availability of ice nuclei providing several pathways for heterogeneous nucleation via *condensation*, *deposition*, *immersion* and *contact freezing.* The number concentration of ice nuclei in the atmosphere is very small compared to the cloud condensation nuclei and this concentration increases with decreasing temperature [*Ludlam*, 1952; *Meyers et al.*, 1992; *DeMott et al.*, 2010] and thus controls the rate of heterogeneous nucleation [*Hagen et al.*, 1981; *Rogers and Yau*, 1988; *DeMott and Rogers*, 1990; *Jeffery and Austin*, 1997; *Pruppacher and Klett*, 1997]. Studies show that suspended particles existing in the atmosphere, either released naturally or through human-intervention becomes activated (i.e., the chemical composition of the particle gets diluted and lowers its freezing point) and may initiate ice formation even at relatively high temperatures [*Rogers et al.*, 1998; *Sassen*, 2002b; *DeMott et al.*, 2003; *Sassen et al.*, 2003b; *Sassen*, 2005; *Seifert et al.*, 2010]. Particles like mineral dust, sea-salt emissions, and soot are commonly recognized particles that act as effective ice nuclei. Once the formation of ice is initiated with the activation of available ice nuclei in the cloud, the existing liquid water droplets are quickly converted to ice particles. This transformational growth of ice particles is referred as the *Wegener–Bergeron–Findeisen process (WBF process)*, owes to the basic fact that the equilibrium water vapor pressure with respect to ice is less than the equilibrium water vapor pressure with respect to water at the same subfreezing temperatures. This property allows the ice crystals to compete for the available water vapor and gain mass by depositional growth [*Wegener*, 1911; *Bergeron*, 1935; *Findeisen*, 1938].

Thereafter, the continued growth of ice particles depends on available water vapor and local thermodynamic conditions. The increasing size of ice particles also increases their fall speeds and allows the particles to escape from the latent heat released during the process; this further promotes the growth of particles through secondary processes involving accretion or riming that are responsible for the complex shapes of ice particles [*Hallett and Mossop*, 1974; *Pruppacher and Klett*, 1997]. Unlike particles in water

(warm) clouds, ice clouds contain non-spherical structures that form in several shapes like plates, solid columns, hollow columns, bullet rosettes and a combination of these. Studies also show that ice clouds forming through different mechanisms are distinct. For example, ice clouds formed through frontal systems have relatively smaller size particles than those formed near the convective centers in the atmosphere [*Stith et al.*, 2002]. Thus, in the context of the above discussion ice formation in the troposphere is apparent, owing to the fact that air masses can easily attain ice super-saturations and also depends on the activation of ice nuclei. However, studies show that 60% of the clouds colder than -10^{o} C contain ice particles in them [*Morris and Braham*, 1968]. An overview of the types of ice clouds observed in the upper and mid-levels of the troposphere along with their formation mechanisms and basic (physical and optical) characteristics follows the discussion.

1.1.1 Upper level clouds

(a) Formation mechanisms

Clouds inhabiting the upper levels of the troposphere predominantly consist of ice particles and are recognized as the family of *cirrus* clouds. These clouds occur in wide varieties of forms and are mostly optically thin, appear as detached white patches or narrow bands, or having fibrous (hair–like) appearance. At such high altitudes and extremely low temperatures, tiny particles freeze homogeneously, thereby forming ice particles for cirrus cloud generation.

Over the past decades, several cirrus cloud studies were performed regionally from both temporary and permanent ground stations [*Mace et al.*, 2001; *Sassen and Campbell*, 2001; *Comstock et al.*, 2002; *Keckhut et al.*, 2006; *Noel and Haeffelin*, 2007; *Goldfarb et al.*, 2012], and globally from surface observations [*Warren et al.*, 1988] and passive satellite sensing [*Wylie et al.*, 1994; *Jin et al.*, 1996; *Wang et al.*, 1996; *Stubenrauch et al.*, 1999; *Chen et al.*, 2000]. In addition to these studies, field campaigns have contributed to our knowledge of cirrus cloud properties, which are very limited and mostly confined to midlatitude and tropical regions. Passive satellite techniques have

obvious limitations identifying optically thin clouds. *Sassen* [2002a] extensively examined cirrus clouds through lidar measurements and visual observations, identifying five major cirrus cloud categories (Table 1.1) according to their generation mechanisms.

Table 1.1: Categories of cirrus clouds based on generating mechanisms*

Category	***Mechanism***
Synoptic	Top–down generation
Injection cirrus	Thunderstorm anvil
Mountain-wave updraft	Orographic, terrain induced
Cold trap	Tropopause–topped thin layer
Contrail – cirrus	Rapid cooling of aircraft exhausts

*Adapted from *Sassen* [2002a]

(i) Synoptic cirrus: Synoptic cirrus clouds are those formed in conjunction with weather systems such as frontal and low-pressure systems, or with jet streams. These weather systems are often associated with large scale uplift of air masses, attaining high ice-supersaturation, which invokes ice formation through homogeneous nucleation from the cloud top zone. This formation mechanism is referred to as a *top-down* generation mechanism for ice.

(ii) Injection cirrus: Injection or anvil cirrus clouds are those formed as a result of spreading anvils associated with deep-convective clouds (*thunderstorm processes*). Strong updraft velocities involved in the convection process support the production of ice crystals in their cloud top zone, which tends to spread and get separated from their convective centers through wind shear and forms as cirrus clouds.

(iii) Mountain-wave cirrus: These clouds are formed as a result of ice crystals production through updrafts induced or enhanced by the mountainous terrain.

(iv) Cold trap – cirrus: This category of cirrus clouds is usually observed in tropical regions at extremely low temperatures of about –70° to –90° C, where they are trapped against the tropopause.

(v) Contrail cirrus: Contrail cirrus clouds are those formed by the exhaust fumes of jet engines in the upper atmosphere.

It is now apparent from these mechanisms that the basic microphysical properties of ice particles in cirrus clouds differ through their genesis and so their radiative effects as studied in detail by *Sassen and Comstock* [2001] and *Sassen et al.* [2001]. However, cirrus cloud formation is also known to be strongly influenced by the prevailing upper-level disturbances and topography of the region is known to have strong influence on the cirrus cloud formation [*Stone*, 1957; *Starr and Wylie*, 1990; *Sassen and Campbell*, 2001]. Thus, long-term regional cirrus measurements in the context of varying geography and weather systems are required to accurately parameterize and represent them in climate models at reasonable meso– and synoptic–scales.

(b) Physical and optical properties

The optical characteristics of cirrus clouds are distinct from other ice clouds by their physical appearance and make their identification easy for any surface observer. *Sassen and Cho* [1992] recognized that types of cirrus clouds could be categorized based on their visual appearance and approximate optical depths (given in Table 1.2).

Table 1.2: Range of visible optical depths for categories of cirrus clouds*

Category	***Optical depth range (τ)***	***Description***
Subvisual	< ~0.03	Invisible against the blue sky
Thin	0.03 – 0.3	Translucent, retains bluish color of sky
Opaque	0.3 – 3.0	Usually appears white
Altostratus	> ~3.0	Disk of sun becomes indistinct

*Adapted from *Sassen* [2002a]

Optically thin (*'translucidus'*) types of cirrus clouds are those through which the blue sky is apparent to a surface observer. At this stage the visible optical depth of the cloud will range from 0.03 to 0.3 and with ongoing development processes, as the cloud attains an optical depth of 3.0, it appears opaque and white (the blue sky is no longer visible), though the disk of sun can still be discernible to the observer. Further, as the cirrus develops and thickens, they will eventually transform in to an altostratus type of cloud where the disk of sun becomes totally indistinct. Such transitions of cloud type from cirrus to altostratus can be observed using ground-based lidar systems as the laser pulses get fully attenuated with the visible optical depth exceeding ~3.0 – 4.0. This optically thin nature and the composition of relatively small ice particles with complex shapes enable cirrus types of clouds to produce spectacular optical effects in the atmosphere such as halos, sun dogs, glorys and arcs [*Sassen et al.*, 1998; *Sassen et al.*, 2003a] under certain varying conditions.

1.1.2 Mid-level clouds

(a) Formation mechanisms

According to the World Meteorological Organization (WMO) cloud classification scheme [*WMO*, 1987], those clouds formed with their base altitudes greater than 2 km AGL (above ground level) are referred to as *mid-level clouds* and are basically of two types: *altostratus* and *altocumulus*. In general these clouds are the product of slow ascent or uplift of air mass over large areas or along frontal zones. The other well recognized mechanisms for these cloud types are through convection and orographic lift of air masses.

Liquid water droplets can exist in the atmosphere in a supercooled state until its temperature reaches the homogeneous freezing point of pure water of about -40^{o} C. However, ice crystal formation in mid-level clouds can still be initiated depending on the availability of activated ice nuclei. Mid-level clouds usually exist as mixed-phase with thin layers (a few hundreds of meters) of supercooled water in the top zones and ice

crystals beneath [*Rauber and Tokay*, 1991; *Shupe et al.*, 2006; *Korolev and Field*, 2008; *Shupe et al.*, 2008a; *Smith et al.*, 2009; *Morrison et al.*, 2012]. Though the general formation of ice in such clouds can be explained by the WBF process (as described earlier), this formation is strictly restricted to conditions only when the ambient vapor pressure (e) is supersaturated with respect to ice (e_i), but subsaturated with respect to water (e_w) [*Matrosov et al.*, 2002; *Korolev*, 2007]. Owing to the fact that at subfreezing temperatures, e_w is always greater than e_i the other two scenarios ($e_w > e > e_i$ and $e_w > e_i > e$) may either cause the simultaneous growth of both water droplets and ice particles, or the water droplets may get evaporated completely depending on local thermodynamic conditions and characteristics of both particle populations [*Korolev*, 2007].

Typical altostratus clouds often resemble cirrostratus clouds in appearance and are usually observed to form in the gradual thickening process of upper level cirrostratus, thus containing large ice particles. The distinction between altostratus and altocumulus clouds can easily be depicted from the visual appearance of the cloud to a surface observer as a result of the distinct thermodynamic phase dominance that also causes differences in scattering of light through them. Altostratus clouds are ice-dominant and not strongly precipitating, while altocumulus clouds are water-dominated. The dominance of ice particles in altostratus gives it a diffuse, fibrous appearance with dull gray shades, whereas in altocumulus type clouds the predominant liquid droplets give it a crisp, sharp-edge look. The other forms of ice clouds that exist in the mid-level of the troposphere are those formed as a result of the glaciation of altocumulus clouds [*Sassen et al.*, 2003b; *Sassen and Khvorostyanov*, 2007, 2008], ice crystal layer clouds that are often residuals of briefly lived thin clouds [*Hobbs and Rangno*, 1998], and those formed under the influence of topography over mountainous terrain.

(b) Physical and optical properties

Unlike cirrus, altostratus clouds are usually optically thick (opaque) and consist of large ice crystals with complex shapes that do not allow simple refraction of sunlight

through them. However, halos are often observed near the tops of altostratus clouds by observers in aircraft, as these cloud tops often reach similar altitudes as cirro-form clouds. Usually the lower portions of altostratus cloud where plate-like crystals fall with their faces downward produce *'sun dogs'*. Ground observers often use the presence of sun dogs to confirm the presence of ice crystals in the altostratus clouds. Altostratus clouds formed at frontal systems often contain relatively low concentrations of large ice particles that obscure the solar disk of the sun as if observed through a ground glass, popularly known as *ground glass effect* [*Hobbs and Rangno*, 1998]. These properties serve to easily identify and discriminate altostratus from cirrostratus. While altostratus clouds are often thick, dark, and obscure the disk of the sun or moon, altocumulus clouds tend to form as relatively thin, cellular structures and are often observed with precipitating ice crystals as long tails or fall streaks referred as *virga,* most of which eventually evaporate in the air before reaching the surface.

The other varieties of mid-tropospheric clouds are mostly transparent with low particle density and sizes that often inhibit the growth of precipitable-sized particles by collision-coalescence processes [*Hobbs and Rangno*, 1998]. Occasionally, these thin clouds can also occur as subvisible types [*Hoff*, 1988] owing to conditions such as: (i) intrusion of mid-tropospheric dry layers, which inhibit diffusional ice crystal growth and trigger the ice-sublimation process under certain conditions that also greatly vary with different synoptic regimes [*Smith*, 1995], (ii) prevalence of cold air over the region aligned with frontal zone favoring high supersaturations required to form ice clouds in the lower and mid-levels of the troposphere – especially during winter and spring as observed by *Lampert et al.* [2009] over the Arctic region, and (iii) the lack of or inadequate aerosols upon which cloud droplets can grow [*Mauritsen et al.*, 2011].

1.2 Cloud observation techniques

The commonly used techniques for cloud observation/measurements are described here with their relative advantages and limitations. The purpose of this brief description is

to introduce that each cloud observation technique is unique in its sensitivity to clouds and emphasize the synergetic use of instruments to better comprehend cloud types.

1.2.1 Surface observations

For over a century, clouds were identified based on the estimated range of their heights and visual appearance as observed by trained weather observers. Here identifying the cloud type is solely based on the meteorological conditions that define the cloud appearance and morphology at the time of observation. In practice, this technique is quite subjective and applicable only when the visibility range is good enough. During night or when the vertical visibility is poor, surface weather observations are difficult. The accuracy of this cloud information depends on the ability of the observer to recognize the cloud type. Records of surface observations show that they often tend to underestimate high-cloud amounts as low-level clouds typically obscure the view of upper level clouds. Furthermore, the network of observers is limited and sparsely located thus preventing a globally uniform characterization of clouds. Despite these challenges, several studies have used surface weather reports to provide global distributions of cloud types and cloud amounts [*Hahn et al.*, 1982, 1984; *Warren et al.*, 1986, 1988].

1.2.2 Radar systems

The beginning of instrumentation for cloud observations started soon after World War II, recognizing the ability of radars to identify atmospheric constituents. Over the years many radar systems have been deployed at weather stations, and temporary and permanent ground observatories. These radar measurements have played a key role in our understanding of cloud microphysics and precipitation processes. Radars measure the backscattered power of emitted microwave radiation after hitting a volume of particles in the atmosphere. Radars are operated under a variety of wavelengths (e.g., 10 cm, 3 cm, 8 mm, 3.2 mm) in the microwave region, each suitable to detect a specific size range of particles. Due to the long radar wavelengths and the small particle size, atmospheric constituents fall in the *Rayleigh scattering* regime and the radar beam can penetrate most

of the clouds (even in multiple layers) in the atmosphere. Radar beams can be strongly attenuated in the atmosphere in the presence of skirts of water vapor absorption lines [*Liebe*, 1985; *Lhermitte*, 1987]. The smallest wavelengths that can be used in the microwave region for remote sensing provide the highest sensitivity to all ranges of cloud particles [*Lhermitte*, 1989] except small sizes of ice or drizzle particles (also aerosols), which do not fall in the *Rayleigh scattering* regime for the radar wavelengths in use.

1.2.3 Lidar systems

Lidar systems are similar in principle to radar systems, but operate in the visible or infrared region of the electromagnetic spectrum. Thus, the shorter wavelengths used with lidar place the atmospheric constituents in the *Mie scattering* regime and are capable of detecting all ranges of cloud particles in the atmosphere [*Collins*, 1966]. Also as a result of such short wavelengths, the lidar pulses often gets attenuated in the dense mass of condensed atmospheric constituents and thus can only penetrate optically thin clouds (e.g., cirrus clouds, thin altostratus clouds).

1.2.4 Passive satellites

Meteorological observations with passive satellite techniques began in the 1960's. Since then, observations of cloud structures at large scales have become accessible and helped improve our knowledge of cloud processes. Passive sensors rely on the solar radiance incident on it, and the emissions of atmospheric particles to detect or identify clouds. Measurements with this technique were made during daytime using visible and at nighttime using infrared wavelength channels. Here *cloud type* can be identified based on cloud properties such as cloud top pressure (heights) and visible optical depth, applicable to a single cloud layer in the obtained scene. Though a variety of algorithms have been developed to retrieve multiple cloud layers using a combination of data sources, one often has to make assumptions on the characteristics of the cloud. However, clouds over regions that provide little contrast with the underlying surface (ice and snow-packed

regions) and observation of low-level clouds remain as major challenges for passive satellite sensing techniques.

1.3 Cloud classification schemes

Traditionally, the accepted standard cloud classification scheme is given by WMO [*WMO*, 1987]. The WMO identifies all tropospheric clouds as 10 types based on their essential visual properties and altitude range of occurrence.

With the evolving cloud observations from several techniques, various cloud classification schemes have been proposed to identify cloud types from the observations. These types are primarily based on the *genera* of the clouds as originally given by Luke Howard [*Howard*, 1803]. The International Satellite Cloud Climatology Project (ISCCP) uses cloud top pressure and visible optical depth to identify cloud types [*Rossow and Schiffer*, 1999]. Threshold-ranges were identified using long-term measurements from multiple ground-based sensors to classify clouds by *Wang and Sassen* [2001]. Several other studies classified clouds from satellite passive sensing data sources like AVHRR, MODIS and a combination of these [*Molders*, 1987; *Welch et al.*, 1992; *Bankert*, 1994; *Baum et al.*, 1997; *Li et al.*, 2007; *Behrangi et al.*, 2010]. There exist large discrepancies among such cloud classification schemes due to the sensitivity of the measurements made. While it is true that no single measurement technique or sensor can provide the required information on all cloud types present under any given condition, the use of multiple sensors at all stations is practically not possible. However, these classification schemes have provided a systematic though limited way to categorize clouds with certain characteristic traits representative of the *cloud type*. Recent lidar [*Winker et al.*, 2009] and radar [*Stephens et al.*, 2002] probing from space, through the CALIPSO and CloudSat missions respectively, provide a uniform and systematic global perspective on the complete vertical structure of the clouds over all scales and in all seasons.

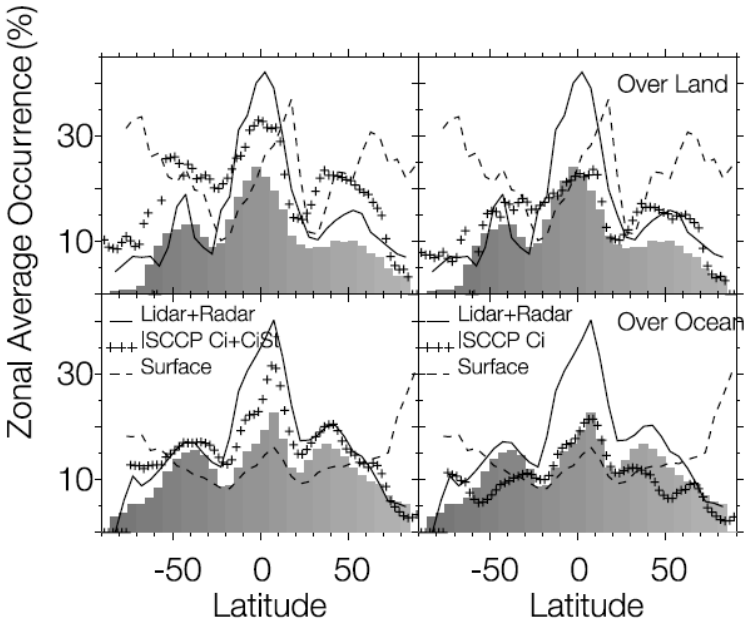

Figure 1.1: Comparison of cirrus cloud occurrences using surface reports, passive (ISCCP), and active satellite sensing [*Sassen et al.*, 2008].

Figure 1.1 presents an illustration taken from *Sassen et al.* [2008] to show that categorization of clouds through different techniques are unique in their own way and are strongly dependent on their sensitivity to the *cloud type* under observation. In this case for the cirrus clouds under observation by each technique: surface observations, passive and active remote sensing through satellites had to rely on different criteria to identify cirrus from other cloud types. The results (Figure 1.1) show a high occurrence of cirrus cloud amounts in the polar regions from surface observations. The other data sources from satellite active remote sensing (radar only – *shown as gray bars*; lidar and radar – *solid line*), and passive remote sensing (ISCCP classification, +*sign*) agree reasonably well, owing to their common observational sensitivities. It remains an open question, whether this over-estimation by surface observations is due to misidentification of cold ice clouds that form in the low and mid-level's as *cirrus* or an artifact owing to the poor sampling statistics in such sparsely populated regions?

What is traditionally known about cirrus clouds from their visual appearance is that they are nearly transparent or optically thin. These optically thin clouds can be completely by lidar measurements as there is little attenuation of the lidar beam. Thus combined visual and lidar observations at ground stations provide a complete and precise, albeit local, characterization of cirrus clouds. Satellite active remote sensing provides an efficient means of studying clouds inhabiting the upper-levels of troposphere. However, these global satellite measurements are not accompanied by ground-based visual observations allowing misidentification of the cloud type. Visual observations avoid confusion of cirrus clouds with other clouds that reside at similar altitudes due to other meteorological processes. A combination of extensive visual observations, ground-lidar measurements, and over-passing satellite measurements of cirrus clouds should be an effective way to resolve the discrepancy in reported occurrence of cirrus clouds over the polar regions. Resolving this discrepancy is one of the objectives for the present work.

1.4 Motivation

Arctic clouds have long been recognized as one of the crucial components that are strongly coupled with several feedback mechanisms in the Arctic and regulate the surface energy budget [*Curry et al.*, 1996]. The net radiative forcing of all types of clouds over the Arctic region has a warming effect on the surface for most of the year [*Curry and Ebert*, 1992; *Intrieri et al.*, 2002], with an estimated annual mean of 40–50 W/m^2 [*Curry et al.*, 1996]. While the formation mechanisms of clouds over the Arctic region vary with the characteristics of the underlying surface, very weak or absence of solar insolation for prolonged periods during winter, extreme low temperatures and surface-temperature inversions create unique environmental conditions over the region that cause the frequent occurrence of multiple layer of clouds [*Pinto*, 1998]. Though these clouds are often optically thin and at relatively low levels, cloud types comprising liquid, ice, and also mixed-phase particles are observed throughout the lower 5 km of the Arctic troposphere. While mixed-phase clouds are more prevalent at low altitudes, clouds above 5 km are found to be predominately composed of ice particles [*Pinto et al.*, 2001].

Arctic mid-level clouds have always been of special interest for climate modelers, owing to the existence of supercooled liquid layers over a large spatial extent that is known to have a substantial radiative impact on the surface energy budget over the region [*Shupe and Intrieri*, 2004; *Zuidema et al.*, 2005]. Several studies have indicated that mixed-phase clouds in the Arctic have a long lifetime that persists for many days and even weeks [*Hobbs and Rangno*, 1998; *Shupe et al.*, 2006; *Verlinde et al.*, 2007; *Morrison et al.*, 2012]. Studies have also reported the existence of ubiquitous thin ice clouds [*Hoff*, 1988] in the low and mid-levels of the troposphere over the Arctic region. However, although low-level ice clouds termed as *'diamond dust'* or *'ice crystal haze'* are well documented [*Curry et al.*, 1990; *Overland and Guest*, 1991; *Curry and Ebert*, 1992; *Hobbs and Rangno*, 1998; *Intrieri and Shupe*, 2004], there has been a dearth of studies of mid-level ice clouds for several reasons: (i) these optically thin clouds are difficult to detect and identify with existing methods and data, (ii) these clouds are not strongly precipitating and do not produce interesting weather, (iii) these clouds have shorter lifetimes and could even dissipate completely under certain conditions. Thus, the primary motivation for our Arctic cloud research is to gain a better understanding of these *types* of ice clouds occurring over such unique environment, in view of their radiative effects.

Recent advances in active remote sensing from satellites are shedding new light on several interesting details about cloud properties that have not known before. While the ability to obtain the vertical structure of clouds from space is costly, the holistic view of *cloud type* from such data has allowed new questions to surface about our traditional understanding of cloud types. This is demonstrated through Figures 1.2 and 1.3 adapted from *Sassen and Wang* [2012], which show the seasonal distribution of mid-level (altostratus and altocumulus) clouds derived from satellite-borne lidar and radar measurements. Sassen and Wang define the seasons as Spring (March-April-May), Summer (June-July-August), Fall (September-October-November) and Winter (December-January-February). The cloud classification scheme here uses a fuzzy logic

classifier, which matches the basic characteristics of cloud type (e.g., height, temperature, phase, horizontal extent, etc.) to assign that cloud to the standard *genera* as defined by the WMO. The fuzzy rules for the mid-level clouds used are shown in Table 1.3 [*Wang*, 2011].

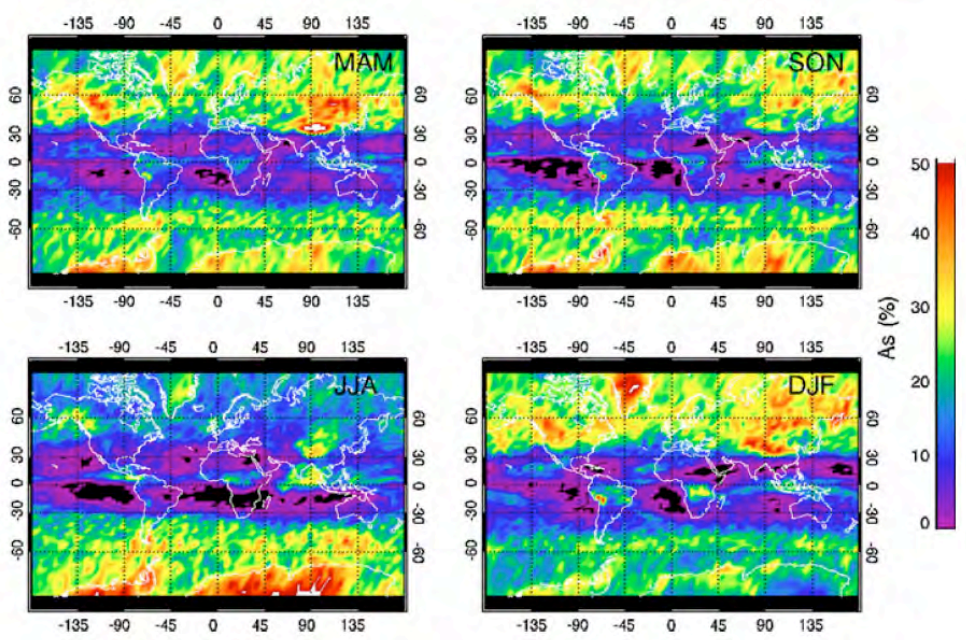

Figure 1.2: Seasonal distribution of altostratus clouds derived from two years of CALIPSO–CloudSat data [*Sassen and Wang*, 2012]. Upper left: Spring, lower left: Summer, upper right: Fall, lower right: Winter.

The altostratus cloud distribution in Figure 1.2 shows a high frequency of occurrence over midlatitudes-to-polar regions, along with the obvious enhancement caused due to the influence of orography and the presence of storm tracks. Whereas, the altocumulus type of cloud occurrences (Figure 1.3) mainly dominate in the tropical belt, and along the midlatitude storm tracks, which is associated with deep convection. The geographical occurrence of altostratus here also suggests the prevalence of thin mid-level ice clouds over the polar regions attributable to: (i) strong frequency of occurrence over the regions other than the extratropical storm tracks. (ii) for the case of classic/standard altostratus type of clouds (where the lidar pulse gets attenuated), which usually forms

through the transition of upper-level cirrostratus, it is fair to think of the association of the high frequency of cloud occurrence for cirrus [*Sassen et al.*, 2008] and altostratus – which is not the case. Thus, we speculate that mid-level ice-dominated clouds occurring over the Arctic region have probably been included in the categorized altostratus sample here. This categorization suggests a need to investigate varieties of mid-level ice clouds other than the standard altostratus/altocumulus to comprehend this type of cloud. With this background, here we propose our research hypothesis as, *"Unlike the basic mid-level cloud type (altostratus), other varieties of transparent ice clouds occur over the Arctic region"*. The relevant questions to understand: (i) are these transparent mid-level clouds are composed entirely of ice particles? (ii) how prevalent are they? (iii) are they linked to synoptic regimes? and (iv) what are their radiative impacts?

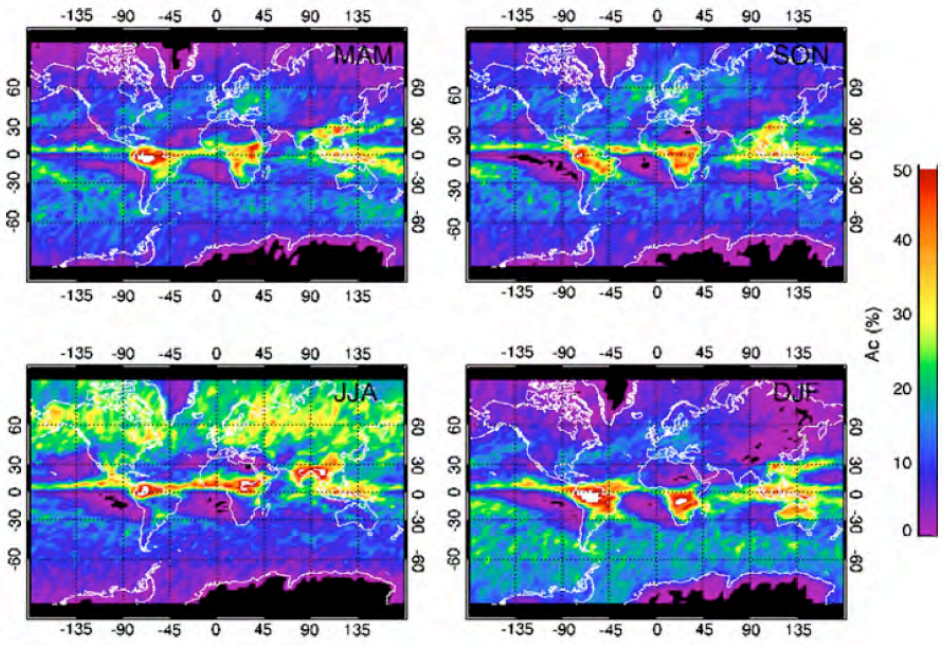

Figure 1.3: Seasonal distribution of altocumulus clouds derived from two years of CALIPSO–CloudSat data [*Sassen and Wang*, 2012]. Upper left: Spring, lower left: Summer, upper right: Fall, lower right: Winter.

Table 1.3: Fuzzy rules for two basic mid-level cloud types*

Property	Altostratus	Altocumulus
Height and Temperature (Base and Top)	Middle base; low base and middle or high top	Middle base; low base and middle top; warm or moderate cloud top temperature
Phase	Ice or mixed-phase	Mixed-phase or water
Precipitation	No precipitation or isolated drizzle	No precipitation or isolated drizzle
Thickness	Moderate or thick or thin ice	Thin or moderate
Horizontal extent	Moderate extent	Isolated or moderated or extended mixed-phase
Cloud cover	Overcast or moderate mid-level ice clouds	Any

*Adapted from *Wang* [2011]

1.5 Objectives and structure of this thesis

The present research is motivated by our need to understand the radiative effects of Arctic ice clouds on the climate system. Specifically we characterize the types of ice clouds forming in the upper and mid-troposphere over the Arctic region and the associated synoptic-scale conditions. The occurrence and properties of these ice cloud types are investigated using the Cloud Polarization Lidar (CPL) system through ground-based observations available from the AFARS (Arctic Facility for Atmospheric Remote Sensing) station located on the University of Alaska Fairbanks campus in Fairbanks, Alaska. The purpose here is to reveal and characterize cirrus clouds and the hypothesized occurrence of varieties of transparent ice clouds in the mid-levels of troposphere over the Arctic region.

This thesis addresses the following questions:

i) How do the macrophysical properties of visually-identified cirrus clouds vary seasonally over a typical sub-Arctic region?

ii) Do varieties of mid-level clouds exist as optically thin layers over the sub-Arctic region, if so what are their properties and how do they vary?
iii) What are the regional weather patterns favorable for the formation of thin ice clouds over the AFARS ground station?
iv) How well are the ice clouds observed over the AFARS station represented in satellite data, and what are the discrepancies found between them?

Our attempt to address these questions begins by studying the climatological properties of transparent ice clouds in the troposphere over the AFARS observation station as measured by ground-based sensors. Here the types of ice clouds were identified entirely based on their visual appearance by a trained observer. The ability of the lidar pulses (0.694 μm) to penetrate these clouds without being attenuated (i.e. only transmissive pulses) is used for the analysis to identify transparent ice clouds. Then a threshold with the maximum cloud top temperature of -38^{o} C is used to extract the mid-level transparent ice clouds from the sample. Examination of the macrophysical properties for visually identified cirrus and transparent mid-level clouds will help us define such cloud properties regionally over our sub-Arctic observation station. Statistical methods will be applied to the MERRA (Modern Era Retrospective analysis for Research and Applications) reanalysis dataset. Weather patterns associated with thin ice cloud formation over AFARS will also be examined.

In this chapter we have presented a general introduction to the mechanism and properties of ice clouds, the observation and measurement of ice clouds, and the categorization of ice clouds. We have also identified the need to comprehend several categories of ice clouds. We describe the types of ice clouds observed over the AFARS station located in central Alaska, along with the data and methods used in Chapter 2. In Chapter 3 we provide an overview of synoptic patterns over the Arctic region and examines the conditions favorable for ice clouds formation over the observation station. In Chapter 4 we describe satellite active remote sensing data from A-Train constellation

and provide a comparison of ice cloud retrievals from both the AFARS station and the A-Train satellites. Finally, in Chapter 5 we present a summary, conclusions and applications of the present work and compare then with previous studies of ice clouds as appropriate.

Chapter 2

Ice clouds over the AFARS site (64.86^{o} N, 147.84^{o} W)

In this chapter, the types of ice clouds forming in the upper and mid-levels of the troposphere over the cloud observation station (AFARS – *Arctic Facility for Atmospheric Remote Sensing*) are presented. AFARS is located at the University of Alaska Fairbanks and has been operational since 2004. This project is a continuation of a research program for high cloud measurements and was previously operational from 1992 – 2002 at the University of Utah, where it was referred as *'FARS'*. Here we use approximately eight years of cloud polarization lidar (CPL) data collected at AFARS, to investigate the types of local ice clouds. This chapter first provides a description of the instruments at AFARS along with their operating principles and sensitivity to clouds. Next, the data collection philosophy and the method used to identify cloud types at AFARS are described. Cloud boundaries are derived using a general cloud detection algorithm, and the meteorological parameters along the cloud boundaries are deduced from the nearest available local radiosonde data. In this chapter through the analysis of AFARS dataset, we obtain:

i) Climatology of ice cloud properties as observed over the AFARS site, and
ii) Characteristic features of the categories of ice clouds.

2.1 AFARS

AFARS facilitates state-of-the-art remote sensors to monitor clouds and aerosols over a typical sub-Arctic environment. AFARS is located in the University of Alaska Fairbanks campus (64.86^{o}N, 147.84^{o}W), which lies in the interior of Alaska at the confluence of the Chena and Tanana rivers with an elevation of 286 m above mean sea

level. The climate of Fairbanks can be described as *continental* with relatively warm summers and very cold winters [*Shulski and Wendler*, 2007]. The city is surrounded by a barrier of hills extending from northeast to southwest (~600 m elevation) and the Alaska Range (~6190 m elevation) to the south, as shown in Figure 2.1. The large longitudinal extent of the Brooks Range (lying over northern Alaska) effectively blocks the intrusion of air from the Arctic Ocean into the Interior, whereas the Alaska Range to the south acts as an effective barrier to the intrusion of warm and moist air from the North Pacific Ocean. Due to such local topography, orographic lifting of air masses is expected to be an important cloud formation mechanism over the region.

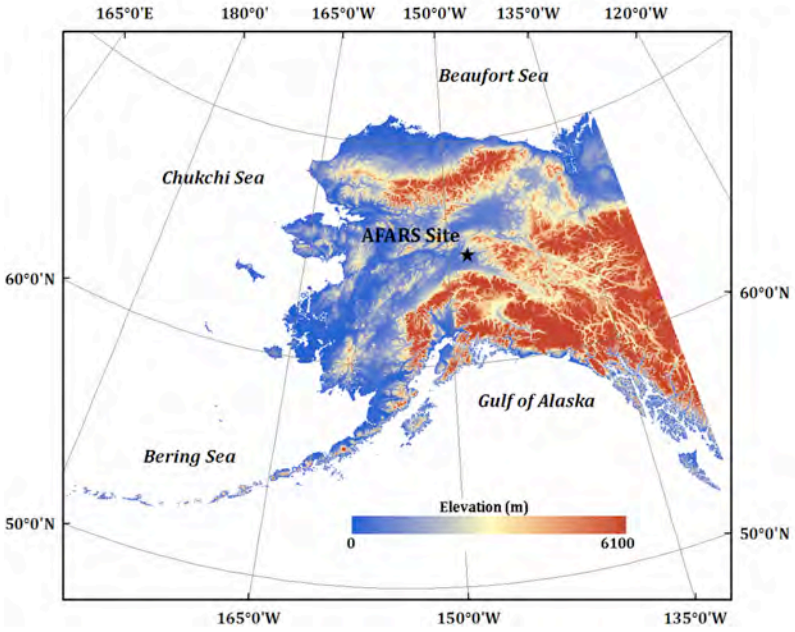

Figure 2.1: Topographic map for the state of Alaska, also showing the location of the AFARS station (star mark).

2.1.1 Instruments and working principles

(a) Cloud polarization lidar

The Cloud Polarization Lidar (CPL) deployed at the AFARS site is a vertical pointing (nadir looking) dual-channel lidar operating at 0.694 μm. This lidar transmits laser pulses generated through a ruby crystal every 10-sec with a peak energy of 1.5 J.

The lidar detects the returned backscattered signal over 2400 range gates. The returned vertical resolution of 6 m for this configuration (Table 2.1) makes it possible to probe the atmosphere up to about 14.5 km altitude with an additional 100 pretrigger points, which are used to estimate the background signal level for each shot.

Table 2.1: Specifications of cloud polarization lidar at AFARS

Operational		
Wavelength (ruby)		0.694 μm
Peak energy		1.5 J
Maximum PRF		0.1 Hz
Pulse width		25 ns
Polarization		Vertical
Beam widths:	transmitter	0.5 mrad
	receiver	1 – 3 mrad
Receiver		28 cm diameter telescope
Detectors		2, PMTs
Positioning		Manual
Data handling		
Channels		Vertical + Horizontal
Vertical resolution		6.0 m
Range gates		2400
Digitizer resolution		10 bit
Storage		Hard drive
Pretrigger points		100

Operations with the lidar are carried with a *turnkey* system and the returned signals detected through photomultiplier tubes (PMTs) are digitized (10-bit) before they are stored on a hard drive. To avoid the saturation of the detector (off-scale data points) from highly backscattering medium in the troposphere, the receiver gain is occasionally reduced and suppressed manually for some time. This operation might lead to a loss of signals even from a narrowly separated upper layer due to the limited dynamic range of the CPL, and such loss of signals are noted as *definite range-limited* attenuation in the field notes by the operator. However, the lidar observations are often affected by the presence of lower level clouds, or thickening mid-level clouds, that lead to the partial or

complete attenuation of laser pulses before reaching the upper levels; these are termed as *probable range-limited*. Usually the lidar is operated in the up-looking nadir direction (zenith), but occasionally the lidar is manually titled to point ~3 – 4^o off the zenith view for some time to detect/confirm the presence of horizontally oriented ice crystals. This off-zenith operation mode owes to the fact that horizontally oriented crystals lying with their faces downward generate high specular backscattering [*Sassen*, 1977] and tend to saturate the detector when viewed in the zenith direction.

Working principle of the lidar:

The power received P(R) as a function of range R, by a monostatic lidar under isotropic scattering assumption can be written as *Scotland et al.* [1971]:

$$P(\lambda,R) = \frac{C(\lambda)}{R^2}.[\beta_a(\lambda,R) + \beta_m(\lambda,R)].exp[-2\int_0^R(\sigma_a(\lambda,r) + \sigma_m(\lambda,r)).dr] \qquad (2.1)$$

Where, $P(\lambda, R)$ is the returned backscattering power,

C is the constant derived for the instrument,

λ is operating wavelength of lidar,

R is the distance of the target from lidar,

σ_m, σ_a are the absorption coefficients of atmospheric molecules and particles, and

β_m, β_a are the backscatter coefficients due to atmospheric molecules and particles.

The backscattering coefficient (β) represents the amount of light scattered in the backward direction from a volume of scatterers and depends on the particle phase function and scattering cross-section. The absorption coefficient (σ) represents the total quantity of light energy removed from the incident field and depends on the particle extinction cross-section. The backscatter and absorption coefficients, which are the unknown quantities in the lidar equation (2.1), can be derived from inversion methods by assuming a value for extinction-to-backscatter ratio (referred as *lidar ratio*) for any given scatterers [*Fernald et al.*, 1972; *Klett*, 1981].

The advantage of using CPL is the ability to discriminate the shape of scatterers as spherical or non-spherical through a derived parameter called *linear depolarization ratio,* which is used to infer the phase of the cloud. The linear depolarization ratio (LDR, denoted as δ) is defined as the ratio of the perpendicular to the parallel polarized backscattered signals from the scatterers. For instance, liquid water droplets of spherical shape retain the polarization state of the incident light, whereas the light incident on non-spherical particles undergoes multiple internal reflections, and produces depolarization of the light [*Liou and Scotland*, 1971]. The corresponding δ values of commonly encountered hydrometeors in the atmosphere as reported by *Scotland et al.* [1971] and *Sassen* [1991] are: water droplets ~0.0, ice crystals and snowflakes ~0.5, and rimed ice and particles with complex surfaces have values more than 0.6.

(b) W-band radar

Table 2.2: Specifications of W-Band radar at AFARS

Operational	
Wavelength (W-band)	3.2 mm
Peak power	1.2 KW
PRF	10 Hz – 100KHz
Pulse width	27 ns
Beam width	0.25^{o}
Receiver diameter	90 cm dish
Receiver gain	57 dB
Maximum scan rate	5.0 deg/sec
Data handling	
Channels	6
Vertical resolution	Max. of 75 m
Range gates	Max. of 600
Pulses averaged	Programmable
Digitizer type	Logarithmic
Storage	Hard drive
Polarization Transmitted	Vert. + Horz.
Received	Vert. + Horz.

The second instrument at AFARS is a vertically pointed Doppler radar operating at 94 GHz (3.2 mm wavelength), which is suitable for observing most cloud types. The technical specifications of the radar are given in Table 2.2. This radar system uses a high pulse repetition frequency that yields a Doppler velocity window of ±8 m/s at a vertical resolution of 75 m. The single-antenna with beam width of 0.25° provides a horizontal sample size of about 20 m at 5 km. Radar operations at AFARS are usually carried out simultaneously with the lidar but operations are limited to times of suitable cloud conditions.

Working principle of the radar:

As the operating principle of radar is similar to that of the lidar with the exception of the wavelengths used, the radar equation can be written in a similar fashion as the lidar equation [*Sassen*, 1987]:

$$P(R) = \frac{C}{R^2}\eta \,.exp[-2\int_0^R (k_a + k_i + k_w)\,.\,dr] \tag{2.2}$$

Where, $P(\lambda, R)$ is the average returned power,

λ, C is operating wavelength and constant of the radar system,

R is the distance from the target to the radar,

η is radar reflectivity, and

k_a, k_i, k_w are the extinction coefficients for moist air, ice and water particles.

At Rayleigh scattering wavelengths, radar reflectivity is defined as the sum of the backscattering coefficients per unit volume and can be expressed as,

$$\eta = \frac{\pi^5}{\lambda^4}|K|^2 \,.\int_0^\infty N(D)\,D^6\,dD \tag{2.3}$$

Where, $|K|^2$ is the dielectric constant for either ice or water particles,

D is the diameter of the particle, and

N is the particle concentration in the diameter interval from D to (D + dD).

Owing to the dependence of the radar reflectivity on the sixth power of particle size (Equation 2.3), the radar can detect only relatively large particles, and the shortest millimeter wavelength that could be used for remote sensing in the microwave region of the spectrum possesses sensitivity to most cloud particles.

(c) IR radiometer

The third instrument at AFARS is an IR radiometer. An IR radiometer is a device used to measure the emitted radiation from any atmospheric constituents within the spectral range of the *atmospheric window* (ranging from 8 – 14 μm). Operations at AFARS use an up-looking IR radiometer with a specifically designed narrow-beam field-of-view (FOV) of about 0.14° to measure emitted radiation from clouds even in the upper levels of the troposphere. In the absence of clouds within the FOV of the device, it records the emitted radiation of water vapor and ozone (gases) in the atmosphere directly above the instrument. The *Brightness temperature* obtained with it can range ~50° to – 80^{o} C with an accuracy of 0.5^{o} C. This radiometer is operated with a similar time resolution as the ruby lidar at 0.1 Hz (i.e., one record for 10-seconds).

2.2 Relevant studies on ice clouds

Studies on ice clouds are mostly confined to upper level cirrus clouds from temporary and permanent observation stations, and field campaigns. For more than a decade, with the extensive use of specifically designed lidars to monitor cirrus clouds, several regional climatologies have emerged from midlatitudes [*Mace et al.*, 2001; *Sassen and Campbell*, 2001; *Giannakaki et al.*, 2007; *Goldfarb et al.*, 2012] and the tropics [*Comstock et al.*, 2002; *Cadet et al.*, 2003; *Thorsen et al.*, 2011] have emerged. Among these, *Sassen and Campbell* [2001] was the first to provide a climatological representation of cirrus cloud properties based on a long-term dataset over the midlatitudes. There are also several studies on mid-level clouds over the tropics [*Yasunaga et al.*, 2006; *Ansmann et al.*, 2009; *Seifert et al.*, 2010; *Zhang et al.*, 2010], midlatitudes [*Hobbs and Rangno*, 1985; *Fleishauer et al.*, 2002; *Hogan and Illingworth*,

2003; *Korolev and Isaac*, 2003; *Smith et al.*, 2009] and the Arctic [*Rangno and Hobbs*, 1991; *Hobbs and Rangno*, 1998; *Pinto*, 1998; *Turner*, 2005; *Zuidema et al.*, 2005; *Shupe et al.*, 2008b]. These studies focus mostly on the mixed-phase cloud properties and low-level ice clouds. The present work exclusively focuses on the ice clouds forming in the upper and mid-levels of troposphere that are transparent to lidar pulses. By analogy, it means the visible optical depths of these ice clouds are less than 3.0 – 4.0.

2.3 Data used

Operations at AFARS have been ongoing since 2004. Operators make daily to weekly cloud and aerosol observations usually during the local-noon overpass times of the *A–Train constellation* of satellites, depending on the weather conditions over the site. Though the primary interest of AFARS is to gather high-cloud measurement, other cloud-types and aerosols in association with upper/mid-level clouds have also been of special interest because of their frequent occurrence. Since AFARS has been operational, about 1000 hours of extended time observations have been made at the site. This dataset provides a unique opportunity to build climatological statistics of the observed clouds with such rarely available ground-based measurements for a prolonged period over a typical sub-Arctic region. The data-record used for the present study spans form February 2004 – June 2012 (Figure 2.2) with an average of 82-hours of observations per month.

Apart from the lidar dataset, field notes maintained by the operator play an important role in our analysis. These field notes describe the general weather associated on the day of operations with several observations/comments, such as: (i) visual attributes (e.g., fibratus, spissatus), (ii) presence of any optical phenomenon (e.g., halos, corona, arcs), (iii) cloud coverage, (v) presence of contrails, (vi) presence of aerosol layers, and (vii) any instrumental disturbance. These comprehensive observations not only exclude the risk of misclassifying clouds using various algorithms, but also are useful in determining the cloud generating mechanisms such as synoptic cirrus, orographic cirrus,

anvil cirrus, contrail cirrus and thin ice clouds formed by depositional nucleation of aerosols.

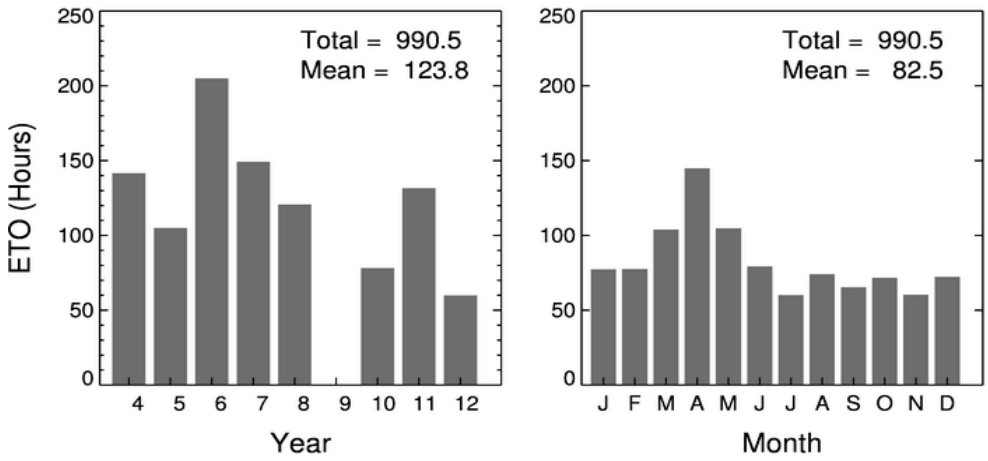

Figure 2.2: Extended time observations record at AFARS from February 2004 – June 2012 used in the present study (yearly – *left*, monthly – *right*).

2.4 Methodology

2.4.1 Identifying cloud types

During the data collection at AFARS, the local weather conditions and the visual morphology of the clouds were observed and noted in routinely maintained field notes by the operator. A single operator (Professor Kenneth Sassen), trained by the National Weather Service, carries out these visual observations of clouds. The operator initially categorizes the cloud (as low, middle and high) based on the approximate altitude level of its occurrence in the atmosphere and matches its characteristic traits with the '*genera'* of cloud types. Basically *cloud type* identification is relied on the traits such as cloud height, color, texture and visibility of the sky through the cloud. At any time during data acquisition, the operator can also use the ability of polarization lidar to confirm or retune his judgment. Thus, clouds at AFARS are categorized entirely based on their visual attributes through real-time inspection with no prior constraints on their properties like height, temperature, phase etc.

2.4.2 Retrieval of cloud properties

The cloud boundary detection algorithm used here is derived from the modified Universal Cloud Detection Algorithm [*Wang and Sassen*, 2001] suitable to retrieve the characteristics in ice clouds. An averaging scheme of three vertical points (18 meters) and 6 shots (1-minute) has been applied to increase the signal-to-noise ratio in the lidar dataset, and the required range-squared correction is applied. The background signal (noise level) in each shot is estimated as *n-times* of the standard deviation of the returned power from last 75 points of the maximum range of the lidar (~14.6 km), where *n* varies between 1–3 and is chosen iteratively by observing the display of data so as to avoid any aerosol layers (if present) and the ambient noise layers identified as cloud by the algorithm. Alternatively, a *threshold* value determined from pretrigger points for each shot used as the background signal. In this algorithm, cloud bases are detected similar to *Sassen and Cho* [1992] as the altitude at which the lidar returned power increases up to 5% of the previous value for at least three consecutive points, and the power at cloud base is above the background noise level. Cloud top height is determined as the altitude above the cloud base where the returned power falls below the chosen background signal level.

It is a well-known fact that lidar can penetrate relatively thin clouds, so it is essential to *flag* the shots as attenuated or transmissive. Cloud tops retrieved from attenuated shots are marked as *apparent tops,* and only *true tops* retrieved from transmissive shots are considered for analysis. A basic framework of all the available data displays is prepared as shown in Figure 2.3, which are checked with the field notes as a measure of quality check of the retrieved cloud types and their boundaries. Climatological statistics for all transmissive ice clouds have been derived for individual layers. In case of multiple cloud layers, if the spacing between them is less than 500 m, such layers have been merged as a single *envelope* layer. The corresponding atmospheric parameters such as temperature, relative humidity, pressure, wind speed, and wind direction representing the thermodynamic properties of both cloud top and base along

with the tropopause limit, are obtained over the cloud layer altitudes from radiosonde data. The local meteorological station is located at the Fairbanks International Airport 4.9 km from AFARS. The radiosonde measurements from the launch at 0000 UTC are normally used for combining with the mid-afternoon AFARS lidar measurements.

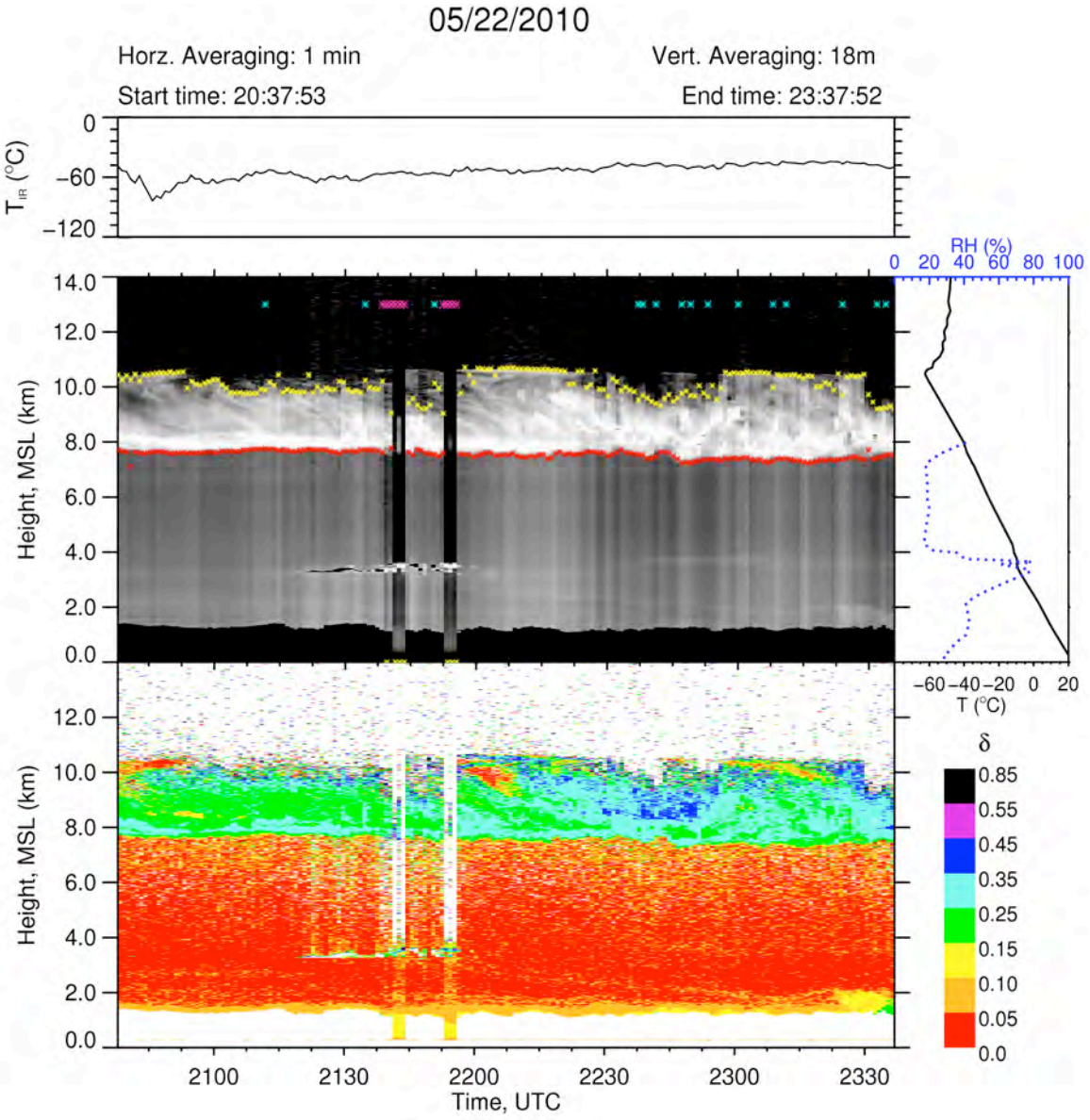

Figure 2.3: Framework of lidar data display used in extracting climatological statistics.

A maximum allowable cloud top temperature (T_{ct}) of –38^{o} C is used to separate mid-level cloud from cirrus cloud, which are termed as '*mid-level ice clouds'* in this analysis. Thus, the sample of upper level ice clouds identified as '*cirrus clouds*' contains all types of cirrus (cirrus, cirrostratus, cirrocumulus, etc.) that are confirmed by their visual appearance. The sample of '*mid-level ice clouds'* consists of types of optically thin altostratus, sometimes with thin embedded altocumulus and thin ice cloud layers left as remnants in the mid-troposphere or formed as a result of other cloud processes (as described in Section 1.1.2). The breakdown of the AFARS data according to these categories is shown in the Table 2.3. In summary, up to 70% of the cloudy profiles from the data record used here are identified as cirrus and 15% as mid-level ice clouds. The dataset is intentionally biased towards cirrus clouds, as measurement of upper level clouds is been the primary objective for the establishment of the AFARS station.

Table 2.3: Breakdown of AFARS data used to derive climatological properties

	*Number of Shots**	*Percentage*
Total data used (472 Independent days)	49150	100
Clouds		
Cirrus clouds	34073	69.3
Mid-level ice clouds	7443	15.1
Definite range-limited	2757	5.6
Probable range-limited	4877	9.9

*1–minute averaged shots

2.5 Results and discussion

The monthly frequency of occurrence for the cirrus and mid-level ice cloud categories are shown in Figure 2.4. The overall trend in both categories of clouds is obviously similar to the trend in the data-records used here. What is of particular interest is the high occurrence of mid-level ice cloud during spring season, compared to the cirrus

clouds that are attributed to the increased cyclonic activity over the Gulf of Alaska. This finding shows the influence of regional synoptic activity conducive for local ice cloud formation over AFARS. Figure 2.4 also shows the monthly normal mean precipitation (data source: http://climate.gi.alaska.edu/Climate/Normals) for Fairbanks. In general, considerable variability in monthly precipitation is observed over the region with a minimum in March of 0.3 inches and a maximum in July of 2.1 inches. While much of the summer and winter precipitation is generated from major frontal systems that cross over the region, convective systems contribute notably to the summer precipitation with July and August being the wettest months. Thus, the AFARS observations show that for the months with least precipitating weather systems (i.e., March and April) cirrus clouds are most common.

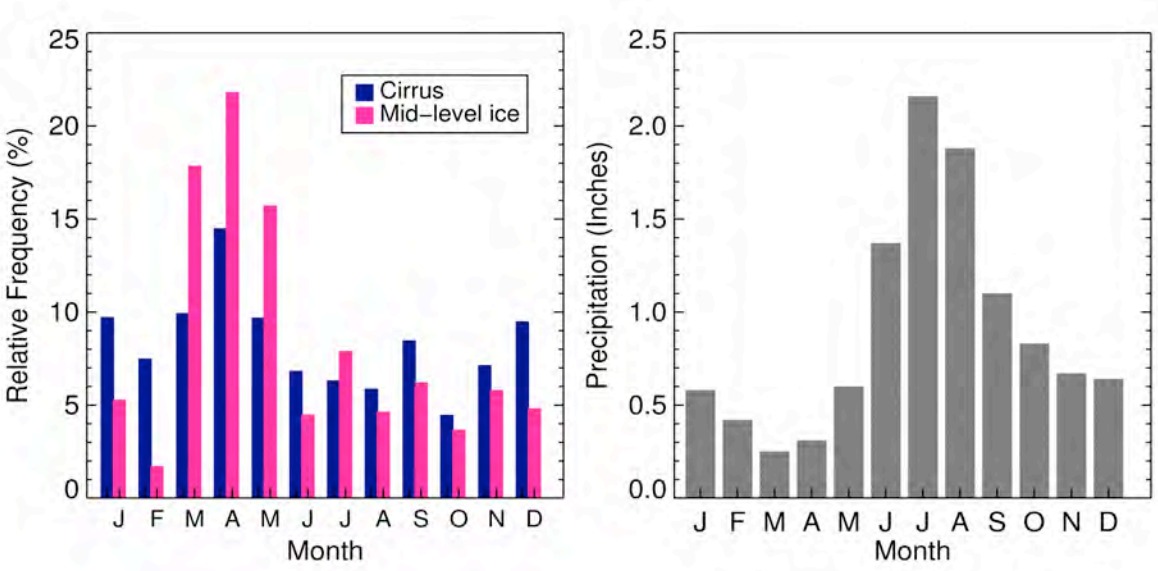

Figure 2.4: Relative frequency of occurrence for cirrus, mid-level ice clouds from the AFARS data being used (*left*) and mean monthly precipitation (*right*) over Fairbanks from 1981 – 2010.

2.5.1 Climatology of ice clouds

(a) Cirrus clouds

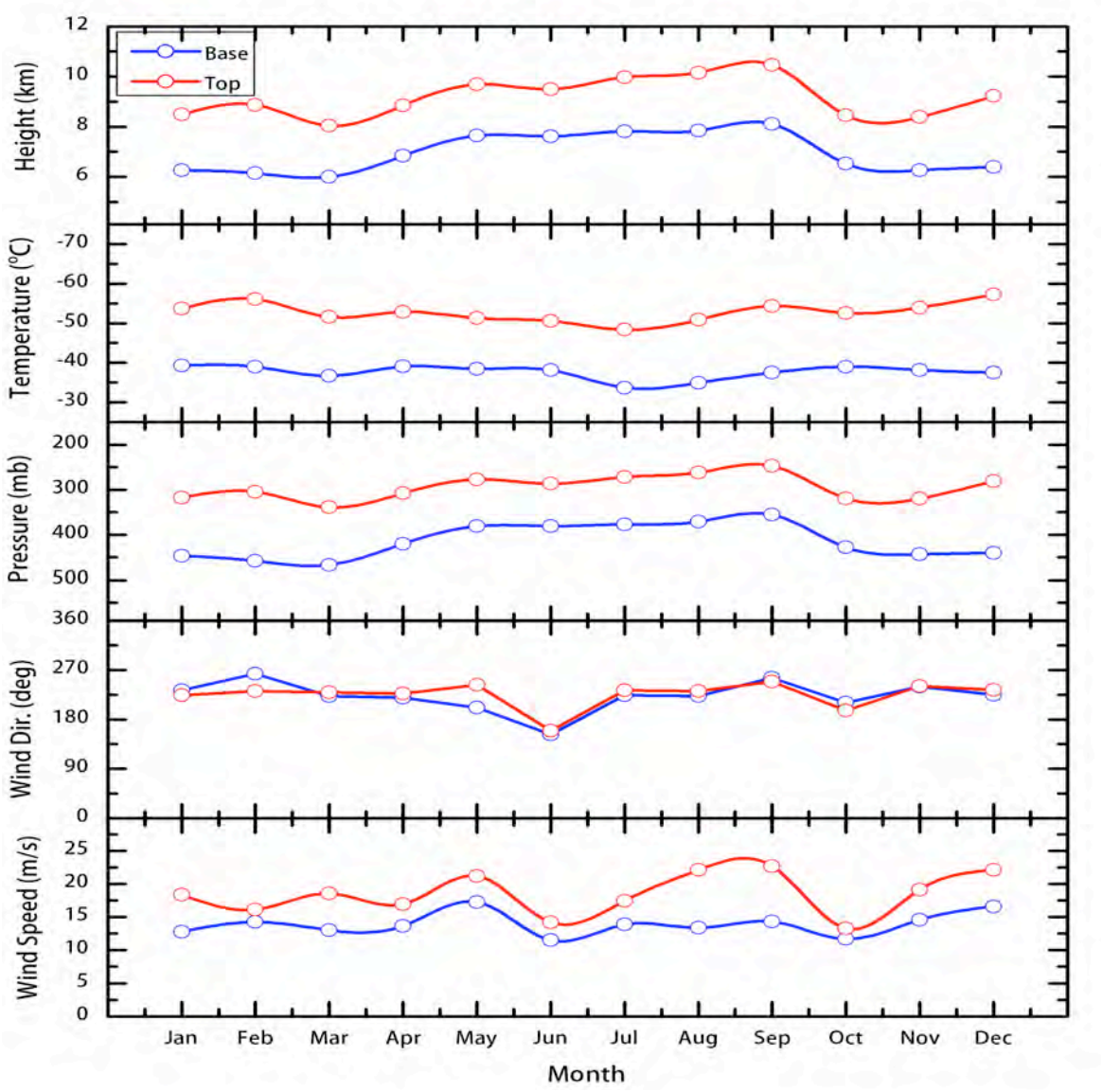

Figure 2.5: Monthly climatological properties of cirrus clouds over the AFARS site.

The monthly and seasonal climatological macrophyiscal properties of cirrus clouds are examined here as follows. The monthly cirrus cloud top/base heights maxima occur during late summer to early fall where the minimum values occur during December to January (Figure 2.5). Here the variations in cirrus cloud altitudes do not show any strong

seasonality, but rather vary with the tropopause height, which marks the boundary of the upper troposphere. The variations in the corresponding atmospheric pressure and temperatures at cirrus altitudes follow the annual cycle of meteorological conditions over the region; cirrus cloud altitudes markedly follow the tropopause level. The variations of monthly mean cirrus cloud top altitudes with the mean tropopause altitudes for cirrus cloudy days are shown in Figure 2.6 to confirm this. Occasionally, cirrus clouds extend beyond 1 – 2 km of the tropopause depending on the amount of ice particles injected into the tropopause layer and the availability of water vapor [*Sassen and Campbell*, 2001]. This is true even in the present case, which can be depicted from the contours showing separation distance of tropopause from cirrus top altitudes.

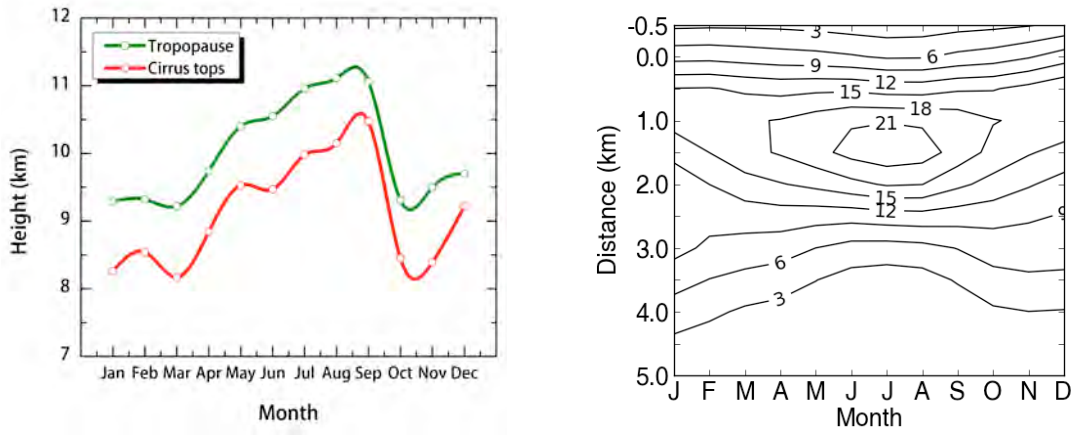

Figure 2.6: Monthly cirrus cloud top, and tropopause heights (left) and contours of distance of separation between them cirrus cloud top and tropopause heights (right) in percent.

Average monthly cirrus top (base) temperature range from –50^{o} C to –58^{o} C (–32^{o} C to –40^{o} C). The monthly mean wind speeds at cirrus altitudes show much undulation with maximum winds (up to 25 m/s) occurring during September, where the airflow is nearly zonal (W). Monthly mean wind directions at cirrus levels clearly depict the influence of the polar jet stream surrounding the Alaska mainland. During winter, the extreme low temperatures over the Arctic region favor the positioning of polar jet streams to the south of Alaska. With the seasonal transition, the jet stream moves over Alaska and its north by

summer. Depending on the meridional temperature gradient, the upper level circulation often forms into deep troughs and ridges over the region (creating long waves or Rossby waves), which causes southerly flow into interior Alaska.

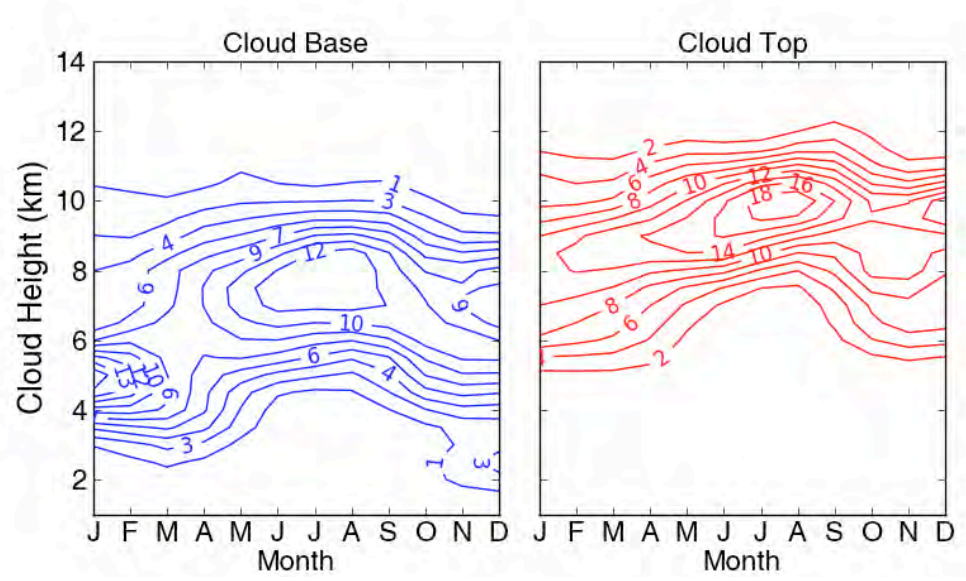

Figure 2.7: Monthly cirrus cloud frequencies (in percent) at AFARS binned for 0.5 km height intervals.

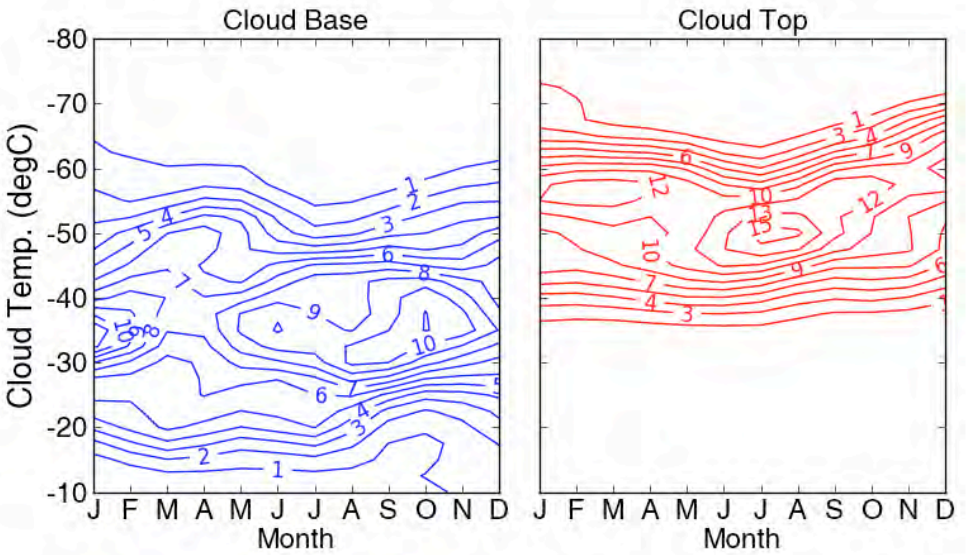

Figure 2.8: Monthly cirrus cloud frequencies (in percent) at AFARS binned for 2.5^{o} C temperature intervals.

Observations of monthly frequencies of occurrences of cirrus clouds (Figures 2.7 and Figure 2.8) show higher occurrences during winter at lower altitudes. It can also be seen that the cirrus base altitude occurrences span a greater range of altitudes in late fall and winter with a gradual decrease in surface temperatures over the region. Table 2.4 provides the seasonal and annual averages of the cirrus clouds as observed over AFARS. It is now apparent that at AFARS, cirrus clouds occur at relatively low altitudes, as one can expect from the lower altitude of the tropopause over the sub-Arctic. Seasonality in the cirrus top/base altitudes can again be observed only with reference to the tropopause heights with the cirrus preferring relatively higher altitudes during spring and summer. This behavior is due to the gradual increase in tropopause height from spring to summer. The seasonality of cirrus macrophysical properties shown here are in consistence with previous climatological studies from *Mace et al.* [2001] and *Sassen and Campbell* [2001].

Table 2.4: Seasonal and annual mean of cirrus clouds for ~8 years over AFARS

	Jan – Mar	Apr – Jun	Jul – Sep	Oct – Dec	Annual
Cloud base					
Height (km)	6.02	7.23	7.92	6.37	6.87
Pressure (hPa)	461.06	402.3	367.93	438.8	418.04
Temperature (^{o}C)	–37.69	–38.27	–36.13	–38.6	–37.73
Wind direction (^{o})	231.58	201.3	239.2	226.0	222.91
Wind speed (m/s)	13.0	13.8	13.9	14.9	13.9
Cloud top					
Height (km)	8.31	9.17	10.2	8.78	9.08
Pressure (hPa)	325.2	296.4	257.2	301.74	297.16
Temperature (^{o}C)	–54.31	–52.76	–53.06	–56.82	–54.06
Wind direction (^{o})	223.89	210.6	240.79	229.45	224.84
Wind speed (m/s)	18.8	17.1	21.2	19.3	18.9
Tropopause separation(km)					
Cirrus days	0.94	1.00	1.11	0.96	1.00
Cloud thickness (km)					
Layer envelope	2.3	1.97	2.29	2.40	2.21

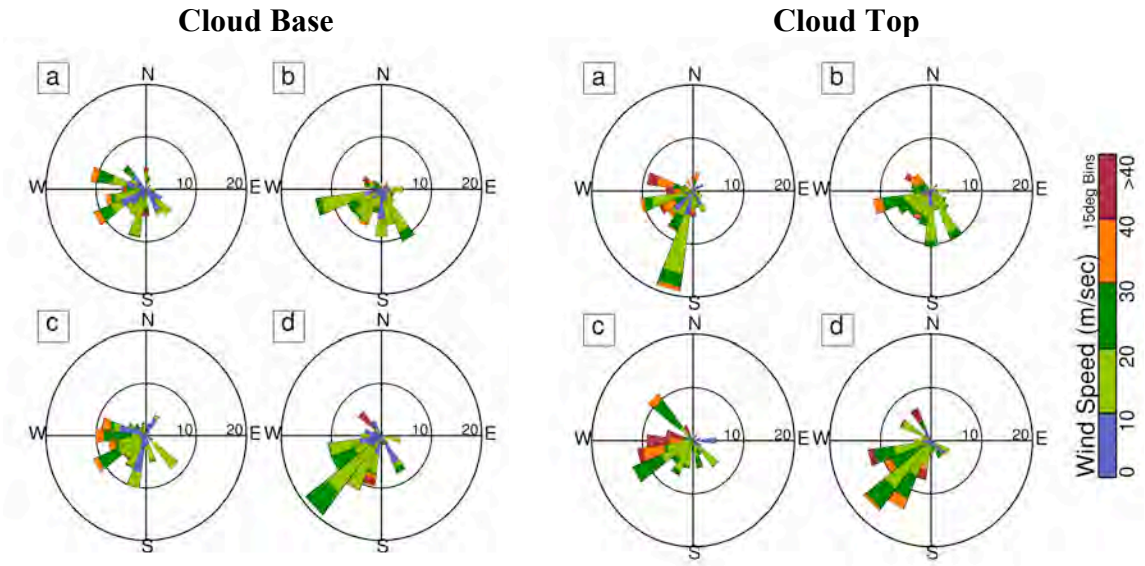

Figure 2.9: Seasonal frequencies (in percent) of wind speed and directions for AFARS cirrus clouds. (a) Winter, (b) Spring, (c) Summer and (d) Fall.

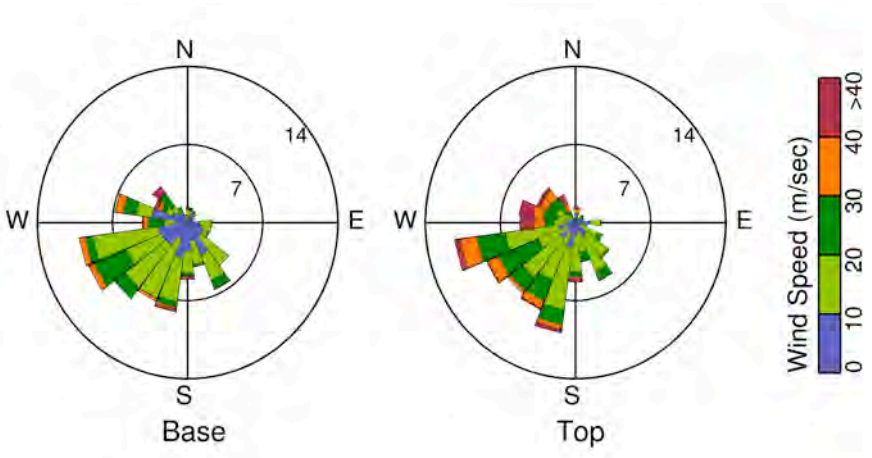

Figure 2.10: Total frequencies (in percent) of wind speed and directions for AFARS observed cirrus clouds.

The variability of wind speed-directions is shown in the Figures 2.9 and 2.10 as the percentage of occurrence of wind (wind roses) binned for every 15 degrees. Winds over 40 m/s indicative of polar jet streams, are evident in winter as well as in summer seasons. As most cirrus cloud-causing winds are observed to be originating from the S–SW direction, it can be said that often over AFARS, cirrus have their genesis from the orographic uplift of air masses along the Kuskokwim mountains and the Alaska Range.

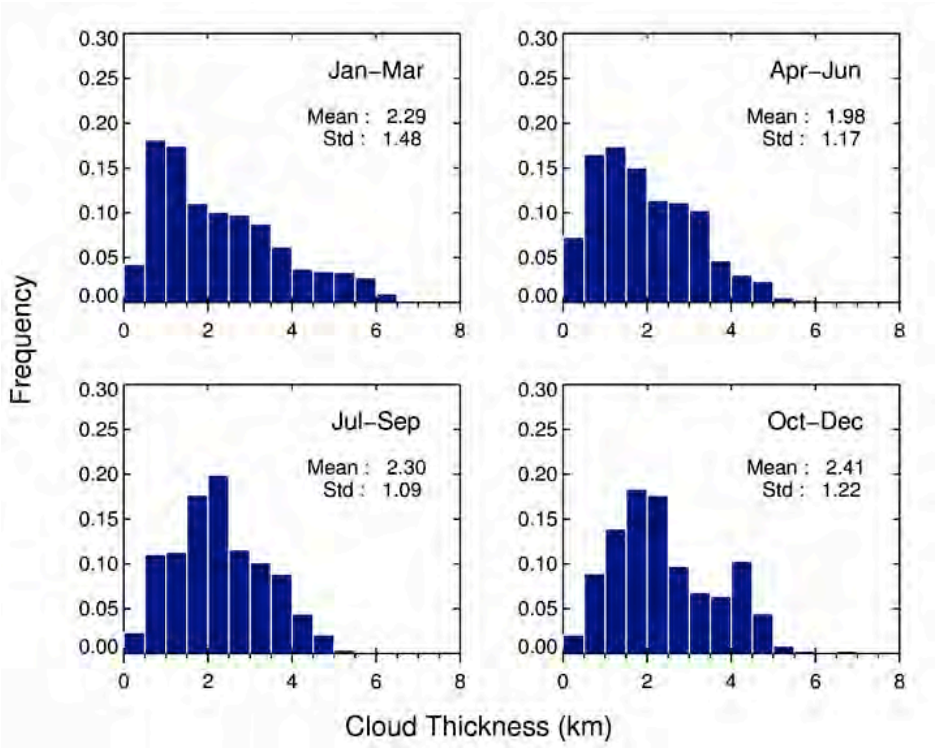

Figure 2.11: Seasonal frequencies of cloud thickness (0.5 km bins) for cirrus clouds over AFARS.

The seasonal distribution of cirrus cloud geometrical thickness is shown in Figure 2.11. The data shows a wider distribution (high standard–deviation) with peak occurrences of thinner cirrus clouds during winter. The long tail of the winter distribution extending to 6 km, represents the gradually thickening of cirrus clouds caused by synoptic activity over the region. Average seasonal cirrus thickness is lowest (1.98 km) in spring, and highest (2.41 km) in fall. The peak occurrence of cirrus cloud thickness gradually shifts to thicker clouds from winter to summer, which can be noticed from the high occurrences of 2 km cirrus thickness during summer. The thinner cirrus clouds are observed during the months (noticeably in June) where the wind direction is nearly southerly indicating orographic formation of cirrus. Thicker cirrus clouds with narrow distribution found in summer can be explained by convective detrainments (thunderstorm activity) that often trigger cirrus cloud formation through their anvil tops. These observations are in consistent with *Sassen and Comstock* [2001], which showed that

synoptically generated cirrus clouds over a midlatitude site have high average cloud thickness than those cirrus clouds generated by anvils or with the influence of orography.

(b) Mid-level ice clouds

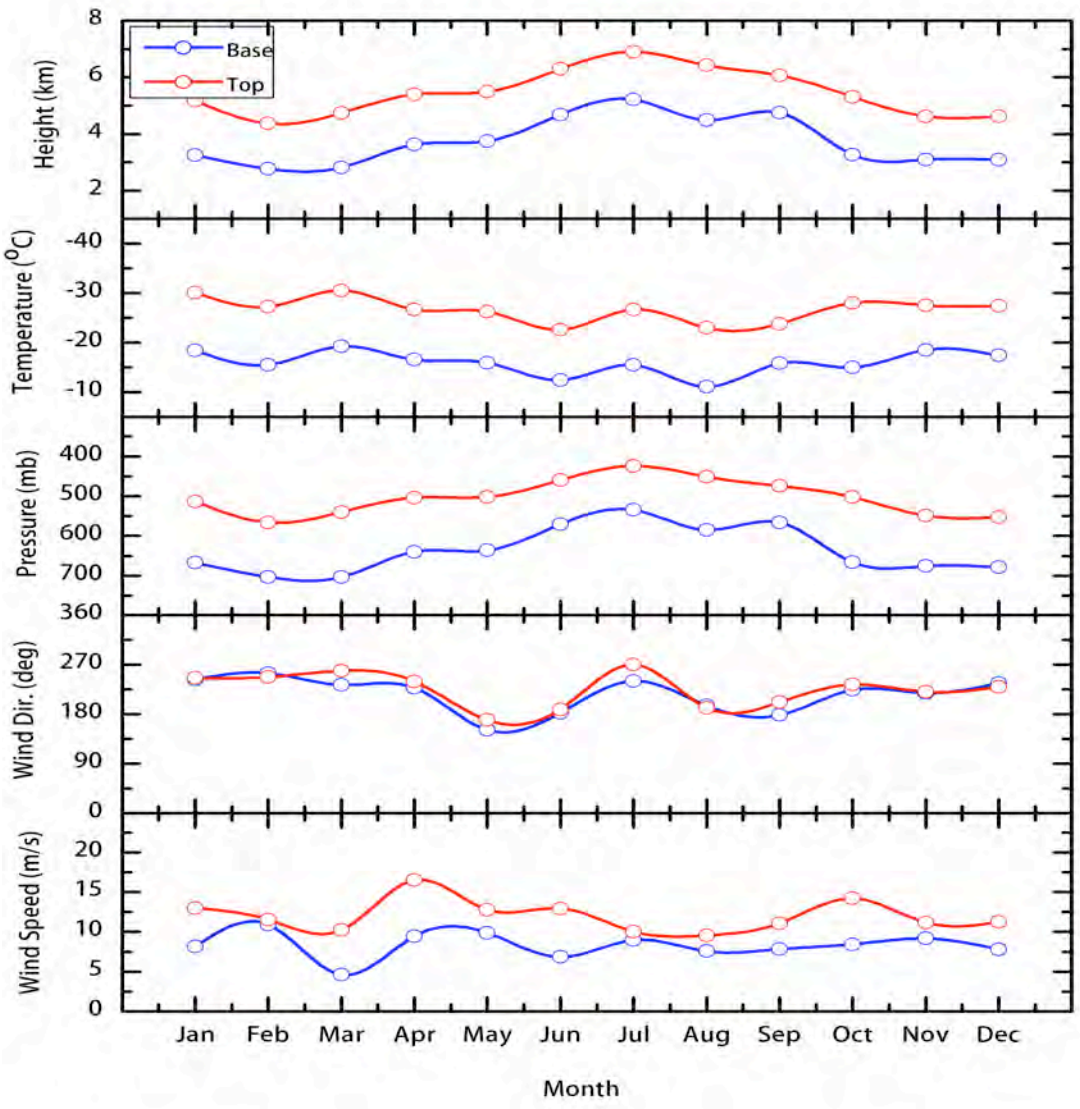

Figure 2.12: Monthly climatological properties of mid-level ice clouds over the AFARS site.

The monthly and seasonal climatological macrophyiscal properties for our mid-level ice clouds are examined here as follows. The monthly mid-level ice cloud top/base altitude (Figure 2.12) maxima occur during summer, and minima occur during winter. This behavior is similar to the trend followed by upper level (cirrus) clouds and in general reflects the annual cycle of meteorological conditions present over the site. It is interesting to observe the variety of wind speeds and directions that cause the local mid-level ice clouds. In contrast to the upper level winds that cause cirrus clouds, the wind direction shows a marked departure from zonal flow to strong southerly flow in summer. The mid-tropospheric winds that cause mid-level ice clouds show such departures during the spring – summer and summer – fall, transition periods. Overall the average monthly wind direction ranges from south-westerly (SW) to westerly (W). Average wind speeds show much variation throughout the year attaining peak winds reaching up to 15 – 20 m/s during spring.

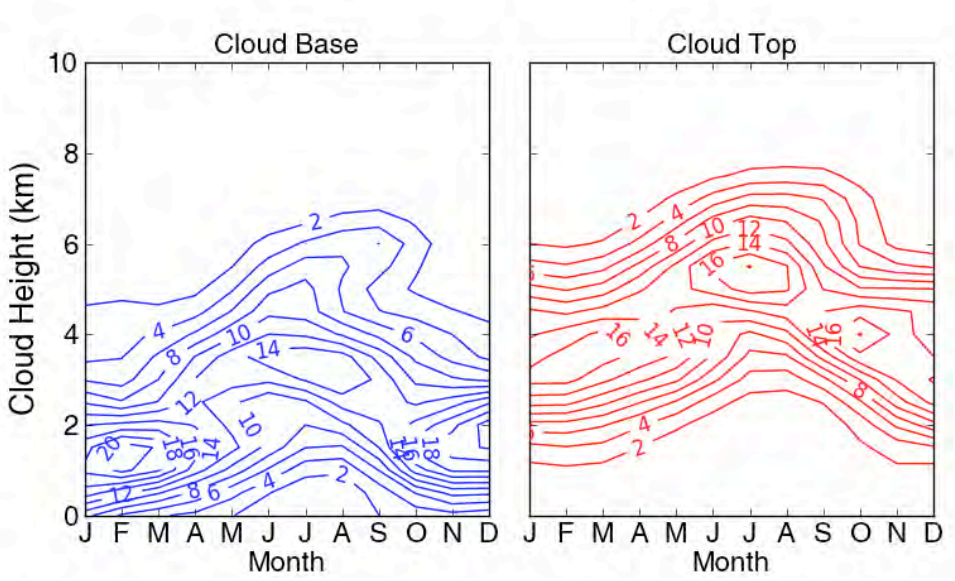

Figure 2.13: Monthly mid-level ice cloud frequencies (in percent) at AFARS binned for 0.5 km height intervals.

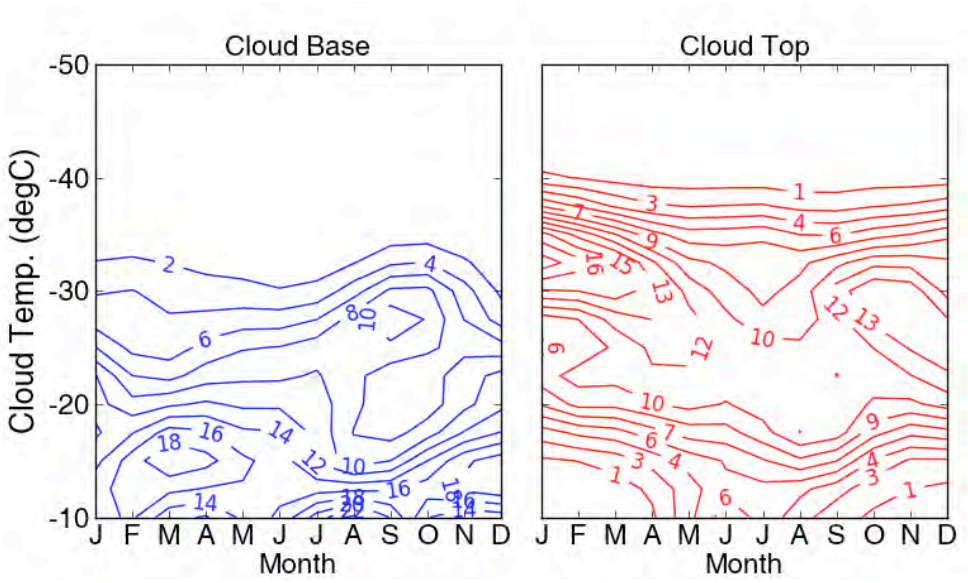

Figure 2.14: Monthly mid-level ice cloud frequencies (in percent) at AFARS binned for 2.5^{o} C temperature intervals.

The monthly occurrence of mid-level ice clouds along the altitude (temperature) is shown in Figure 2.13 (Figure 2.14). Mid-level ice clouds are found more commonly in the lower levels of the troposphere, near 2 km, during winter. Most mid-level ice cloud top temperatures range from –33^{o} C extend to higher temperatures. Especially during spring, where relatively high occurrences of mid-level ice clouds are observed at warm temperatures from –10^{o} C to –20^{o} C, these clouds can be explained through the depositional growth of ice particles on the often occurring diffuse aerosols layers over the station. Long-range transport of aerosols such as dust storms from Asia, sporadic episodes of forest fire smoke from northern China and eastern Russia are commonly observed over the AFARS site during spring. Several studies like *Sassen* [2005], *Sassen and Khvorostyanov* [2008], and *Atkinson et al.* [2013] have documented several noticeable episodes of such ice cloud formation at mid-levels of the troposphere over the AFARS site.

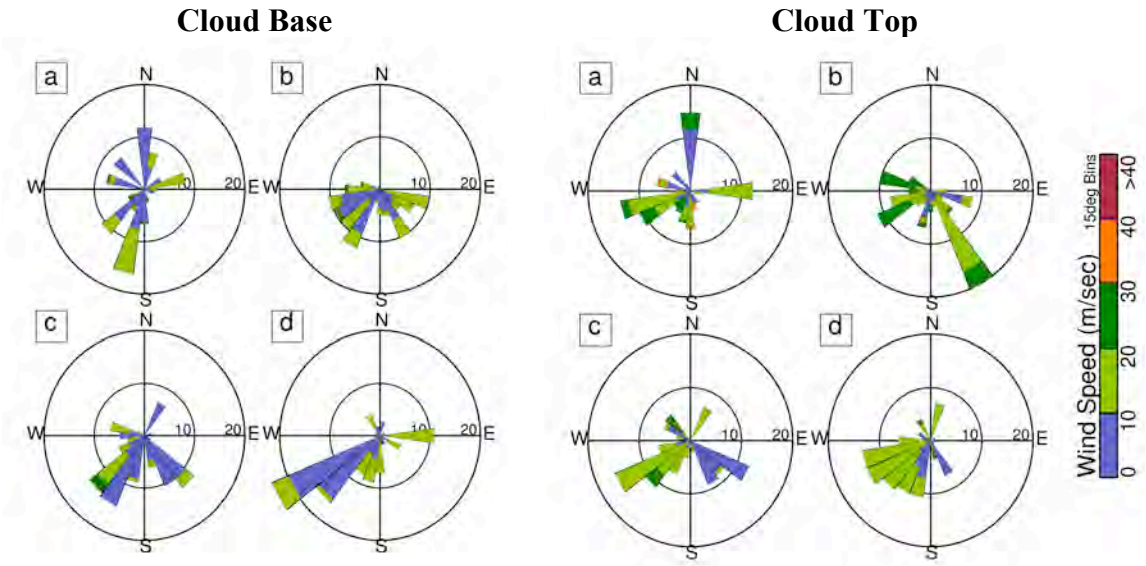

Figure 2.15: Seasonal frequencies of wind speed-direction for AFARS mid-level ice clouds. (a) Winter, (b) Spring, (c) Summer and (d) Fall.

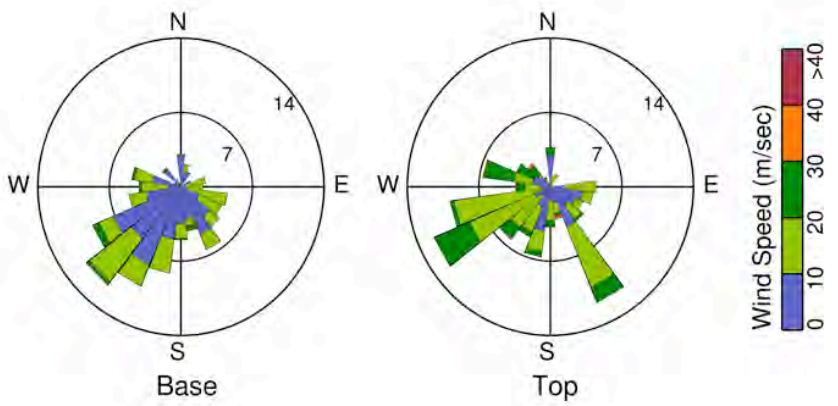

Figure 2.16: Total frequencies (in percent) of wind for AFARS mid-level ice clouds.

The variability of wind speed and direction at mid-level ice cloud altitudes are shown in the Figures 2.15 and 2.16. Seasonal and annual macrophysical properties of mid-level ice clouds are given in Table 2.5. The wind speeds range from 0 – 20 m/s and occasionally exceed 20 m/s near mid-level ice cloud top altitudes. The overall average directional wind forming mid-level ice clouds originated from south-westerly (SW). In contrast to the winds causing cirrus clouds, there are periods of wind flow from the southeast that are associated with up to 10% of the total mid-level ice clouds.

Table 2.5: Seasonal and annual mean of mid-level ice clouds for ~8 years over AFARS

	Jan – Mar	Apr – Jun	Jul – Sep	Oct – Dec	Annual
Cloud base					
Height (km)	2.87	3.78	4.76	3.15	3.68
Pressure (hPa)	696.8	630.92	565.49	672.36	641.28
Temperature (^{o}C)	–19.05	–15.86	–13.65	–16.94	–16.41
Wind direction (^{o})	232.05	198.91	199.93	211.53	203.54
Wind speed (m/sec)	7.5	9.3	8.0	9.5	8.5
Cloud top					
Height (km)	4.76	5.53	6.46	4.89	5.42
Pressure (hPa)	537.87	498.09	449.62	531.7	504.07
Temperature (^{o}C)	–30.46	–26.10	–24.27	–27.72	–27.08
Wind direction (^{o})	242.06	196.98	207.23	229.97	214.7
Wind speed (m/sec)	11.7	14.7	10.0	11.0	12.6
Cloud Thickness					
Layer envelope (km)	1.88	1.74	1.69	1.73	1.76

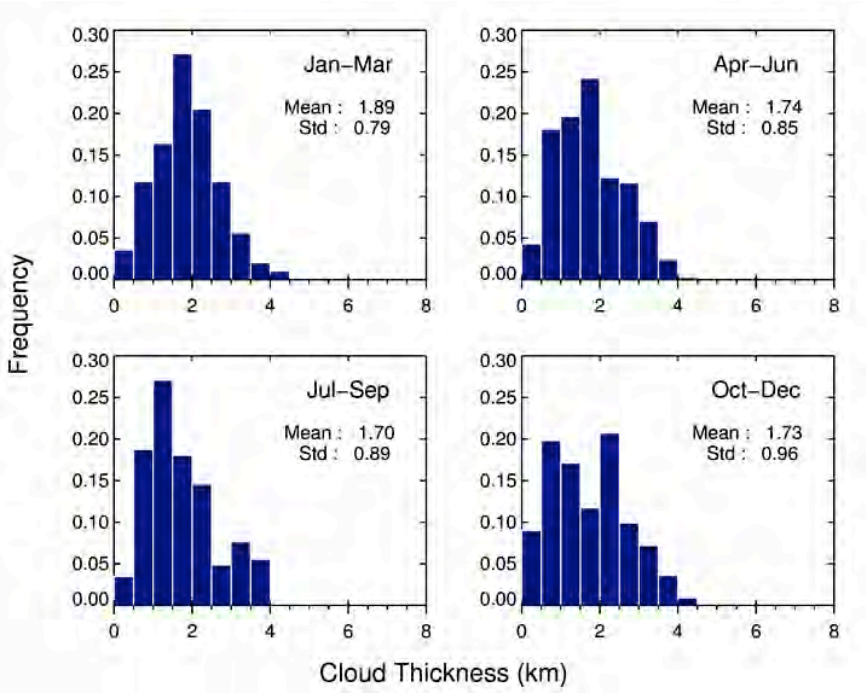

Figure 2.17: Seasonal frequencies of cloud thickness (0.5 km bins) for AFARS mid-level ice clouds.

The seasonal distribution of mid-level ice cloud geometrical thickness is shown in Figure 2.17. For all the seasons the cloud thickness are less than 4.5 km. The most common thicknesses are 1.75 km in winter and spring, and 1.25 km in summer. In fall the cloud thickness shows a bi-modal distribution with peaks at both 0.75 and 2.25 km. The average seasonal mid-level ice cloud thickness is lowest (1.7 km) in summer and highest (1.9 km) in winter. As expected, the mid-level ice clouds are thinner than cirrus clouds. Recall that the mid-level ice clouds presented here are those found at mid-levels in the troposphere and are transparent to lidar pulses.

2.5.2 Characteristics of ice clouds

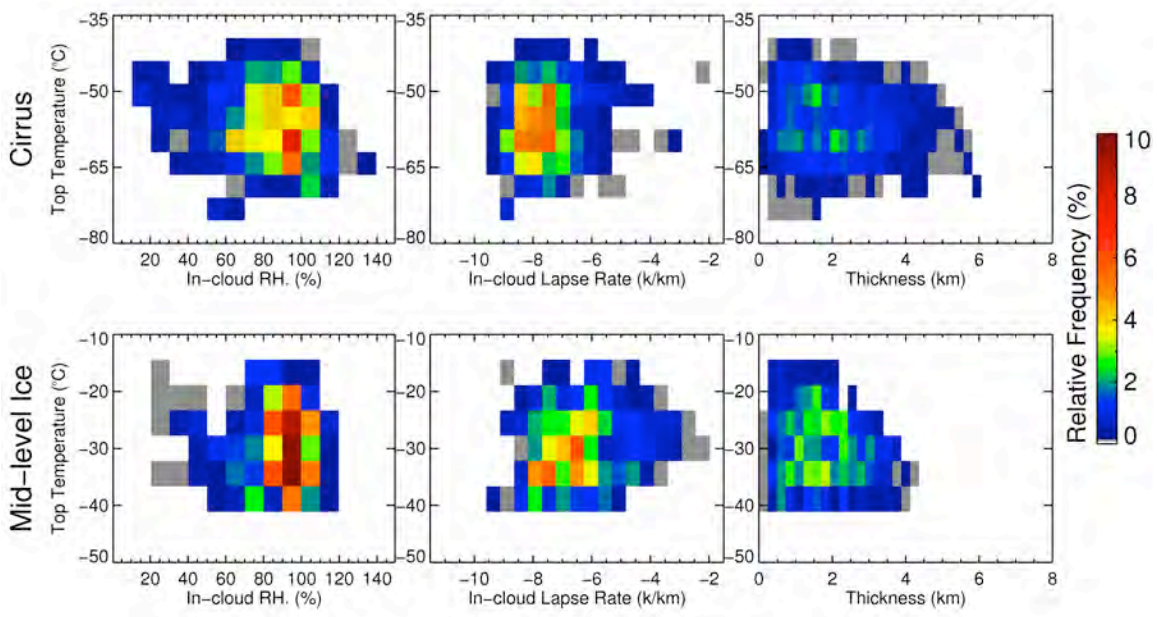

Figure 2.18: Thermodynamical characteristics derived for cirrus and mid-level ice clouds.

In order to understand the thermodynamical characteristics of the retrieved transparent ice clouds, we examine the atmospheric RH_{ice} and stability (Figure 2.18) of the cloud layer. Relative humidity with respect to ice is computed from the humidity with respect to water and temperature values acquired from local sounding data using the

formulation of *Murphy and Koop* [2005]. The average of all bins inside the cloud layer is determined and denoted as In-cloud RH_{ice}. Further, a temperature profile interpolated to the resolution of the lidar bins is used to calculate the lapse rate inside the cloud layer, which is indicative of the atmospheric stability in the cloud.

In the case of cirrus clouds, 79% of the derived In-cloud humidities are sub-saturated with respect to ice, while 21% are supersaturated. For mid-level ice clouds 81% are sub-saturated and 19% are supersaturated with respect to ice. The observations are not consistent with the field campaign measurements and simulations of RH_{ice} in cirrus clouds that show high supersaturation values [*Jensen et al.*, 2001; *Ovarlez et al.*, 2002; *Haag et al.*, 2003; *Strom et al.*, 2003]. This finding could be possibly due to the envelope method used here for the retrieval of cloud boundaries, since sub-saturated In-cloud RH_{ice} would cause rapid sublimation of cloud water. But the AFARS data collection records with 2 – 3 hrs time periods suggest that the local cirrus clouds are persistent. However owing to the uncertainties from radiosonde measurements in upper levels of the troposphere, our observations are consistent with the studies of *Comstock et al.* [2004] and *Kay et al.* [2007], which reported similar percentages of In-cloud humidities sub-saturated with respect to ice using Raman lidar measurements over midlatitude sites. Our derived In-cloud lapse rates indicate that most of the clouds (cirrus: 70%, mid-level ice: 59%) are stable with respect to the pseudo-adiabatic lapse rate for ice. Our observations also show fewer cloud layers are unstable (cirrus: 30%, mid-level ice: 41%). This behavior could be due to mixing of cloud layers and air, which has also reflected in the In-cloud humidities. Recall, that our algorithm for the retrieval of cloud properties follows an envelope method, which often merges several thin cloud layers with spacing less than 500 m between the multi-layered cloud boundaries.

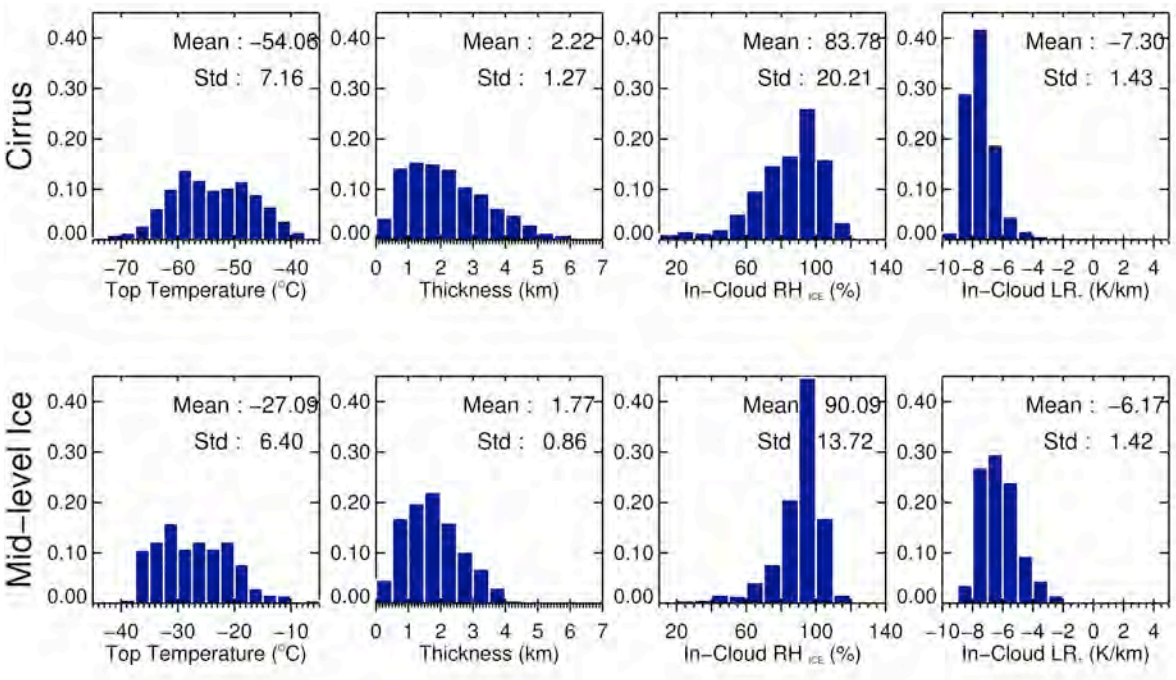

Figure 2.19: Probability densities for cirrus and mid-level ice: cloud top temperatures, thickness, and In-cloud humidities with respect to ice and In-cloud lapse rates.

The probability density functions (PDFs) of cloud top temperature, cloud thickness, In-cloud humidities and In-cloud lapse rates for cirrus and mid-level ice cloud categories are shown in Figure 2.19. Here the cirrus cloud top temperature distribution appears to be bimodal with peaks around –50° C and –60° C, that represent two distinct groupings of cirrus clouds. The former temperature represents those cirrus clouds formed through anvil bits from cumulonimbus or through orographic uplift. The latter temperature represents those cirrus clouds formed in the vicinity of the tropopause, as a result of synoptic activity or from strong updrafts that inject supercooled liquid water from cumulonimbus clouds into region of much lower temperatures. The mean tropopause temperature over the AFARS site is found to be about –57° C from the radiosonde observations. It is also observed that there are only 1 – 2% of cirrus clouds warmer than –40° C. These may be due to long fall streaks extending from the cirrus base. Observations from our field notes confirm that the use of –38° C threshold to separate mid-level ice clouds has not excluded any visually identified cirrus clouds from the sample used here. This suggests that

homogeneous nucleation is the dominant mechanism for our local cirrus cloud formation, as also evident from the climatology of cirrus derived from other ground-based lidars [*Mace et al.*, 2001; *Sassen and Campbell*, 2001; *Comstock et al.*, 2004].

For mid-level ice cloud type ~40% of the clouds occur within the temperature range –30^o C to –38^o C and the remaining 60% of clouds are observed to form in the range of –30^o C to –10^o C. Our mid-level ice cloud temperature and thickness show two distinct groupings around –35^o C and –25^o C with increased cloud thickness (Figure 2.17). This distribution could possibly arise from the variety of cloud formation mechanisms. It should be remembered that these mid-level ice clouds include: thin altostratus formed in the transition phase from cirrostratus to altostratus before the cloud is dense enough to block the sun (or attenuate lidar pulses), ice clouds left behind in typical altocumulus clouds after the precipitation in the form of virga and ice clouds formed as a result of glaciated altocumulus through heterogeneous depositional nucleation process.

2.6 Summary

The data presented here reveal the climatological macrophysical properties of transparent ice clouds ($\tau < 3.0 – 4.0$) that form in the upper and mid-levels of the troposphere. A unique extensive high-resolution lidar dataset with visual observations of cloud types is used for this purpose. The average values of the local cirrus cloud properties from the ~8-yr data are as follows. For cirrus cloud base: 6.87 km height, 418 hPa pressure, –37.7^o C temperature, 13.9 m/s wind speed, and 223^o wind direction. For cirrus cloud top: 9.08 km height, 297 hPa pressure, –54.1^o C temperature, 18.9 m/s wind speed, and 225^o wind direction. The data further support the assessments from previous cirrus cloud climatologies [*Sassen and Campbell*, 2001; *Comstock et al.*, 2004] that, cirrus cloud macrophysical properties are seasonally dependent and generally follow the annual cycle of the tropopause over any region. Most cirrus cloud occurrence limited to cloud top temperatures below –40^o C indicates homogeneous nucleation of particles as the dominant mechanism for cirrus formation.

Transparent ice clouds with top temperatures greater than –38^{o} C is categorized as mid-level ice clouds. The average values of the local mid-level ice cloud properties from the ~8-yr data are as follows. For mid-level ice cloud base: 3.68 km height, 641 hPa pressure, –16.4^{o} C temperature, 8.5 m/s wind speed, and 203^{o} wind direction. For mid-level ice cloud top: 5.42 km height, 504 hPa pressure, –27.1^{o} C temperature, 12.6 m/s wind speed, and 215^{o} wind direction. Our sample of mid-level ice clouds includes: (i) transparent altostratus, (ii) remnants of altocumulus layer, (iii) ice cloud layers formed from depositional growth of ice particles without initial liquid phase, and (iv) orographic uplift of the airmass. The prevalence of these types of ice clouds over the Arctic region in view of their radiative implications has to be further explored.

Chapter 3

Ice clouds over Fairbanks: influence of weather patterns

In general, ice clouds forming in the upper troposphere are referred to as 'cirrus clouds' and are well-known as a product of a variety of meteorological processes (e.g., frontal systems, jet streams, mountain waves, and deep convection, etc.) [*Stone*, 1957; *Starr and Wylie*, 1990; *Sassen and Campbell*, 2001], whereas clouds formed in the mid-troposphere are most commonly formed by uplift of air masses along frontal systems. Thus, it is essential to understand the link between the weather patterns and these cloud-type occurrences, which are also strongly influenced by the topography of the region. This chapter starts with a discussion of previous studies relating cirrus clouds and prevailing weather patterns, followed by a general overview of synoptic features observed over the Arctic region. Later, the methodology used to understand the observed weather patterns for such types of cloud formation over the AFARS site is presented. In this chapter, we obtain the typical synoptic conditions favorable for local ice cloud formation.

3.1 Why are cirrus cloud occurrences linked to weather patterns ?

Before the satellite era, reports from weather forecasters usually stated cirrus as benign cloud forms that were used as an aid in predicting the onset of bad weather [*Wylie*, 2002]. *Stone* [1957] was the first to make an extensive analysis from aircraft data and surface observations to augment cirrus cloud occurrence from weather patterns. His work also points out the most likely location for cirrus on the northward flowing side of Rossby wave troughs from the trough axis to the ridge. *Conover* [1960] identified that

most cirrus bands occur in southwesterly flows on the warmer side adjacent to the jet stream core. *Reuss* [1967] reported that the occurrence of cirrus bands along the frontal zone is located just above the layers of strong vertical wind shear. Later, *Menzel et al.* [1992] provided statistical probabilities of cirrus occurrence related to wind patterns and confirmed that most cirrus occurs south of the jet core with the winds accelerating. Thereafter the reported global distribution of cloud type occurrences evolved as more extensive satellite measurements became available [*Warren et al.*, 1988; *Wylie et al.*, 1994; *Jin et al.*, 1996; *Randall et al.*, 1996; *Wang et al.*, 1996; *Wylie and Menzel*, 1999]. This generation of studies revealed that cirrus clouds occur most frequently over the Inter-Tropical Convergence Zone (ITCZ), mid-latitude storm belts (30^o to 50^o latitude), and regions where enhanced topography causes uplift of large air masses. Several ground-based studies [*Sassen and Cho*, 1992; *Sassen and Campbell*, 2001] and field campaigns [*Starr and Wylie*, 1990] further augmented the concept that cirrus properties vary significantly according to their geographical locations and prevailing upper-level disturbances.

In general, cirrus clouds form in the upper levels of the troposphere where the ambient humidity is very low. The moisture required for cloud formation is supplied by atmospheric processes and is eventually removed through sedimentation of ice crystals in the form of fall streaks. Usually, along the upper-frontal zones or any large-scale disturbance that cause substantial instability of the air mass, considerable quantities of moist air will be advected to reach the upper levels supporting cirrus development. *Soden and Schroeder* [2000] showed that the main source of upper tropospheric water vapor in tropical regions is by convection, whereas for mid-latitudes it is mostly through frontal systems. Also ice particles formed in cumulonimbus clouds due to strong updraft velocities can easily reach the upper levels of the troposphere and can inject water vapor or ice particles through wind shear in favor of cirrus formation and maintenance [*Richman*, 1981]. Thus, in view of the cirrus formation mechanisms (described in

Chapter 1) it is important to understand the influence of prevailing weather and the regional topography on the cirrus cloud properties.

3.2 Synoptic features over the Arctic region

Researchers commonly use several definitions of the Arctic region depending on their purpose. The most widely used definition include (i) the region above the *Arctic Circle* (66.32^{o} N) which marks the latitudes above which the sun does not set on the summer solstice and does not rise on the winter solstice, (ii) the region north of *Arctic tree line,* which serves as the landscape boundary between the tundra and boreal forests, (iii) the region of higher latitudes where the average daily summer temperature does not rise above 10^{o} C [*Gordon*, 2005]. For the present study, we consider the Arctic as the region northward of 60^{o} N latitude consistent with the classical delineation of the polar circulation cell.

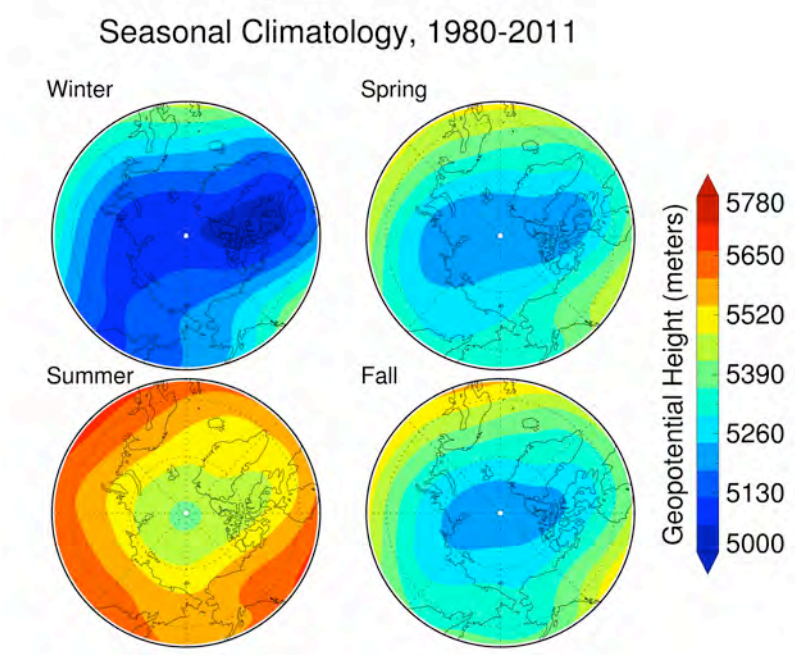

Figure 3.1: Seasonal climatological features at 500 hPa level over the Arctic region.

The MERRA (Modern Era Retrospective analysis for Research and Applications) monthly datasets provided by NASA (http://disc.sci.gsfc.nasa.gov/daacbin/DataHoldings.pl) are used here to understand the synoptic climatological features over the Arctic region. The primary feature of the atmospheric circulation over the Arctic region (Figure 3.1) is the *cyclone or polar vortex* found in the middle and upper troposphere. The polar vortex is a large-scale cyclone system surrounding the *polar high* and lies in the wake of the *polar front*. During winter, the extreme low temperatures over the region cause high meridional temperature gradient and position the vortex as deep troughs over eastern North America, eastern Asia and the western part of Eurasia. During summer as the temperatures over the surrounding land-mass rises, meridional temperature gradient relaxes, weakening this cyclonic system and makes the vortex more symmetric.

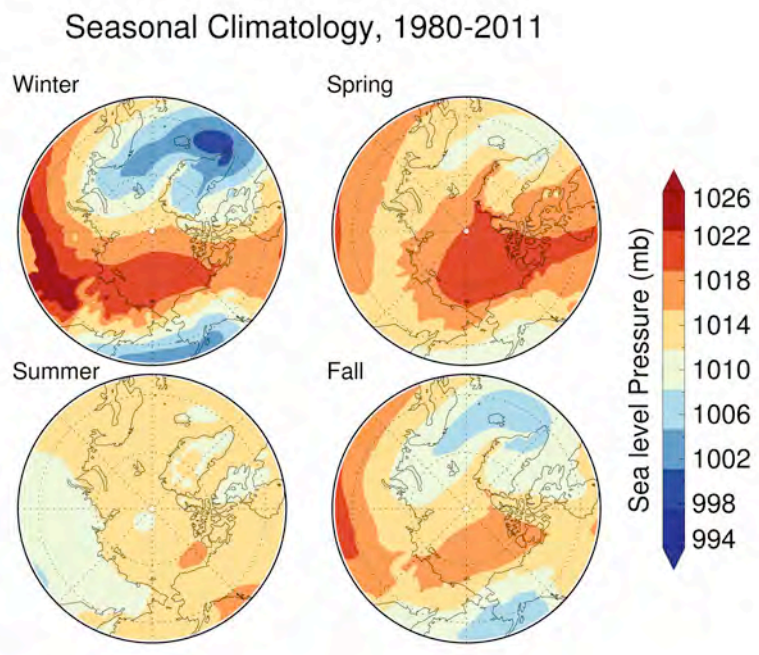

Figure 3.2: Seasonal climatological features at sea level over the Arctic region.

The dominant features observed at the sea level (Figure 3.2) over the Arctic region are the: (i) Aleutian low – located over the North Pacific near the Aleutian Islands, (ii) Icelandic low – located over the North Atlantic between Iceland and southern Greenland,

and (iii) Siberian high – located over east central Eurasia. The Aleutian low and Icelandic low are characterized as semi-permanent low-pressure systems maintained by low-level thermal effects of the relatively warm underlying oceans. These features, due to their positions downstream of the mid-tropospheric trough (Figure 3.1), cause strong Positive Vorticity Advection (PVA) and are thus potential zones for regional cyclogenesis. These two features are weaker during summer and more intense during winter. The other synoptically active regions, where cyclogenesis occurs frequently during winter are the Greenland Sea–North Atlantic, western Canada, and the Norwegian Sea–Baffin Bay areas. During summer, cyclogenesis peaks over the central Arctic Ocean as a result of migrating systems that form rapidly over the Eurasian continent and Arctic Ocean [*Serreze*, 1995; *Serreze and Barrett*, 2008]. While more cyclones are formed in summer with long duration, winter cyclones are more intense than those formed during summer [*Brummer et al.*, 2000; *Zhang et al.*, 2004]. The Siberian high is a very cold, shallow feature maintained by long-wave radiative cooling. The onset of summer almost replaces the Siberian high by relatively low-pressure system and is responsible for most precipitation across East Asia. During winter, the Siberian high is at its maximum strength and responsible for the drier conditions and low temperatures [*Serreze and Barry*, 2005]. Another surface high-pressure system that often exists over the Beaufort Sea (also referred to as the *Beaufort high*) plays an important role in the large-scale atmospheric circulation variability over the Arctic. During summer, the Beaufort high has strong influence on sea ice extent variability over the western Arctic [*Ogi and Wallace*, 2007].

Another synoptic feature over the Arctic region is the formation of small-scale intense cyclones, termed *Polar lows*. Polar lows are meso-scale cyclone systems with intense low-level wind speeds that form only over sea during winter when cold polar air moves over relatively warm water [*Rasmussen*, 1979; *Businger*, 1985]. These cyclones are known to appear along typical spatial patterns with maximum density over three regions: between Greenland and Iceland, south of Iceland and off the Norwegian coast

[*Bracegirdle and Gray*, 2008]. Recent studies also show that amplified changes in Arctic climate have relatively decreased the occurrence of polar low frequency over the North Atlantic [*Zahn and von Storch*, 2010].

With this background knowledge, we now examine the types of flow prevailing over Alaska for the AFARS observed cirrus cloud days.

3.3 Data and methodology

To understand the prevailing weather patterns favorable for local ice cloud formation in Fairbanks, we apply a statistical procedure to categorize the synoptic conditions of the AFARS observed on cirrus cloud days. The spatial extent surrounding the AFARS site is shown in Figure 3.3 extending from 180^{o} W to 118^{o} W and 44^{o} N to 84^{o} N is chosen for the analysis that should be sufficient to capture any synoptic-scale feature.

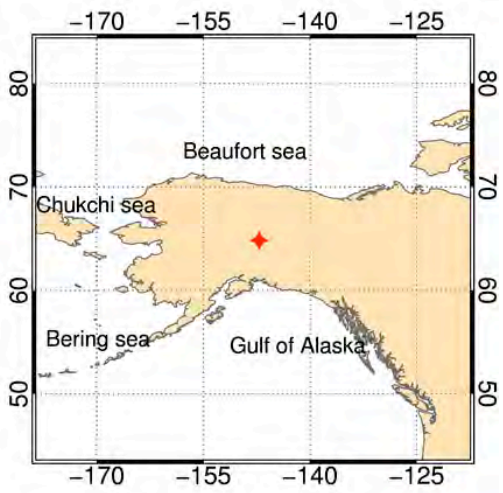

Figure 3.3: Spatial extent of the study area around the AFARS site (red mark).

The total number of independent days cirrus clouds observed over the Fairbanks region from February–2004 to June–2012 in accordance with the AFARS data collection philosophy are 443 (Figure 3.4), with an average of about 30 days for each month. The

MERRA daily datasets provided by NASA (http://disc.sci.gsfc.nasa.gov/daac-bin/DataHoldings.pl) are used in the present analysis. This reanalysis data is available from 1979 to present, gridded with 1.25^{o} x 1.25^{o} spatial and 3 hr temporal resolution, respectively on 42 pressure levels from 1000 to 0.1 hPa [*Lucchesi*, 2012]. For the current study, we used geopotential heights, wind speeds, wind directions at 500 hPa and 250 hPa pressure levels and also sea level pressure fields near the time of AFARS observations (~0000 UTC) for the cirrus cloud days.

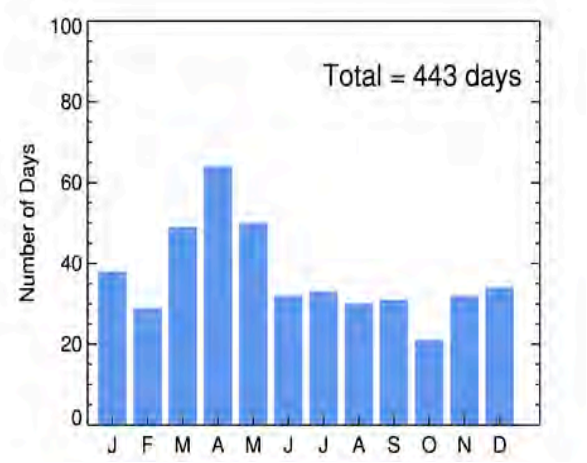

Figure 3.4: Monthly number of days cirrus clouds were observed over AFARS from 2004 – 2012.

Statistical techniques have been in use for categorizing weather patterns from the early 1970s [*Barry and Carleton*, 2001]. Since then, several synoptic climatological studies [*Christensen and Bryson*, 1966; *Craddock and Flintoff*, 1970; *Kruizinga*, 1979; *Richman*, 1981; *Crane and Barry*, 1988; *Davis and Kalkstein*, 1990; *Bonell and Sumner*, 1992; *Davis and Walker*, 1992; *Kalkstein et al.*, 1996] have developed and employed statistical procedures successfully to derive realistic weather patterns representative of a region or hemisphere. In general, all of these studies describe the synoptic patterns influence on weather process, and there are no comprehensive studies relating synoptic patterns to cloud formation. On the other hand, only field campaign measurements of clouds detail the synoptic conditions during their measurements. A recent study

[*Mulmenstadt et al.*, 2012] identifies prevailing meteorological regimes using long-term surface observations to study the cloud formation over an Atmospheric Radiation Measurement (ARM) site at Barrow, Alaska.

The use of statistical methods to categorize synoptic patterns is an apparent objective procedure requiring the analyst to make important choices suitable for his goal. For our purpose, we have followed a two-way cluster method similar to *Davis and Walker* [1992]. The data processing scheme used here can be detailed in five steps: (i) normalize the data, (ii) apply principal component analysis (PCA) procedure to the normalized data, (iii) apply hierarchical clustering method using average linkage method to the unrotated component scores, (iv) choose optimum number of clusters and compute their centers as the mean scores of the clusters, (v) apply k-means clustering to the component scores using the derived cluster centers as input, producing the final cluster solution. Initially, the data is normalized for each grid point by making the mean value equal to zero and normalizing the occurrence equal to one for all cirrus days of study. In the second step, as the geopotential height fields are known to be collinear in nature, it is subjected to PCA to reduce the dataset to fewer components, which explains a significant amount of variance in it. The PCA method is applied here using the correlation matrix of the dataset as input, and twelve principal components were retained whose Eigen values are greater than or equal to one representing a cumulative variance of 95.93%. The third step of processing involves hierarchical clustering of the obtained unrotated component scores. Hierarchical clustering starts with individual members in the dataset as a cluster and keeps merging the clusters based to the chosen distance measure. Here, an average linkage method with *squared euclidean* distance measure is used. The optimum number of clusters is identified using both pseudo-F and pseudo-T^2 indexes [*Calinski and Harabasz*, 1974; *Davis*, 1988]. We find that the optimum number of clusters to be 20 clusters in the present study.

An average linkage procedure uses the similarity measure determined by the mean distance between pairs of all members weighted by the total number of members. Such a procedure is well known for its tendency to produce compact, spherical clusters and also clusters with a very small number of members [*Hawkins et al.*, 1982; *Kalkstein et al.*, 1987]. These small clusters formed are identified as typical outliers or conditions with unusual weather [*Kalkstein et al.*, 1987; *Davis*, 1991] and can be avoided in climatological studies by choosing only clusters with members more than a chosen *threshold* (e.g., 2%) of the sample size [*Davis and Walker*, 1992; *Sassen and Campbell*, 2001]. In other words, from the obtained clusters only those clusters that contain at least 2% of the observations will be considered. This choice reduced the 20 clusters derived from average linkage method to only 9 clusters. In the fourth step, mean component scores were calculated for each of these clusters. Finally, in the fifth step all of the extracted twelve component scores were subjected to the k-means procedure providing the calculated nine cluster centers as input: this helps in achieving smaller within-cluster variations than using average linkage method alone [*Milligan*, 1980]. The k-means (supervised) clustering uses randomly selected or user specified points as initial centers and iteratively groups all the observations nearer to its mean value [*MacQueen*, 1967]. With this, all of the cirrus cloud days used in the analysis are assigned a cluster identity (1 – 9).

3.4 Results and discussion

The mean of variables geopotential height, winds at 500 and 250 hPa pressure levels, and the sea level pressure are plotted in Figures 3.5 – 3.7 for each of the identified nine synoptic flow associated patterns. The monthly frequency of occurrence of these synoptic types as categorized for the cirrus days is shown in Figure 3.8.

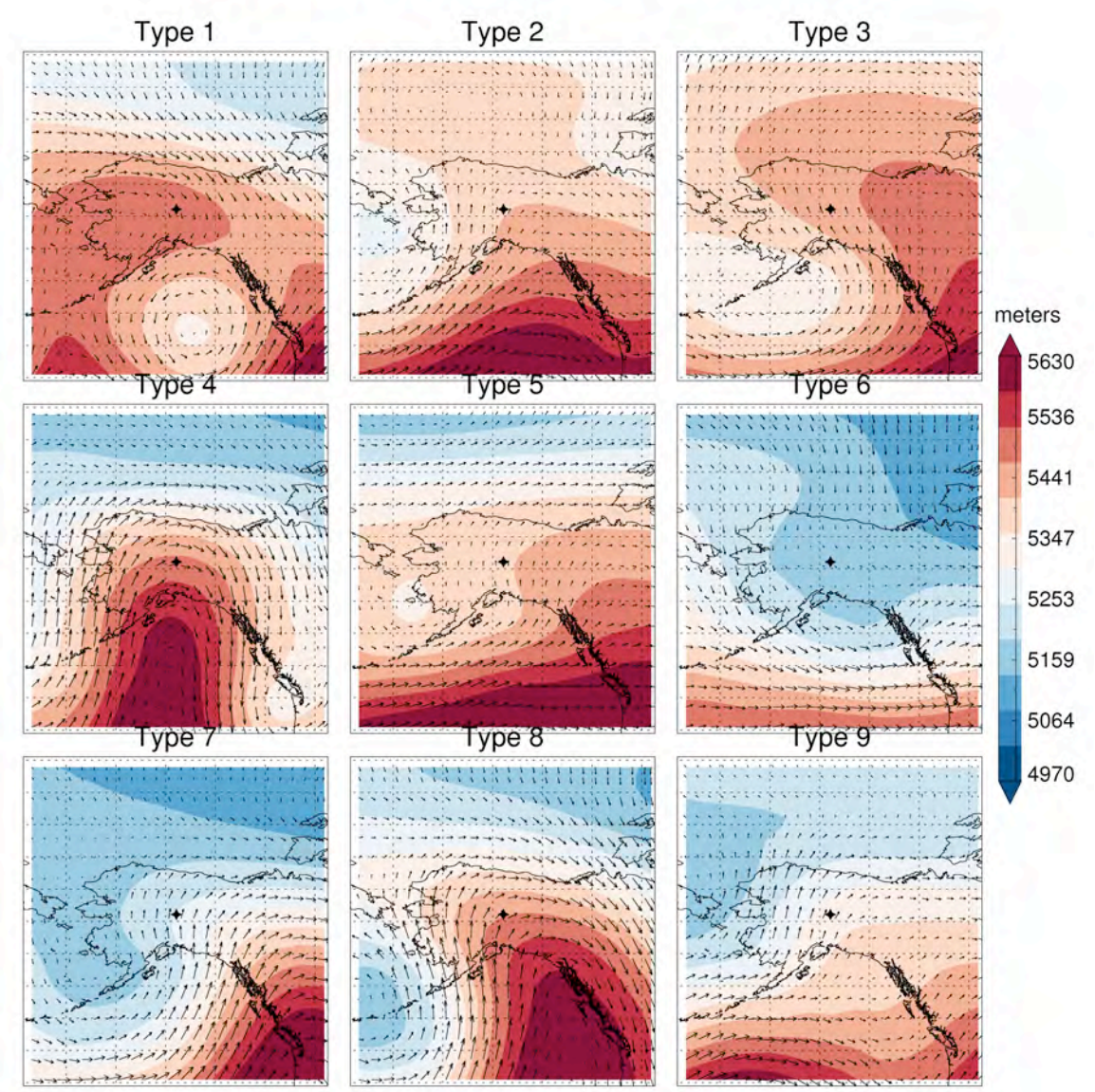

Figure 3.5: Average geopotential height and winds as observed at 500 hPa pressure level for each of nine synoptic pattern. The height contours are drawn at 60 m intervals and a long complete arrow (maximum length) represents 40 m/s of wind speed.

3.4.1 Description of the synoptic patterns

Type 1: This synoptic pattern shows a zonal flow of warm moist air to Interior Alaska regions represented by an elongated ridge from SW to interior, with a cut-off low observed over Gulf of Alaska from the surface up to higher levels of the troposphere. Surface conditions are found to be dominated by high pressures over the Interior

throughout the northern parts including the Beaufort high and a weak cyclonic system with mean sea level pressure (MSLP ~1003 hPa) over the Gulf of Alaska. This type of flow is favored during the transition period of the seasons (i.e., March, May and August) and is observed for ~8% of cirrus cloudy days.

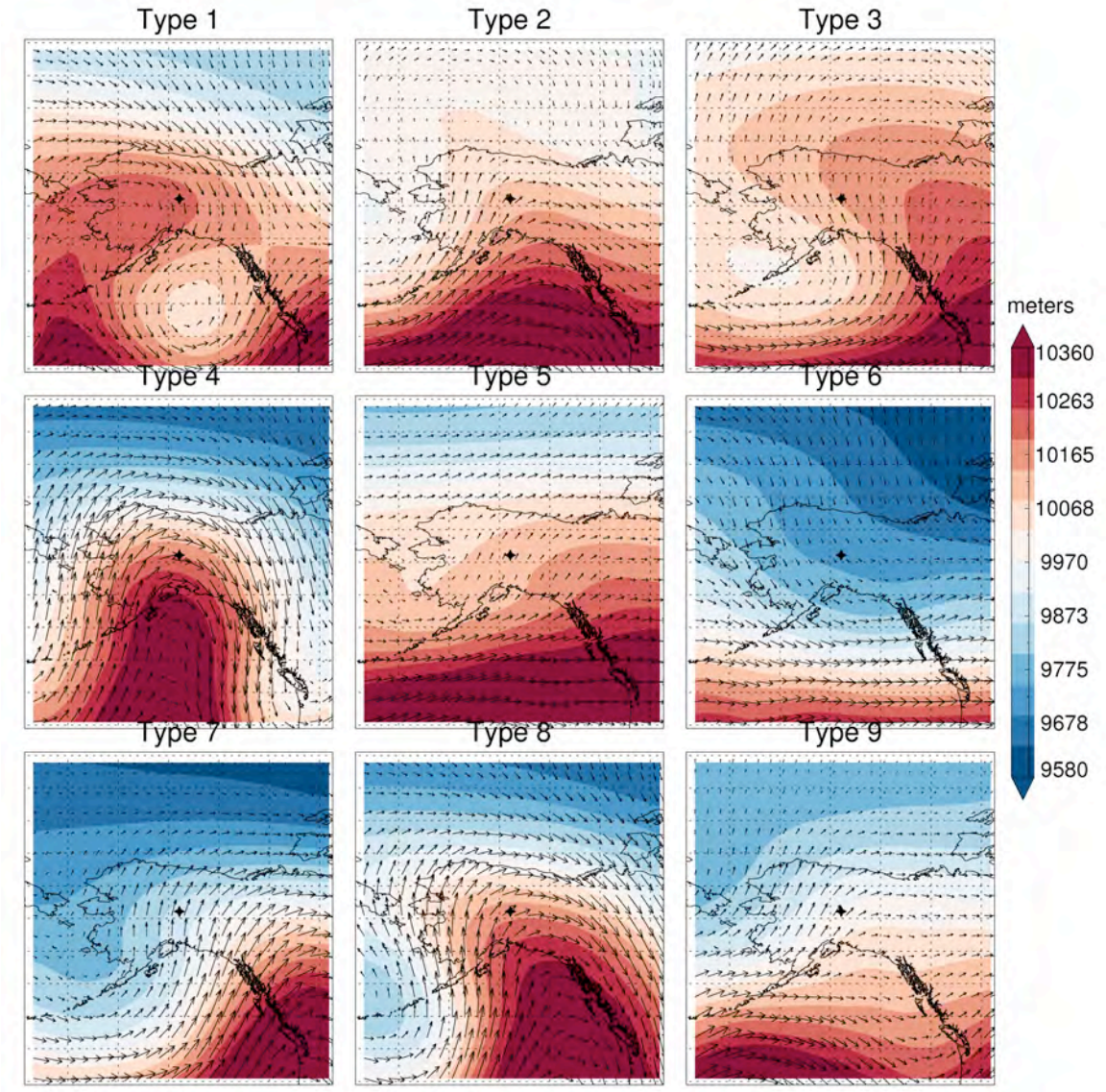

Figure 3.6: Average geopotential height and winds as observed at 250 hPa pressure level for each of nine synoptic pattern. The height contours are drawn at 60 m intervals and a long complete arrow (maximum length) represents 40 m/s of wind speed.

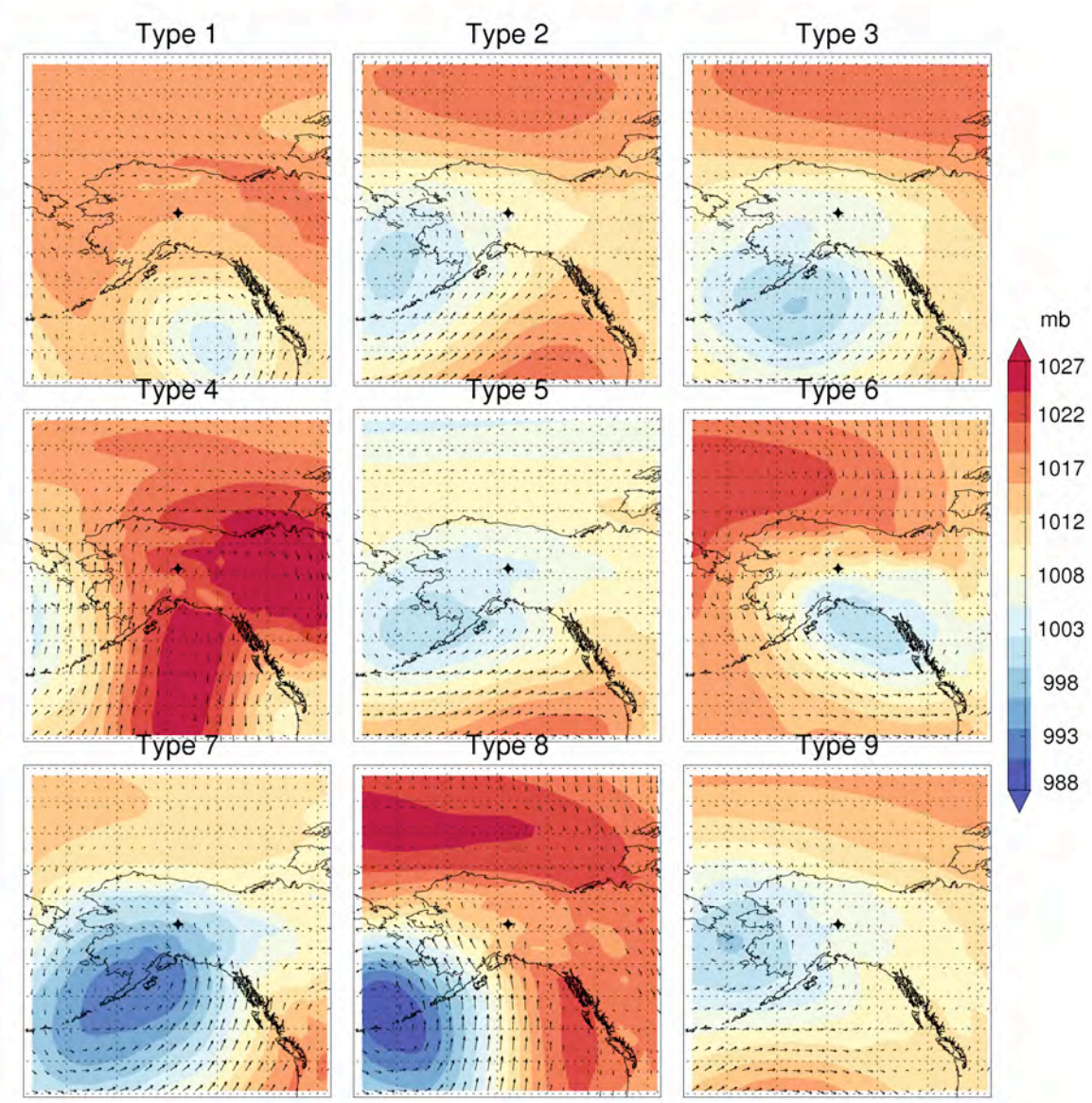

Figure 3.7: Average sea level pressure contours shown here are drawn for 3 hPa intervals and winds are as observed from 850 hPa pressure level for each of nine synoptic pattern. Long complete arrow (maximum length) represents 40 m/s of wind speed.

Type 2: This synoptic pattern shows a southwesterly flow of warm moist air to the Interior. It is represented by a ridge extending from the south as observed in the middle to higher levels, and supported by a moderate surface cyclonic system (MSLP ~1000 hPa) over the Bering Sea. Surface conditions indicate a strong Beaufort high (MSLP ~1025

hPa) and an anticyclonic flow in the Pacific towards the continental States. This type of flow is observed almost throughout the year (~18% of cirrus cloudy days) and occurs most commonly in the spring and summer months.

Type 3: This synoptic pattern shows a south-southeasterly flow of relatively warm and dry air. The intensified pacific-trough (negatively-tilted) and extended ridge to the Interior represents a matured stage of the conditions observed in the Type-2 pattern. Here the surface conditions are characterized by moderate pressure over the Interior along with an intense High over the Beaufort Sea (MSLP ~1025 hPa) and a strong cyclonic system (MSLP ~998 hPa) over the Aleutian Islands extending to the Gulf of Alaska, displacing the ridge much to the south-east of Alaska towards the continental States. This type of flow most commonly occurs in the spring and summer months and is observed for ~14% of cirrus cloudy days.

Type 4: This synoptic pattern exhibits a central deep-ridge towards the Interior extending from the south of Alaska. South-southwesterly flow with strong winds up to 26 and 45 m/s are observed at the 500 hPa and 250 hPa pressure levels, respectively, due to the placement of polar jet stream almost over the entire Alaska mainland. Surface conditions are characterized by high pressures ~1027 hPa over the Interior extended from the north-east including the eastern part of the Canadian province and towards south over the entire Gulf of Alaska. This flow type is observed for ~6% of cirrus cloudy days and occurs only during the winter and spring seasons with no occurrence during the summer/early fall periods.

Type 5: This synoptic pattern shows a southerly and southwesterly flow to the Interior from 500 hPa and 250 hPa pressure levels, respectively, indicating the presence of some wind shear over the region. Moderate to high wind speeds up to 25 m/s persist in the mid and upper levels as the extending ridge from eastern parts intrudes, veering winds to the Interior. Surface conditions are characterized by the complete dissipation of the Beaufort

high and a moderate cyclonic system (MSLP ~1000 hPa) over the Alaska Peninsula extending towards most of the southwestern parts of Alaska. This flow type is observed for ~13% of cirrus cloudy days and has pronounced occurrence in the mid-summer and fall seasons.

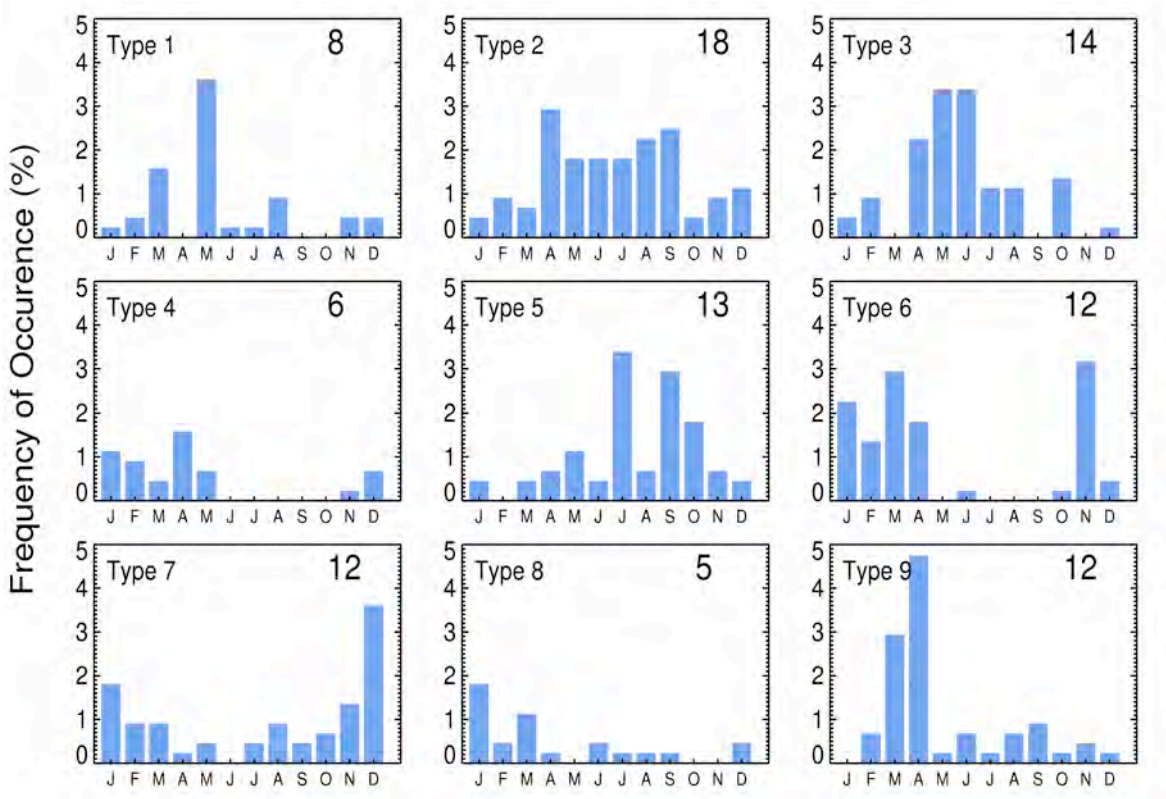

Figure 3.8: Percentage monthly frequency of occurrences for all synoptic patterns. The number shown in each figure is total frequency (in percent) for that type of flow.

Type 6: This synoptic pattern shows a northerly flow of dry cold air to the Interior represented by a trough extending from the northeast. A moderate surface cyclonic system (MSLP ~1000 hPa) is observed along the southeastern parts into the Gulf of Alaska and surface high pressures (MSLP ~1027 hPa) extending to the Interior from the north-northwestern parts including the Beaufort high. This flow type is observed for ~12% of cirrus cloudy days and is dominant in the winter and also shows its occurrence during the onset of winter and spring seasons.

Type 7: This synoptic pattern shows a southerly flow to the Interior represented by a trough over the Pacific and ridge extending from eastern parts of Alaska. Surface conditions indicate a strong cyclonic system (MSLP ~990 hPa) over the Aleutian Islands to the Interior and low to moderate pressures accumulating over the Beaufort Sea. This flow type occurs almost throughout the year (~12% of cirrus cloudy days) and is more pronounced during the winter.

Type 8: This synoptic pattern shows a southerly flow to the Interior regions represented by an intense trough over the Pacific and a negatively tilted ridge extending towards the northeast. Surface conditions features intense cyclonic system (MSLP ~985 hPa) over the Aleutian Islands with moderate to high pressures over the interior parts extending through out, and indicates a matured stage of synoptic conditions observed in Type-7 flow pattern. This flow type is observed for ~5% of cirrus cloudy days and mostly favored in the winter and early spring periods.

Type 9: This synoptic pattern shows a southwesterly flow to the Interior parts of Alaska represented by a trough along the northwestern region. Surface conditions are characterized by a moderate cyclonic system (MSLP ~1000 hPa) over the Bering Sea extending towards the interior with low-moderate pressures over the Pacific and Beaufort Sea. This flow pattern is observed for ~12% of cirrus cloudy days and has much pronounced occurrence during the spring season.

3.4.2 Monthly variations of derived patterns

To understand how these synoptic patterns are related to each other or evolve, we derived simple correlations between their monthly frequencies of occurrences (shown in Table 3.1) that are statistically significant at the 95% significance level, ($\alpha = 0.05$) of the total cirrus cloudy days used in the analysis.

These can be interpreted as, for example: Type 9 and Type 4 flows exhibit highest positive correlation and has dominant occurrence in spring, i.e., most of the times when Type 9 pattern occurs the probable chances of occurring Type 4 pattern is high. The patterns Type 3 show high correlation with Type 1 and Type 2 and are observed dominantly during spring. The pattern Type 5 shows low (0.31) but statistically significant correlation with Type 2 and has dominant occurrence during the summer and fall periods. From Table 3.1 and Figure 3.8, it is now apparent that even within a month, a variety of synoptic patterns occur over the region as evident from all statistically significant correlations that are positive.

Table 3.1: Pearson's correlation coefficients derived between monthly frequencies for each synoptic type. *Italicized values* are statistically significant at 0.05 significance level from Student's T-test

	Type 1	Type 2	Type 3	Type 4	Type 5	Type 6	Type 7	Type 8	Type 9
Type 1	1.00								
Type 2	–0.01	1.00							
Type 3	*0.38*	*0.40*	1.00						
Type 4	0.07	0.04	0.09	1.00					
Type 5	–0.16	*0.31*	–0.09	–0.51	1.00				
Type 6	–0.07	–0.43	–0.44	*0.44*	–0.50	1.00			
Type 7	–0.08	–0.45	–0.54	*0.21*	–0.33	*0.18*	1.00		
Type 8	–0.09	–0.45	–0.32	*0.38*	–0.35	*0.47*	*0.30*	1.00	
Type 9	–0.08	*0.43*	0.08	*0.51*	–0.20	*0.40*	–0.31	0.04	1.00

3.4.3 Seasonal variations of derived patterns

Further in view of the seasonality, the two most recurring patterns were derived as shown in Table 3.2. These two most recurring patterns represent about 40–50% of the cirrus days during winter, spring, fall and up to 64% of cirrus days during summer.

Table 3.2: Most frequently occurring synoptic conditions in the seasons

	Most recurring synoptic flow		*Combined Frequency (%)*	
	First	*Second*	*Total*	*Relative to seasons*
Winter	Type 6	Type 7	10.1	38.8
Spring	Type 3	Type 2	15.6	47.2
Summer	Type 5	Type 2	13.6	64.0
Fall	Type 7	Type 6	9.5	48.3

In general, the upper level synoptic flow pattern that influences weather over Alaska is the polar jet stream pattern found over the 300 – 250 hPa pressure level. The geographical location of Alaska positions the polar jet stream along the Arctic front, to its north in winter and well on its path or towards south in the summer. The presence of the Aleutian low and Beaufort high almost throughout the year; partly maintained by the action of the Arctic frontal zone and the downstream of mid/upper level tropospheric ridge at varying directions over/around the Alaska mainland are the primary controls of prevailing weather systems.

During winter, under normal conditions the air circulation is zonal to the north of Alaska along the Arctic front. Cold-dry air masses from the Arctic oceans often reach Interior through northerly or northwest flow. This synoptic condition (Type 6) under moderate to high surface pressure over the Interior brings most clear skies in winter. This pattern also prevails in transition periods (spring and fall). *Mock et al.* [1998] investigated the synoptic climatological patterns over Beringia (Eastern Siberia till Alaska) and described the occurrence of such synoptic flow in winter as common and very rare in summer. As the anticyclonic conditions prevail over the Interior regions, the mid-tropsopheric ridge is displaced to the southeastern parts of the Alaska that strengthens the Aleutian low favoring local cyclogenesis. This synoptic pattern (Type 7) occurrs in winter and fall months is consistent with *Serreze and Barry* [2005] and is responsible for

the stronger winds over the southeastern Alaska coast that advects warm, moist air from the North Pacific to the Interior regions. These two patterns (Type 6 and Type 7) are dominantly observed for 38% and 48% of cirrus days over AFARS during winter and fall seasons.

During transitional seasons the jet stream flow pattern often lies over the Alaska mainland while it moves north and south of it. This often causes marked departures of zonal flow to southerly towards the Interior region. This is clearly reflected in the upper level (for cirrus clouds, Figure 2.4) and mid-level ice cloud (Figure 2.11) climatologies. As the Pacific anticyclonic system moves to the north displacing the Aleutian low to the Bering Sea, a mid-tropospheric ridge is placed exactly over the Gulf of Alaska extending towards the mainland. This pattern (Type 2) causes warm air advection from pacific to the Interior through southwesterly flow. The increasing solar radiation to the continental states intensifies the North Pacific high-pressure system causing a negative tilt to the tropospheric ridge extending it to the northern parts of Alaska. This pattern (Type 5) causes strong warm air advection to the Interior through southerly flow, while the Aleutian low moves to its mean position. The patterns Type 2 and Type 5 dominantly observed for about 64% of cirrus days over AFARS in summer. As the Aleutian low further intensifies with the prevalent vorticity advection, it moves south-east in the Gulf of Alaska before it dissipates. This pattern (Type 3) advects warm and dry air mass to the Interior along the long trajectory over continental states. The patterns Type 2 and Type 3 dominantly observed for about 47% of cirrus days over AFARS in spring.

3.5 Summary

With the assertion that cirrus cloud formation is strongly coupled to regional upper level synoptic disturbances, it is required to understand the prevailing weather conditions during the observed cirrus cloudiness. To achieve this, a two-way clustering technique is applied to a reanalysis dataset and the prevailing synoptic conditions for cirrus cloudy days over the AFARS station are derived. Nine distinct synoptic patterns were identified

that provide apparent thermodynamic conditions for the observed cloudiness. These patterns are consistent with the climatological studies that include: zonal flow conditions, the placement of mid-tropospheric ridge around the Alaska mainland with south-westerly flow, and the placement of polar jet streams directly over the Interior Alaska causing meridional flow. The frequency of occurrence for the nine synoptic patterns ranges from 5 – 18%. The highest occurrence is observed for the Type 2, which advects warm moist air from the North Pacific to the Interior Alaska dominant during spring and summer seasons. It should be remembered that the persistence of these synoptic patterns varies greatly depending on the day-to-day weather variables. However, it is now apparent from our observations that cirrus cloudiness over AFARS is greatly influenced by the regional synoptic disturbance in upper levels of the troposphere.

Chapter 4

Ice clouds over Fairbanks: ground-based and satellite view

Although ground-based remote sensing techniques are providing consistently accurate information (as studied in Chapter 2), better comprehension of cloud processes can be obtained by monitoring cloud properties over large spatial scales. Space-borne measurements of clouds have proved to be an inevitable tool over the last few decades, while the validation of these measurements are still required to ensure the correct interpretation and to ignore unreliable data due to several possible contaminants. Many uncertainties in understanding cloud processes still remain as per the limitations of the technique used. Evolving data from recent active remote sensing satellites overcomes many limitations of the passive satellites and are providing unprecedented information about the vertical structure of cloud/aerosol properties over global scales. In this chapter, we introduce the CALIPSO and CloudSat instruments with their sensitivity to detect various atmospheric constituents. Next, we describe the view of ice clouds from both ground and space measurements and comparison of retrievals of clouds over the AFARS site is made. From this study, we obtain assessment of CALIPSO cloud retrievals.

4.1 *A–Train* constellation

This satellite constellation refers to a group of satellites that orbits in close proximity to each other allowing for synergy between different probe missions. The A–train also known as the *Afternoon-Train* is one such constellation, currently with six polar orbiting satellites (Table 4.1), one of each launched by French agency Centre National d'Etudes Spatiales (CNES), one launched by the Japan Aerospace Exploration Agency

(JAXA), and the remaining four by the U.S agency National Aeronautics and Space Administration (NASA).

Table 4.1: Purpose of different satellite missions in A-Train constellation*

Satellite	***Description***	***Launched by***
Aqua	Instruments on-board measures visible, infrared, microwave radiation. Observations are used for comprehensive studies on water-budget for the Earth system	NASA On May 4, 2002
Aura	Instruments on-board provides limb sounding and nadir imaging of the distribution of key atmospheric pollutants and greenhouse gases	NASA On July 15, 2004
PARASOL	Acquires polarized light measurements of clouds and aerosols in the earth's atmosphere	CNES On Dec 18, 2004
CALIPSO	Carries a space-borne polarization lidar with a infrared radiometer and observes the vertical distribution of cloud and aerosols	NASA, CNES On April 28, 2006
CloudSat	Carries a cloud profiling radar used for detailed study of clouds in the earth's atmosphere	NASA On April 28, 2006
GCOM-W1	Operates microwave scanning radiometer for measuring precipitation, water vapor, snow depth, sea water temperature and winds over the oceans	JAXA On May 18, 2012

* From http://atrain.nasa.gov

These six satellites fly in a 705–km sun-synchronous orbit above the Earth's surface with a velocity of about 7 km/s and crossing the equator at around afternoon (~1:30 pm) and midnight (~1:30 am). The A–train travels northward during the day half-orbit and southward during the night half-orbit and repeats the equivalent ground track every 16 days. The objective of such a constellation is to provide simultaneous observations of Earth's processes or constituents from several instruments with a time lag ranging from

few seconds to a few minutes (Figure 4.1), which would not be possible to acquire from ground-based or air-borne measurements for large spatial scales.

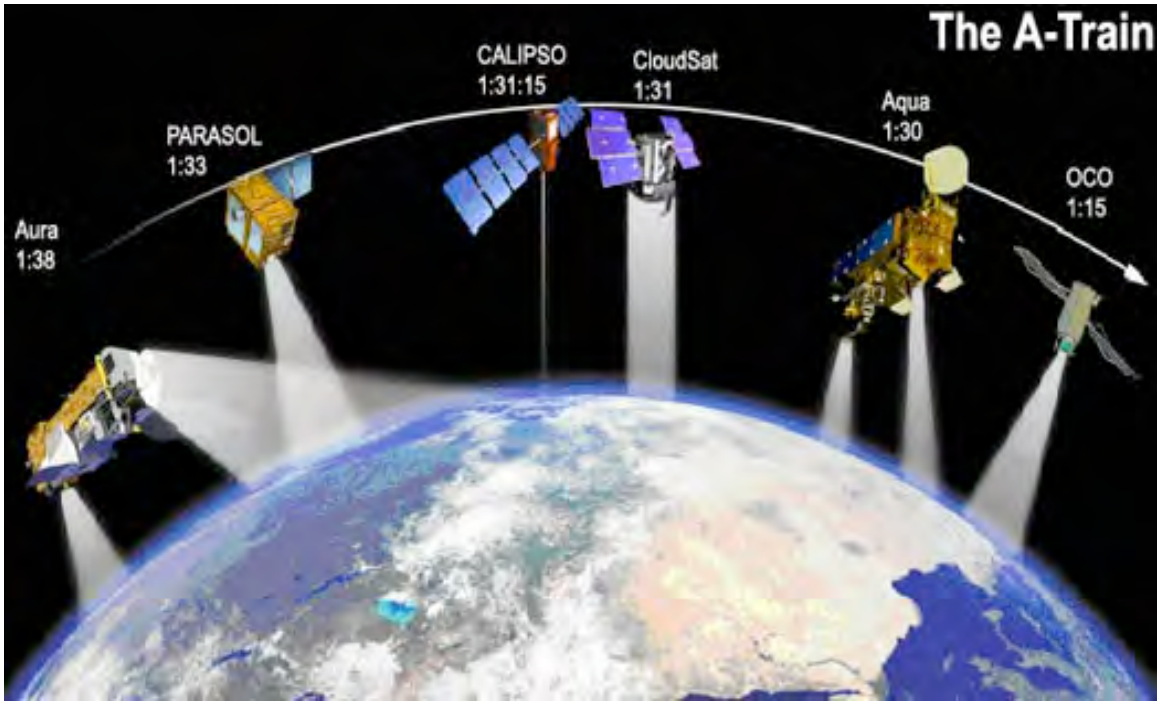

Figure 4.1: A-Train constellation of satellites with times of crossing equator for each mission. (*Note:* In the present A-train constellation CALIPSO precedes CloudSat by 120 seconds owing to the re-activation of the CloudSat satellite and joining the A-Train again from May 2012 after its malfunctioning in April 2011).

4.2 CALIPSO

The payload of CALIPSO (Cloud–Aerosol Lidar and Infrared Pathfinder Satellite Observation) satellite comprises three instruments that can be used to observe the properties of cloud and aerosol particles: the CALIOP (Cloud-Aerosol Lidar with Orthogonal Polarization) lidar, IIR imaging infrared radiometer, and a Wide Field Camera (WFC).

4.2.1 CALIOP

CALIOP uses a Nd:YAG laser to generate 20 nsec pulses of 110-mJ energy at 0.532 μm and 1.064 μm wavelengths. The emitted laser light is directed through beam expanders with an angular divergence of 100 μrad achieving a beam diameter of 70 m on the ground. The lidar pulse repetition at the rate of 20.16 Hz allows for a sampling of a complete atmospheric profiles every ~333 m on the ground. The main components of the receiver subsystem are a 1-m wide telescope and three detectors – one for the 1.064 μm channel and two for the parallel and perpendicular polarization of the 0.532 μm channel. The laser pulses are transmitted as linear polarized output and a beam splitter used in the receiver system allows for the separation of 0.532 μm parallel and perpendicular components of the polarized returned signal.

Table 4.2: Spatial resolutions of the downlinked CALIPSO data*

Altitude Region with Mean Sea Level		*Horizontal Resolution (m)*	*Vertical Resolution (m)*	
Base (km)	*Top (km)*		532 nm	1064 nm
30.1	40.0	5000	300	–
20.2	30.1	1667	180	180
8.2	20.2	1000	60	60
–0.5	8.2	333	30	60
–2.0	–0.5	333	300	300

*From PC-SCI-202.01

Analog signals acquired by the CALIOP are analyzed for several on-board functions including digitization, averaging and background subtraction before the data is down linked to the ground-receiving station. An altitude-dependent on-board averaging scheme (Table 4.2) is implemented on the data to provide reliable signals owing to the fact that the atmosphere is more spatially uniform with increasing altitude and thus signals from higher levels in the atmosphere tend to be very weak, requiring more samples to be averaged.

4.2.2 Imaging infrared radiometer (IIR)

The IIR operates in the thermal infrared region of the spectrum at 8.65 μm, 10.6 μm and 12.05 μm to produce brightness temperature of the targets viewed. An on-board calibration of data is performed with a specifically designed black body to maintain the accuracy of the measurements. Acquired IR data can be used in conjunction with lidar products to estimate the size of cloud particles and infrared emissivity based on certain assumptions.

4.2.3 Wide field camera (WFC)

WFC is a single channel imager operating at a visible wavelength (0.65 μm), and captures images over a 60 km swath centered with the lidar measurements. One pixel of this CCD (charge-coupled device) camera represents an area of 125 m x 125 m on the ground. These images can be used in conjunction with the CALIOP data to provide meteorological context over any region and aid in correct registration of lidar foot prints during daytime operations, while images from infrared imager is used for nighttime operations.

4.3 CALIPSO data products

CALIPSO data is available for scientific research through NASA Langley Research Center (http://eosweb.larc.nasa.gov) and is provided as several products based on the geophysical variables retrieved for the observed cloud and aerosol layers. Since the beginning of the CALIPSO mission, several versions of data products have been released with improvements in the quality of the products for each release. The present thesis uses CALIPSO Version–3 data products, which are provided with improved quality mainly for daytime calibration [*Powell et al.*, 2009] and cloud – aerosol discrimination [*Liu et al.*, 2009].

Initially, the down linked CALIPSO data are analyzed for geolocation of the lidar footprint, determination of instrument calibration constants and estimation of the range to

produce attenuated backscattering profiles as Level-1 product. The cloud and aerosol layers are identified from backscatter data using a specifically designed algorithm referred to as Selective Iterative BoundarY Locator (SIBYL) [*Vaughan et al.*, 2009]. This algorithm allows for the detection of atmospheric constituents at multiple horizontal averaging resolutions such as 5 km, 20 km and 80 km. The detected cloud or aerosol layer at any averaging resolution is removed from the data and a backscattering profile is reconstructed as if the layer were never present before, and passed on to another horizontal averaging resolution. In this way, the SIBYL algorithm can retrieve even tenuous clouds and aerosol layers by achieving a sufficient signal-to-noise ratio from the backscattered signals. The retrieved cloud features at any resolution are resampled and provided in data products accordingly. Once a feature is identified, the CALIPSO data processing algorithm constructs and examines multidimensional PDFs for optical and physical properties of the feature layer to flag it as either aerosol or cloud [*Liu et al.*, 2009]. Data products are reported with various quality flags that show the confidence level in layer classification (CAD score) and their uncertainties in the retrieval of extinction or optical properties.

4.4 Ground and space view of ice clouds

Despite the fact that the measurements are made with a similar sensitivity of instruments, there exist subtle distinctions between the observation of different types of clouds from both ground and space platforms. To illustrate these differences, a set of observations from AFARS and the corresponding observations from CALIPSO and CloudSat satellites as they overpass AFARS are presented. The CloudSat satellite carries a 94-GHz cloud profiling radar and orbits the earth in the A-Train with a time lag of few seconds relative to the CALIPSO satellite.

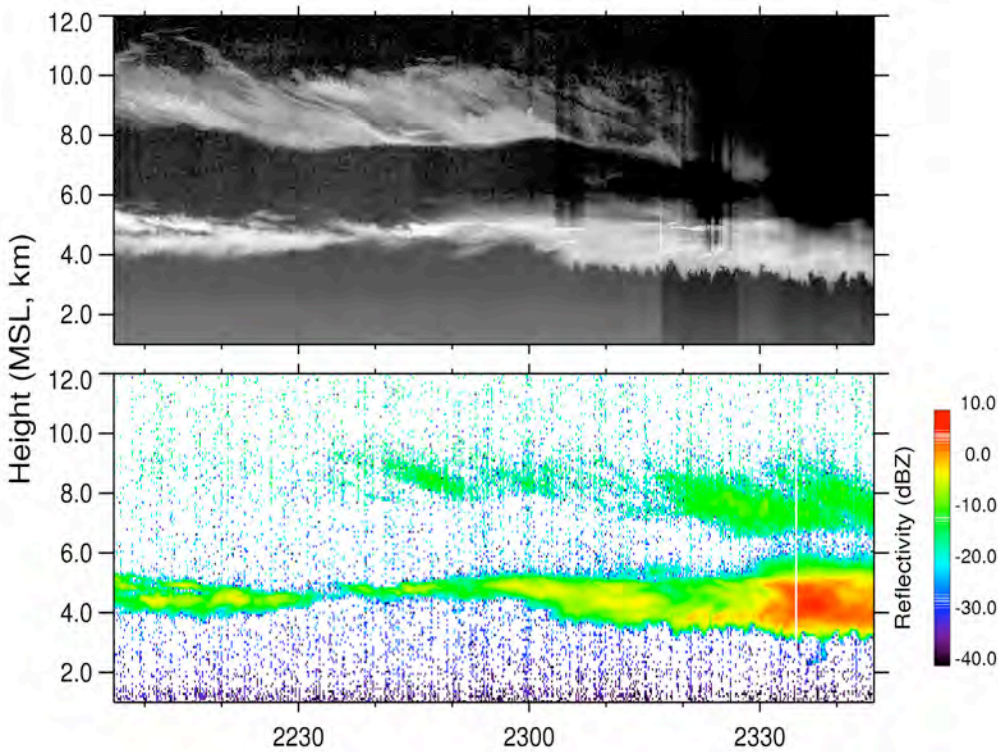

Figure 4.2: Lidar returned power (*above*) and radar reflectivity (*below*) as observed from the AFARS ground station on August 30, 2012.

The simultaneous lidar and radar observations from AFARS (shown in Figure 4.2) highlight the different sensitivities of the lidar and radar instruments. The ruby lidar returned power signal is expressed in a logarithmic gray scale (where white represents high power) and the radar reflectivity is expressed in dBZ for the observation period, given in UTC. Here, the upper level cloud extending from ~8.0 – 10.5 km is a cirrostratus, which is sensitive only to the lidar and only detected by the radar after ~2240 UTC. This behavior is due to the presence of small ice particles in the cirrostratus that is below the sensitivity limits of the W-Band radar (3.2 mm wavelength) in use. With time, as the cloud evolves and larger ice particles form, the radar detected this cloud (~2240 – 2345 UTC).

The relatively thin mid-level cloud extending from 4 – 6 km altitude is identified as altostratus, which dominantly contains ice crystals that are sensitive to both the lidar and radar. The relatively thicker mid-level cloud between 3 – 6 km altitude at 2300 UTC is also identified as an altostratus, although supercooled liquid altocumulus cloud layers are sometimes found embedded. This behavior is the typical scenario of mid-level clouds containing mixed-phase particles, with supercooled liquid layers near the cloud top. The supercooled liquid layers causes strong backscattering of the laser pulses that also gets attenuated there, beyond which it cannot detect the upper cloud layer. The dominant presence of ice particles in the cloud produces high depolarization (δ ~0.35 – 0.55, not shown here). Thereafter, the glaciation of a supercooled liquid layer produces what is traditionally known as a dense altostratus, which attenuates the laser pulse (the solar disk becomes indistinct for a surface observer). This is reflected again in radar reflectivity that can detect both the cloud layers (altostratus and cirrostratus, from ~2320 – 2345 UTC).

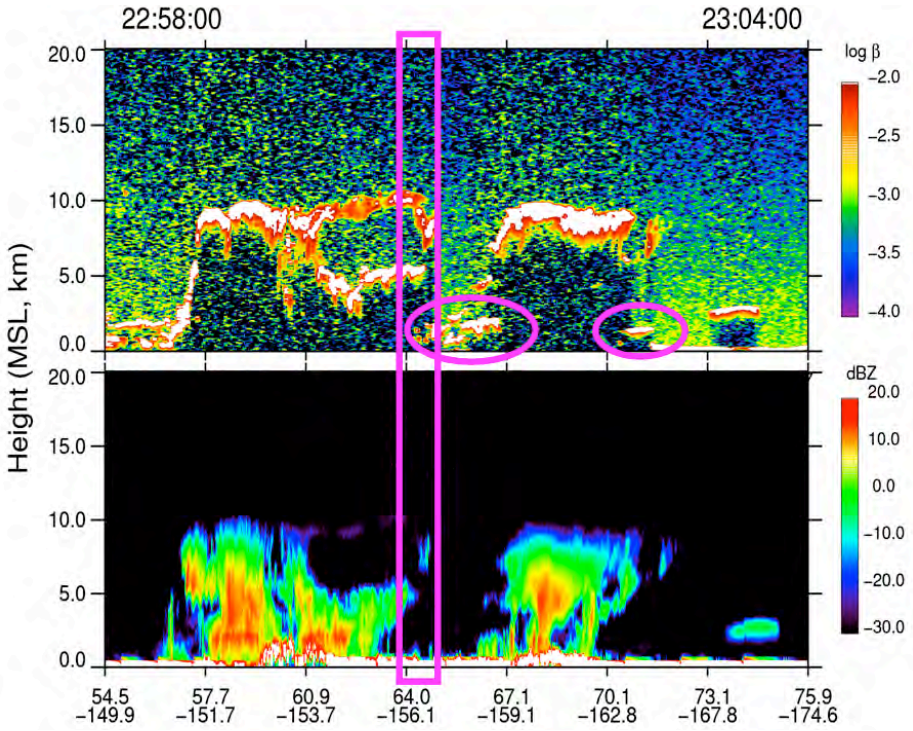

Figure 4.3: Lidar backscattering (*above*) and radar reflectivity (*below*) as observed from CALIPSO and CloudSat satellites on August 30, 2012.

The lidar backscattering and radar reflectivity as observed from CALIPSO and CloudSat for the nearest transect of satellites during the same time is shown in Figure 4.3 (Note: that the AFARS site is located at 64.86^o latitude – pink box). In this case, there are several cloud types that can be possibly identified as cirrostratus, cumulonimbus (*cumulus congestus*), and other mid and low-level clouds. For the case of the two precipitating cumulonimbus cloud systems here, which produce large particles due to strong updraft velocities, CALIPSO can detect only a top-portion of the cloud and then gets attenuated, whereas CloudSat can detect the entire cloud from its top through to the ground surface where particles are precipitating from it. The upper troposphere cloud extending from ~8 – 10 km over the latitudinal belt 60^o – 64^o is identified as cirrostratus, which is completely detected by CALIPSO and only partially by CloudSat. This behavior is due to the small ice particles present in the top zones of cirrus clouds. There are some clouds at lower-levels that are observed only by CALIPSO and not by CloudSat (shown with pink circles). The other possible scenario where such low-level clouds often remain undetected (> 10%, *Okamoto et al.* [2010]) by CloudSat are: (i) contamination from surface clutter that produces strong reflectivity (noise) near the surface, (ii) attenuation of radar pulses in optically thick clouds which considerably reduces the reflectivity near the surface. The apparent differences between ground-based and satellite perspective of observing cloud types can now be summarized as:

Ground-based perspective

(a) Lidar probing

i) View of clouds at higher altitudes (such as cirrus types) is often blocked by the presence of low-level water clouds that partially or totally attenuate the laser pulse.

ii) For mid-level clouds, which are often comprised of thin supercooled liquid layers near the cloud top zone, only the cloud base can be detected before the laser pulse gets attenuated.

Satellite perspective

(a) Lidar probing

i) Higher altitude clouds are always observed and are not affected by the presence of any types of low-level clouds.

ii) In the case of mid-level clouds with supercooled liquid layers, only cloud top can be detected.

(b) Radar probing

i) There are no differences in reference to the platform (ground-based or space-borne) of measurements as radar wavelengths (3.2 mm here) can penetrate multiple cloud layers and only becomes attenuated under moderate to heavy precipitation conditions.

4.5 Comparison studies

There are numerous studies comparing passive satellite and ground-based measurements. Studies like *Wu et al.* [2009], *Protat et al.* [2010], and *Noh et al.* [2011] presented comparison of data from the A-Train satellites with air-borne measurements of cloud properties for data products validation purposes. For the present case of active satellite sensing, which is relatively new (since, June 2006), there are limited studies that make comparison of the cloud macrophysical properties retrieved from both platforms. *Plana-Fattori et al.* [2008] was the first doing a comprehensive comparison of ground-based and space-borne lidar measurements. While they found consistency to an extent between both measurements, they identified that the sources of discrepancies are numerous, and their effects are difficult to quantify with traditional analysis methods. *Dupont et al.* [2010] and *Thorsen et al.* [2011] presented a comparison of macrophysical and optical properties of clouds retrieved from ground-based and space-borne lidars. They found reasonable agreement between the measurements through statistical methods, while accounting for the discrepancies in the sampling and resolution of the measurements made. *Hoareau et al.* [2013] also compared cirrus cloud occurrences over midlatitude site derived from ground-based lidar with CALIPSO retrievals and found

about 5% mean difference of cloud occurrence. Thus, the key here, to make a valid comparison is to understand the differences in observations from both platforms and to accommodate statistically significant nearly coincident samples. The purpose for the present work is to compare of the macrophysical properties of types of ice clouds retrieved over the AFARS station (as described in Chapter 2) and to assess how the properties retrieved from ground-based sensors are represented in the satellite data.

4.6 Data and methodology

For the purpose of comparing cloud retrievals from ground-based and space-borne lidars it is required to understand the essential characteristics of the instruments that define the quality of the measurements, nature of observations from both platforms (discussed in section 4.4) and the algorithms used to detect cloud layers in both datasets. The characteristics of the ground-based and space-borne lidar used for comparison are given in Table 4.3.

Table 4.3: Characteristics of ground-based and space-borne lidars used for comparison

	AFARS	*CALIPSO*
Platform	Ground	Space-orbit: About 705 km altitude above earth's surface moving at 7 km/s speed
Wavelength	694 nm (‖, ⊥)	532 nm (‖, ⊥), 1064 nm
Pulse energy	1.5 J	110 mJ
Repetition rate	0.1 Hz	20.16 Hz
Pulse width	25 ns	20 ns
Range resolution: vertical	6 m	30 m (0 to 8 km) 60 m (> 8 km)
Horizontal		333 m
Beamwidth/FOV: transmitter	0.5 mrad	100 mrad
Receiver	1 – 3 mrad	130 mrad
Receiver: telescope	28 cm diameter	1 m diameter
Altitude range of measurement	0.5 – 14 km	0 – 30 km

From the perspective of zenith looking ground-based lidar, the volume of the atmosphere sampled is small (narrow field-of-view) for each shot of laser pulse and are localized, i.e., representative of the area. The high pulse energy (1.5 J) and sampling resolution of the ground-based lidar provides sufficient signal-to-noise ratios to detect even tenuous clouds and aerosols in the troposphere. Thus, our ground-based measurements can serve as *truth-values* in assessing and validating satellite measurements. From the satellite perspective, which is several hundreds of kilometers away from the targets and moving at high speed, the volume of atmosphere sampled for each laser shot is small (very narrow swath) over large horizontal distance. Thus, satellite measurements are susceptible to high noise levels and it is required to average large samples to attain sufficient signal-to-noise ratios to detect targets. This scenario is further complicated for the daytime measurements, which are contaminated by intense solar noise that makes the detection of thin targets more difficult. For comparison of measurements from both platforms, the spatial extent sampled by the satellite should be a compromise with considerable area around the ground station representative of the properties derived. Such analysis can also be useful to acquire statistical information between temporally consistent samples. Here, we use ground-based lidar observations derived from 1-min averaged shots at AFARS and CALIPSO derived cloud observations from the 5-km resolution cloud product.

4.6.1 Sampling

Since the launch of CALIPSO, the total number of days with AFARS observations is 173 days (June 2006 – June 2012). CALIPSO orbital overpasses within the varying grid resolutions for AFARS cloud days were examined and a grid resolution that accommodates profiles from both datasets is chosen for comparison. A spatial extent of 2.0^{o} x 6.0^{o} (latitude x longitude) around the site is selected, which provides 82 matching days with AFARS observations. Choosing larger spatial extents around the site, tests were performed but it does not notably increase the number of matching days or samples consistent with AFARS observations. The orbital overpasses are selected only if there are

more than 20 profiles in the transect within the grid, i.e., a transect extending more than 100 km near or around the site. As observations at AFARS are routinely taken around ~0000 UTC, only daytime CALIPSO observations within ± 1.5 hrs of 0000 UTC are considered for the analysis. This prevents bias of the measurements from sources such as, due to diurnal cycles and development of other clouds, etc. Once the profiles from CALIPSO data are extracted in this way, a transparency test is applied. This test looks for a valid cloud or aerosol layer below the cloud in question or surface returns to flag the profile as either transmissive or attenuated. This transparency test is used as a proxy to identify clouds with visible optical depths of $\tau < 3.0 - 4.0$ [*Sassen*, 2002; *Sassen et al.*, 2008; *Sassen and Zhu*, 2009]. As described in the section 4.4, satellite active remote sensing can always detect higher-level clouds and the presence of low-level clouds has no effect, whereas ground-based sensors cannot always detect high-level clouds due to the presence of low-level clouds. This fact can induce a bias towards the higher altitude clouds in the samples for comparison, but this should not be a problem in this case as we intend to make a comparison of transparent clouds (i.e., where the laser pulses can completely penetrate the clouds without being attenuated). Thus, only those profiles flagged as transmissive were selected and the identified cloud layers in them are categorized as cirrus and mid-level ice clouds using the maximum cloud top temperature as -38^{o} C for mid-level ice clouds (as described in Chapter 2).

Table 4.4: Cloudy profiles used for comparison from the 82 matching days with CALIPSO overpasses for 2.0^{o} x 6.0^{o} grid resolution around the AFARS site

	Total	*Cirrus clouds*	*Mid-level ice clouds*
AFARS (1 min-profiles)	8975	5606	897
CALIPSO (5 km-profiles)	2553	1298	584

The amounts of transparent cirrus and mid-level ice cloud profiles extracted and used for comparison from both AFARS and CALIPSO datasets are given in Table 4.4. The monthly distribution of transparent cloud profiles obtained for all the matching days in the comparison are shown in Figure 4.4, expressed as percent of the total number of samples. The relative occurrence frequency for *cirrus types* of clouds ranges from 4% to 17% for AFARS and 2% to 20% for CALIPSO, with maximum occurrence in January and minimum occurrence in December. The relative occurrence frequency of samples for *mid-level ice* clouds ranges from 1% to 23% for AFARS and 0.5% to 15% for CALIPSO. As found for cirrus clouds, both AFARS and CALIPSO report a high frequency of occurrence of mid-level clouds in January and a low frequency of occurrence in December. However, are differences greater than 5% between the AFARS and CALIPSO measurements of mid-level cloud occurrence in March, May, June, and July. The monthly distribution of cirrus cloudy profiles from AFARS and CALIPSO agree better than the distribution of mid-level ice clouds derived from AFARS and CALIPSO.

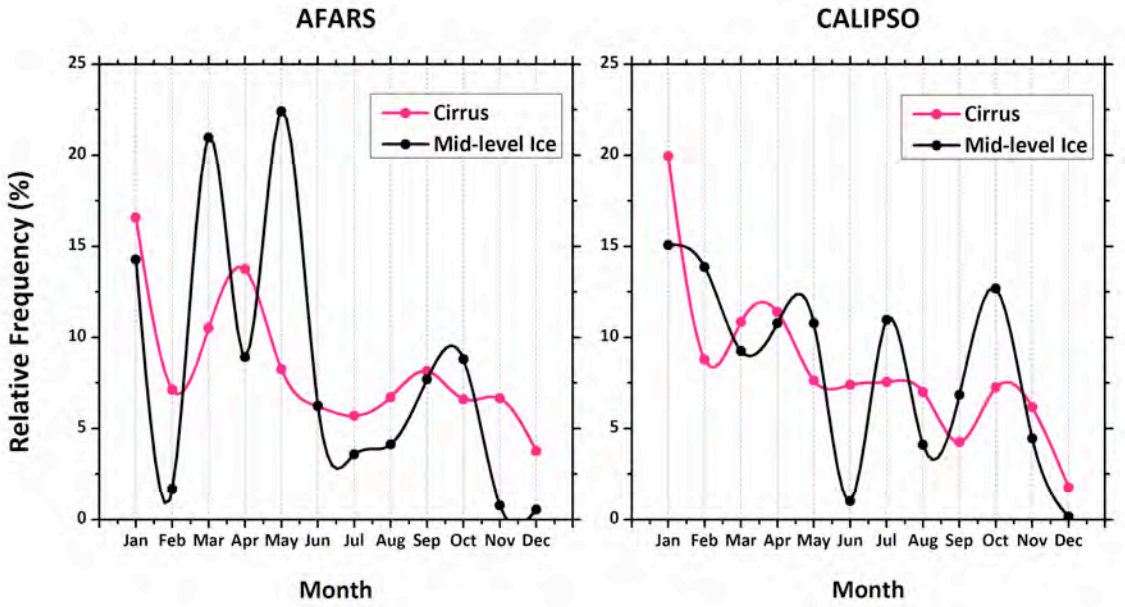

Figure 4.4: Monthly distribution of transparent cloudy profiles available from AFARS (*left*) and CALIPSO (*right*) observations.

4.6.2 Effect of resolution

The ground-based lidar data used here retrieves cloud properties at an averaged 1-minute temporal and 18 m vertical resolution, whereas the CALIPSO data to be used here provide cloud information at 5 km horizontal and 30 – 60 m vertical resolution (see Table 4.2). Apart from the formation mechanisms of clouds the spatial variability of the observed clouds depends on the wind speed over the region [*Pappalardo et al.*, 2010]. The spatial extent sampled by the ground-based lidar in 1-minute can be estimated through the advection of wind over its field-of-view in the atmosphere. From Chapter 2 we know that, at cirrus and mid-level ice cloud top altitudes over AFARS, the mean wind speeds are 18.9 and 12.6 m/s. This fact gives the equivalent spatial extent sampled by our ground lidar for 1-minute observations as 1.13 km and 0.8 km respectively. An increase in sampled extent by ground observations can be obtained by averaging more shots (say 5 minutes). However, the effect of resolution in our case could result in higher cloud occurrences in the CALIPSO data as also shown by *Thorsen et al.* [2011].

4.6.3 Effect of multiple layers

Macrophysical properties derived from AFARS dataset use a single resolution scheme (1-minute shots) and *envelope method* (Chapter 2). Here, the fine resolution of the AFARS lidar is sufficient to retrieve even tenuous cloud layers. Thus, the identified cloud layers from each lidar shot are merged such that top altitude is derived from the topmost cloud layer and base altitude from lowest cloud layer forming an envelope for that particular cloud type. Whereas the CALIPSO data processing algorithm uses multiple-resolutions (5 km, 20 km, 80 km) to gain sufficient signal-to-noise ratios and retrieve even tenuous cloud layers, which are often overlapping. i.e., cloud retrieved at 5 km resolution could have its top or base altitude within the cloud layer retrieved at coarser resolution. Thus, to make fair comparisons, the identified cloud layers at different resolutions of CALIPSO data should be merged such as to create an *envelope* similar to the procedure used in the AFARS analysis. Nonetheless, the use of large spatial

averaging in CALIPSO data leads to several cloud layers in a single profile compared to other ground-based lidar retrievals [*Dupont et al.*, 2010; *Thorsen et al.*, 2011].

4.7 Results and discussion

The macrophysical properties of cirrus and mid-level ice clouds from AFARS and CALIPSO datasets are examined here. These observations are shown as probability density functions (PDFs) with bin size 0.5 km in Figure 4.5, and are derived for the 82 matching days considering a grid box of 2^{o} x 6^{o} around the AFARS site.

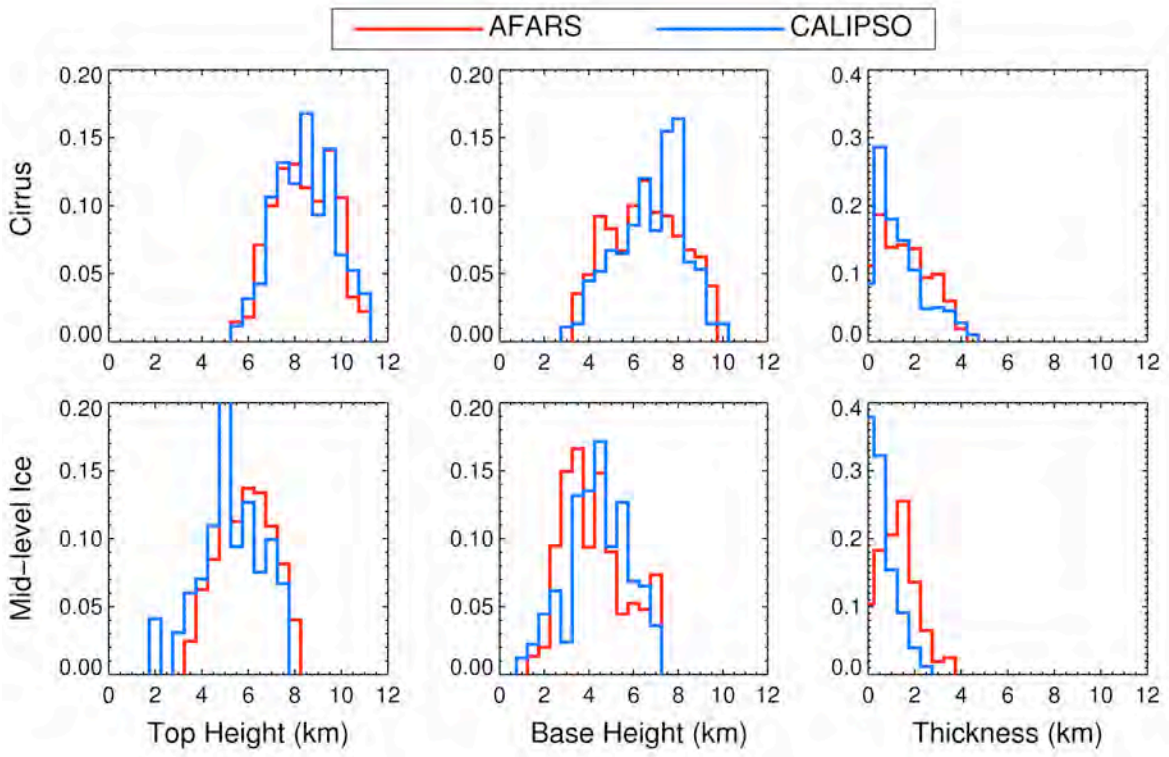

Figure 4.5: Probability density functions (PDFs) of macrophysical properties for cirrus and mid-level ice clouds from 82 matching days of AFARS and CALIPSO (derived from 2^{o} x 6^{o} grid resolution around the site) observations.

In the case of cirrus clouds, the top altitude distributions show strong agreement in both datasets and range from 4 – 12 km, with a relatively high peak in CALIPSO data at 8.5 – 9 km. The high occurrence of cloud top altitude in CALIPSO is quite expected, as a result of different viewing positions (from space and ground). The cloud base altitudes distributions show more variations ranging from 2 – 11 km, specifically, near 5 km and 8 km. AFARS derived cirrus cloud base altitudes occur more frequently near 5 km than those derived from CALIPSO. Whereas at 8 km altitude, CALIPSO derived cirrus cloud bases occur more frequently than those from AFARS. Despite the expected differences, overall there is a good agreement of the range of top and base altitudes and thickness of cirrus clouds. It is observed that a higher frequency of thinner cirrus clouds is retrieved from CALIPSO than those retrieved from AFARS. Recall that CALIPSO cloud detection algorithm uses 5 km, 20 km 80 km (multi-resolutions) signal-averaging scheme, which could identify more tenuous cloud layers in the atmosphere.

In the case of mid-level ice clouds, the top altitude distributions from AFARS range from 3 – 9 km, whereas, in CALIPSO they range from 1 – 8 km. Both datasets show multiple peak occurrences of mid-level ice cloud top altitudes in the 5 km and 6 km bins, with CALIPSO alone identifying cloud top altitudes down to 1-km. Recall that ground-based lidar measurements are often limited by the presence clouds at low levels of the troposphere. The mid-level ice cloud base altitude distributions show a lot of variations with peak occurrences in the 3 km and 5 km bins for AFARS. A similar trend is observed for CALIPSO altitudes with a shift in peak occurrences in the 4 km and 5.5 km bins. The cloud thickness distribution derived from AFARS ranges up to 4 km and from CALIPSO only up to 3 km, showing that CALIPSO derived mid-level ice clouds are much thinner than those of AFARS.

The macrophysical properties derived here do not qualify for standard statistical significance tests due to: (i) uneven sampling from both datasets, (ii) auto-correlation between the samples from each transect in the orbital overpass or even in lidar shots

within its time period of limited operation on day. Thus, the variation in such samples cannot be directly calculated as standard deviation, but can be explained by pseudo-standard deviation, which represents the width of the distribution. Pseudo-standard deviation is calculated as the Interquartile range (IQR) divided by 1.35 [*Lanzante*, 1996], where IQR is the difference between the upper quartile (quartile of order 0.75) and the lower quartile (quartile of order 0.25).

Table 4.5: Mean and pseudo-standard deviation for cirrus clouds marcophysical properties from AFARS and CALIPSO observations

Property	*AFARS*		*CALIPSO*		*Difference,*
	Mean	*PseudoSD*	*Mean*	*PseudoSD*	*AFARS – CALIPSO*
Cloud Top Height (km)	8.596	1.568	8.663	1.468	– 0.067
Cloud Base Height (km)	6.750	2.015	7.011	1.616	– 0.261
Cloud Thickness (km)	1.846	1.348	1.651	1.067	0.214

Table 4.6: Mean and pseudo-standard deviation for mid-level ice clouds macrophysical properties from AFARS and CALIPSO observations

Property	*AFARS*		*CALIPSO*		*Difference,*
	Mean	*PseudoSD*	*Mean*	*PseudoSD*	*AFARS – CALIPSO*
Cloud Top Height (km)	6.047	1.274	5.471	1.305	0.576
Cloud Base Height (km)	4.509	1.454	4.632	1.319	– 0.123
Cloud Thickness (km)	1.538	0.821	0.839	0.526	0.699

Table 4.5 and Table 4.6 provide the mean properties for cirrus and mid-level ice clouds retrieved from both platforms with the estimated pseudo-standard deviation and the observed differences. The mean and pseudo-standard deviation values are calculated using the number of samples/profiles satisfying the criteria for cirrus and mid-level ice clouds from both datasets, as shown in Table 4.4. It is observed that the mean cloud top/base altitudes for cirrus clouds are higher for CALIPSO than AFARS. While, the mean cloud top altitude for mid-level ice clouds is higher for AFARS than CALIPSO. The mean cloud thickness for cirrus and mid-level clouds derived from AFARS is higher than those derived from CALIPSO. These observations are consistent with the previous studies *Dupont et al.* [2010] and *Thorsen et al.* [2011], comparing cloud macrophyiscal properties derived from ground-based lidar to space-borne lidar. The differences in properties derived from both datasets for cirrus clouds agree to from –0.26 km to 0.21 km with a strong agreement for cirrus top altitudes, whereas, the mid-level ice cloud properties agree to –0.123 km to 0.7 km. The differences in cloud thickness for both cirrus and mid-level ice clouds are high because of the apparent higher signal levels in AFARS than those in CALIPSO.

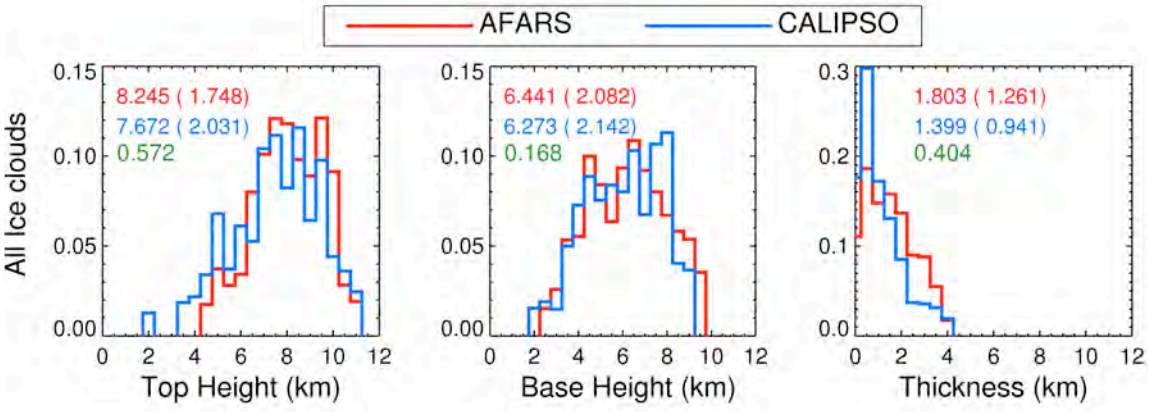

Figure 4.6: Probability density functions (PDFs) of macrophysical properties for transparent ice clouds from 82 matching days of AFARS and CALIPSO (derived from 2^{o} x 6^{o} grid resolution around the site) observations. The numbers shown are mean, pseudo-standard deviation (*in brackets*) and difference between AFARS and CALIPSO (*Green color*).

To further evaluate the occurrence and macrophysical properties of clouds in both datasets, the PDFs are also derived for all transparent ice clouds (both cirrus and mid-level ice clouds) as shown in Figure 4.6. It is observed that the cloud top altitudes from CALIPSO show high occurrences in the lower altitudes up to 6 km than from AFARS. This difference is also reflected in the cloud base altitudes up to 3 km, which can be explained by accounting for the presence of lower level clouds that always restrict the ground-based lidar operations. Attenuated profiles due to lidar signal saturation and presence of low-level clouds are up to 15.5% of the total AFARS dataset (Chapter 2 – Table 2.3). The mean cloud top/base altitude for all ice clouds is higher for AFARS than CALIPSO. But, the mean cloud thickness for all ice clouds is still higher for AFARS (1.8 km) than CALIPSO (1.4 km), similar to the observation made with cirrus and mid-level ice clouds. This finding suggests that, this difference is attributed from CALIPSO dataset that identifies several cloud layers in a profile. In other words, this difference is due high levels of noise in the CALIPSO. Recall, the datasets used for comparison are daytime measurements and CALIPSO daytime datasets is highly contaminated with solar noise levels.

4.8 Summary

Datasets from both ground-based lidar and space-borne lidar are evaluated for the consistency of macrophysical properties retrieved for lidar transparent ice clouds. Assessment of retrieved properties from ground-based and satellite measurements are required to make effective use of the complimentary nature of these observations. The main sources of discrepancies for our analysis are found to be: (i) the presence of low-level clouds, and (ii) effect of signal-to-noise ratio for the two observations. Despite these discrepancies in the cloud occurrence distributions, the overall macrophysical properties retrieved from two platforms of measurements show good agreement to within –0.3 to +0.7 km. The differences in cloud properties derived from AFARS and CALIPSO for cirrus clouds shows strong agreement than those for mid-level ice clouds. This needs to be explored in future studies.

Chapter 5

Conclusions

In view of the present uncertainties in modeling the radiative effects of ice clouds, understanding the varieties of ice clouds forming in the troposphere, their prevalence, and macro- and micro-physical properties is required. Most importantly, true identification of the cloud type and its composition represents a foremost step in this process. Evolving studies from new datasets through satellite active remote sensing have augmented our knowledge of the prevalence of ice clouds that vary greatly not only over geographical regions, but also with their altitude of occurrence in the troposphere. With such perspective, attempts to identify cloud types based solely on the *genera* (altitude range of occurrence) of clouds could lead to spurious inferences on the role of a particular cloud type, and this identification needs to be improved. The research presented here exclusively deals with ice clouds transparent to lidar probing that are limited to visible optical depth (τ) 3.0 – 4.0, and can be summarized in two parts, which concerns: (i) the comprehensive description of visually identified cirrus clouds, and (ii) the occurrence of mid-level ice clouds, along with their macro-physical properties over a typical sub-Arctic region. For this purpose, an extensive dataset obtained through ground-based lidar at the AFARS station is used. Our study also includes a preliminary assessment of space-borne lidar retrieval of ice clouds through the use of CALIPSO dataset.

Traditionally established permanent weather stations with sensitive instruments to observe clouds are essential and found to be very useful in understanding the locally formed varieties of clouds. Specifically those which are supported by visually identified

cloud type observations during data collection, such as the case with the AFARS station, gains an additional advantage in delineating the properties for those varieties of clouds without any prior constraints with altitude/temperature range and cloud phase. Cloud types at AFARS have been identified (Prof. Kenneth Sassen) by visual observations on the basis of its characteristic traits such as: transparency of cloud, color, and optical phenomenon if any. We used about 8-yrs of lidar dataset collected at AFARS and only transparent ice clouds through which lidar pulses can penetrate without being completely attenuated. It means that the visible optical depths of these ice clouds are limited to 3.0 – 4.0, beyond which the two-way penetration of the lidar pulse cannot exist. In general, *'cirrus clouds'* are ice-dominant clouds forming in the upper levels of the troposphere and are relatively optically thin. Thus from the sample of transparent ice clouds collected at AFARS, a threshold temperature of –38^{o} C is chosen to separate the clouds forming in the mid-levels of the troposphere (i.e., cloud top temperatures warmer than –38^{o} C) are termed as *'mid-level ice clouds'*. Low-level or warm clouds have been discarded from the entire sample by using a maximum allowable cloud base temperature of –10^{o} C. We derived macrophysical properties such height, thickness, and temperature for both cirrus and mid-level ice clouds. Despite the basic differences that arise due to the presence of low level clouds obstructing the view of ground-based lidars, transparent ice cloud occurrences over AFARS agrees well with the trend of precipitating weather systems over the region (Figure 2.4). The results presented here contribute to a climatological representation of cirrus clouds and mid-level ice clouds occurrence over a typical sub-Arctic region.

5.1 AFARS – cirrus clouds

The average values of our AFARS local cirrus cloud properties from the ~8-yr data are as follows. For cirrus cloud base: 6.87 km height, 418 hPa pressure, –37.7^{o} C temperature, 13.9 m/s wind speed, and 223^{o} wind direction. For cirrus cloud top: 9.08 km height, 297 hPa pressure, –54.1^{o} C temperature, 18.9 m/s wind speed, and 225^{o} wind direction. The average cirrus cloud geometrical thickness is about 2.21 km. Considering

the high resolution of AFARS extended time dataset and visual observations used to identify cloud types, the climatological findings reported here serves as a reference to test the climate-model cloud (height/temperature) forecasts and satellite retrievals of cirrus clouds over the Interior Alaska region. In agreement with previous cirrus studies, it is observed that AFARS cirrus cloud heights do not follow any trend but generally vary with the local tropopause level. The monthly distribution of cirrus cloud occurrences reveals that cirrus extends to lower levels during winter. This arises from the geographical location of the AFARS site where polar-frontal outbreaks are not uncommon during the cold season. Our observations show that visually identified AFARS cirrus cloud top temperatures are dominant below -40^{o} C, supporting the theory that the homogeneous nucleation of particles is the dominant mechanism for cirrus cloud formation. The influence of orography for cirrus cloud formation is quite noticeable from the observed wind directions at cloud top and base altitudes because of our local terrain features. Seasonality in cirrus clouds forming mechanisms is evident from the cloud thickness distributions and wind directions.

Several studies have shown that cirrus clouds are a product of weather processes. Thus, it is essential to understand the weather patterns over the AFARS station, as the above reported findings are likely to be specific for the Interior Alaska region. For this purpose, a two-way clustering technique is applied to reanalysis dataset to identify the synoptic patterns conducive for the observed cirrus cloud formation over the AFARS station. Nine synoptic patterns consistent with the climatological lidar studies were identified to prevail over AFARS during the observed cirrus cloudiness. It is observed that the polar jet stream pattern found about 300 – 250 hPa pressure levels is the basic upper-level synoptic feature influencing the cirrus clouds over Alaska. This feature is displaced much further south of Alaska during winter and to the north of Alaska during summer, while it is overhead for most of the transitional periods. The movement of this feature along with the Beaufort high and Aleutian low primarily controls the weather over Alaska. Depending on the meridional temperature gradient, a mid-tropospheric ridge

is often in place extending into Interior Alaska at varying ridge axis positions that advects warm moist air from the North Pacific to the Interior through southwesterly flow. The other patterns include zonal flow during transitional seasons, southeasterly-southerly flow caused by deep extended ridges during spring-summer, and southwesterly-westerly flow caused by polar jet stream overhead, cold air intrusion through northerly flow during winter. Though surface features vary greatly with intensity and their mean location, the upper-level synoptic disturbance clearly explains the favorable conditions for the formation or transport of cirrus clouds over the AFARS site (Interior Alaska). It should be remembered that upper-level synoptic disturbances causes cirrus cloud formation, whereas the surface features may exhibit a cause-and-effect relationship depending on the local thermodynamic conditions.

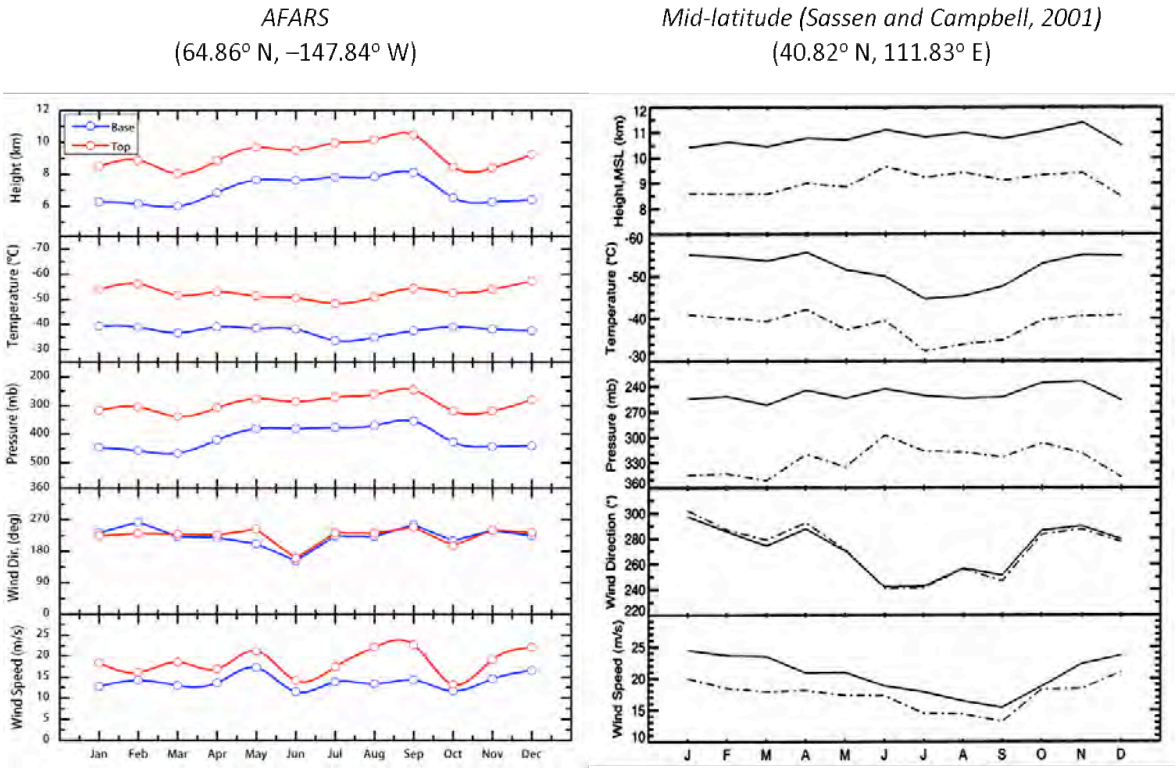

Figure 5.1: Comparison of cirrus cloud climatological properties derived from two distinct geographical zones (base/top: blue-dashed/red-solid).

Here we compare the exclusive cirrus cloud climatologies obtained from visually identified cloud types from two distinct geographical regions. Figure 6.1 shows the essential macrophysical properties of cirrus clouds derived from AFARS (sub-Arctic) and a midlatitude site [*Sassen and Campbell*, 2001] in Salt Lake city, Utah. Comparison of the macrophysical properties reveals similar variations for both regimes, in that cirrus cloud heights tend to follow the local tropopause trend. The monthly average cirrus cloud top temperatures show much warmer temperatures during summer for the midlatitude site; this can be attributed to the prevalence of monsoonal conditions where cirrus cloud formation occurs through anvil blow-off. However at AFARS, the decrease in cirrus cloud mean temperature during summer is not as prominent, as expected. The mean annual cirrus cloud top temperature at the sub-Arctic site (–54.1^{o} C) and midlatitude site (–53.9^{o} C) is found to be quite similar. Distinct weather patterns exist between these regions that cause cirrus clouds such as: the sub-tropical jet stream, and Pacific Ridge in midlatitudes, and the polar jet stream, and North Pacific Ridge over the sub-Arctic region. The new finding with this comparison is that the visually identified cirrus cloud properties over any region vary only due to the regional influences that are responsible for those cloud formations. This also supports our assertion that to identify cirrus clouds elsewhere (any geographical location) which lack visual observations, a minimum cloud top temperature as –38^{o} C can be employed.

5.2 AFARS – mid-level ice clouds

The average values of our AFARS local mid-level ice cloud properties from the ~8-yr data are as follows. For mid-level ice cloud base: 3.68 km height, 641 hPa pressure, –16.4^{o} C temperature, 8.47 m/s wind speed, and 204^{o} wind direction. For mid-level ice cloud top: 5.42 km height, 504 hPa pressure, –27.1^{o} C temperature, 12.6 m/s wind speed, and 215^{o} wind direction. Seasonal occurrences of mid-level ice clouds show high values during spring, attributed to the increased regional cyclonic activity. Also from our field notes it can be observed that most aerosol layers (dust) occur over AFARS during spring, which could initiate ice formation in the troposphere at much warmer temperatures, such

as –15^{o} C to –25^{o} C. Observations of mid-level ice cloud top/base temperatures entail the occurrence of horizontally oriented ice crystals in most clouds, that can also be confirmed from the field notes and examination of data displays. Our sample of mid-level ice clouds observed at AFARS are: (i) transparent altostratus, (ii) remnants of altocumulus layer, (iii) ice cloud layers formed from depositional growth of ice particles without initial liquid phase, and (iv) orographic uplift of airmass. With these observations, we provide evidence for our hypothesis that the mid-level ice clouds are prevalent over the sub-Arctic region. The exact mechanisms and contribution of several atmospheric/cloud processes in the formation and maintenance of mid-level ice clouds are not unknown and beyond the scope of the current study. In reference to the current cloud classification schemes implemented for remote sensing observations, these transparent mid-level ice clouds are broadly categorized as altostratus clouds [*Sassen and Wang*, 2012]. Such a classification scheme based on *genera of clouds* could be misleading in assessing the net radiative effect of mid-level clouds and should be improved by including visual traits of the cloud types. Unlike the transparent mid-level ice clouds studied here, the classic/standard altostratus clouds are those, which obscure the disk of sun or moon for a surface observer. By analogy, this means the lidar pulses operating in visible wavelengths will be completely extinguished.

5.3 Assessment of CALIPSO ice cloud retrievals

Comparison of transparent ice cloud – macrophysical properties derived from ground-based lidar at AFARS are made with CALIPSO measurements. For the time period considered (i.e., June 2006 – June 2012), ice clouds are observed for about 173 independent days over the AFARS station. In order to obtain statistically consistent samples from CALIPSO orbital overpasses with respect to our AFARS samples, we have chosen a grid resolution of 2.0^{o} x 6.0^{o} (latitude x longitude) around the AFARS site. Using similar criteria for cirrus and mid-level ice clouds as with AFARS data, ice cloud properties from the CALIPSO dataset are retrieved. Owing to the perspective of the platform of measurements, it is observed that at lower altitudes the occurrences of ice

clouds is more common in CALIPSO than in AFARS data. The mean cirrus cloud top and base altitudes derived from AFARS are found to be lower than the cirrus cloud altitudes derived from CALIPSO, whereas the cirrus cloud geometrical thickness is higher for AFARS data than those derived from CALIPSO. For the case of mid-level ice clouds, the properties (cloud top altitude and geometrical thickness) derived are higher for AFARS than those derived from CALIPSO with the exception of cloud base altitude. The comparison of all transparent ice cloud macrophysical properties (cirrus as well as mid-level ice clouds) shows higher mean values for clouds observed from AFARS than from CALIPSO. This is evident from the higher signal levels in AFARS than those in CALIPSO. Thus, it can be understood that the discrepancies in these datasets can be attributed to sources such as: (i) the presence of low-level clouds, and (ii) lidar system signal noise. Despite these discrepancies, the overall agreement for macrophysical properties derived from the two platforms is found to be good and with a mean difference of –0.3 to +0.7 km.

The key findings of my study are as follows:

1. The AFARS observations have shown that sub-Arctic cirrus clouds have similar mean cloud top temperatures, but occur at lower altitudes than those at midlatitudes.
2. The AFARS observations have shown that sub-Arctic cirrus clouds are associated with different weather patterns than found at midlatitudes. The formation of cirrus is strongly associated with the North Pacific ridge over Alaska.
3. The AFARS observations show that transparent mid-level ice clouds occur commonly in the sub-Arctic, often appear visually similar to cirrus, but are found ~2 km lower in the troposphere.

Based on this study the following future studies are recommended:

1. Based on the initial comparison of observations from AFARS and the CALIPSO satellite, the depolarization capabilities of both instruments should be explored

further to understand the microphysics of ice-clouds over the Arctic. Such a study would allow formal intercomparison and evaluation of the observations from the ground station and the satellite, and set the foundation for studies of mixed-phase clouds.

2. Use the CALIPSO observations to extend the scope of the AFARS observations of mid-level ice clouds to understand their distribution over the entire Arctic region and assess their radiative impact on the surface energy budget.

Thus, while long-term data from ground-based stations like AFARS provides a basis for both mesoscale and climatological studies of cloud types, continuing data from both current *A-Train* satellites and future missions (e.g., Earth Clouds, Aerosols and Radiation Explorer (EarthCARE), scheduled to launch in late 2015) is critical for developing a global and complete understanding of ice clouds and their role in the Earth's climate system.

REFERENCES

Ansmann, A., M. Tesche, P. Seifert, D. Althausen, R. Engelmann, J. Fruntke, U. Wandinger, I. Mattis, and D. Muller (2009), Evolution of the ice phase in tropical altocumulus: SAMUM lidar observations over Cape Verde, *Journal of Geophysical Research-Atmospheres*, *114* (D17208), 1-20.

Atkinson, D. E., K. Sassen, M. Hayashi, C. F. Cahill, G. Shaw, D. Harrigan, and H. Fuelberg (2013), Aerosol properties over Interior Alaska from lidar, DRUM Impactor sampler, and OPC-sonde measurements and their meteorological context during ARCTAS-A, April 2008, *Atmospheric Chemistry and Physics*, *13* (3), 1293-1310.

Bankert, R. L. (1994), Cloud classification of AVHRR imagery in maritime regions using a probabilistic neural-network, *Journal of Applied Meteorology*, *33* (8), 909-918.

Barry, R. G., and A. M. Carleton (2001), *Synoptic and dynamic climatology*, 637 pp., Routledge, New York and London.

Baum, B. A., V. Tovinkere, J. Titlow, and R. M. Welch (1997), Automated cloud classification of global AVHRR data using a fuzzy logic approach, *Journal of Applied Meteorology*, *36* (11), 1519-1540.

Behrangi, A., K. Hsu, B. Imam, and S. Sorooshian (2010), Daytime precipitation estimation using bispectral cloud classification system, *Journal of Applied Meteorology and Climatology*, *49* (5), 1015-1031.

Bergeron, T. (1935), On the physics of clouds and precipitation, *Proces Verbaux de l'Association de Météorologie* (IUGG), 156-178.

Bonell, M., and G. Sumner (1992), Autumn and winter daily precipitation areas in Wales, 1982-1983 to 1986-1987, *International Journal of Climatology*, *12* (1), 77-102.

Bracegirdle, T. J., and S. L. Gray (2008), An objective climatology of the dynamical forcing of polar lows in the Nordic seas, *International Journal of Climatology*, *28* (14), 1903-1919.

Brummer, B., S. Thiemann, and A. Kirchgassner (2000), A cyclone statistics for the Arctic based on European Centre re-analysis data, *Meteorology and Atmospheric Physics*, *75* (3-4), 233-250.

Businger, S. (1985), The synoptic climatology of polar low outbreaks, *Tellus*, *37A* (Polar low Special Issue), 419-432.

Cadet, B., L. Goldfarb, D. Faduilhe, S. Baldy, V. Giraud, P. Keckhut, and A. Rechou (2003), A sub-tropical cirrus clouds climatology from Reunion Island (21°S , 55°E) lidar data set, *Geophysical Research Letters*, *30* (3), 1-4.

Calinski, T., and J. Harabasz (1974), A dendrite method for cluster analysis, *Commun. Stat*, *3*, 1-27.

Chen, T., W. B. Rossow, and Y. C. Zhang (2000), Radiative effects of cloud-type variations, *Journal of Climate*, *13* (1), 264-286.

Christensen, W., and R. A. Bryson (1966), An investigation of the potential of opponent analysis for weather classification, *Monthly Weather Review*, *94*, 697-709.

Collins, R. T. H. (1966), Lidar: A new atmospheric probe, *Quarterly Journal of the Royal Meteorological Society*, *92*, 220-230.

Comstock, J. M., T. P. Ackerman, and G. G. Mace (2002), Ground-based lidar and radar remote sensing of tropical cirrus clouds at Nauru Island: Cloud statistics and radiative impacts, *Journal of Geophysical Research-Atmospheres*, *107* (D23), AAC 16-01-AAC 16-14.

Comstock, J. M., T. P. Ackerman, and D. D. Turner (2004), Evidence of high ice supersaturation in cirrus clouds using ARM Raman lidar measurements, *Geophysical Research Letters*, *31* (11), 1-4.

Conover, J. (1960), Cirrus patterns and related air motions near the jet stream as derived by photography, *Journal of Meteorology*, *17*, 532-546.

Craddock, J. M., and S. Flintoff (1970), Eigenvector represenations of northern hemispheric fields, *Quarterly Journal of the Royal Meteorological Society*, *96*, 124-129.

Crane, R. G., and R. G. Barry (1988), Comparison of MSL synoptic pressure patterns of the Arctic as observed and simulated by the GISS general circulation model, *Meteorological Atmospheric Physics*, *39*, 169-183.

Curry, J. A., and E. E. Ebert (1992), Annual cycle of radiation fluxes over the Arctic Ocean - Sensitivity to cloud optical properties, *Journal of Climate*, *5* (11), 1267-1280.

Curry, J. A., W. B. Rossow, D. Randall, and J. L. Schramm (1996), Overview of Arctic cloud and radiation characteristics, *Journal of Climate*, *9* (8), 1731-1764.

Curry, J. A., F. G. Meyer, L. F. Radke, C. A. Brock, and E. E. Ebert (1990), Occurrence and characteristics of lower tropospheric ice crystals in the Arctic, *International Journal of Climatology*, *10* (7), 749-764.

Davis, R. E. (1988), The development of a spatial synoptic climatological index for environmental analysis, *Ph.D Dissertation*, *University of Delaware, Newark, Delaware*, 210.

Davis, R. E. (1991), A synoptic climatological analysis of winter visibility trends in the Mideastern United-States, *Atmospheric Environment Part B-Urban Atmosphere*, *25* (2), 165-175.

Davis, R. E., and L. S. Kalkstein (1990), Using a spatial synoptic climatological classification to assess changes in atmospheric-pollution concentrations, *Physical Geography*, *11* (4), 320-342.

Davis, R. E., and D. R. Walker (1992), An upper-air synoptic climatology of the Western United-States, *Journal of Climate*, *5* (12), 1449-1467.

DeMott, P. J., and D. C. Rogers (1990), Freezing nucleation rates of dilute-solution droplets measured between -30^{o}C and -40^{o}C in laboratory simulations of natural clouds, *Journal of the Atmospheric Sciences*, *47* (9), 1056-1064.

DeMott, P. J., K. Sassen, M. R. Poellot, D. Baumgardner, D. C. Rogers, S. D. Brooks, A. J. Prenni, and S. M. Kreidenweis (2003), African dust aerosols as atmospheric ice nuclei, *Geophysical Research Letters*, *30* (14), 1-4.

DeMott, P. J., A. J. Prenni, X. Liu, S. M. Kreidenweis, M. D. Petters, C. H. Twohy, M. S. Richardson, T. Eidhammer, and D. C. Rogers (2010), Predicting global atmospheric ice nuclei distributions and their impacts on climate, *Proc Natl Acad Sci USA*, *107* (25), 11217-11222.

Dupont, J. C., M. Haeffelin, Y. Morille, V. Noel, P. Keckhut, D. Winker, J. Comstock, P. Chervet, and A. Roblin (2010), Macrophysical and optical properties of midlatitude cirrus clouds from four ground-based lidars and collocated CALIOP observations, *Journal of Geophysical Research-Atmospheres*, *115* (D00H24), 1-15.

Fernald, F. G., B. M. Herman, and J. A. Reagan (1972), Determination of aerosol height ditribution by lidar, *Journal of Applied Meteorology 11*, 482-489.

Findeisen, W. (1938), Kolloid-meteorologische Vorgänge bei Neiderschlags-bildung, *Meteor. Z*, *55*, 121-133.

Fleishauer, R. P., V. E. Larson, and T. H. Vonder Haar (2002), Observed microphysical structure of midlevel, mixed-phase clouds, *Journal of the Atmospheric Sciences*, *59* (11), 1779-1804.

Fu, Q., and K. N. Liou (1992), On the correlated K-distribution method for radiative-transfer in nonhomogeneous atmospheres, *Journal of the Atmospheric Sciences*, *49* (22), 2139-2156.

Giannakaki, E., D. S. Balis, V. Amiridis, and S. Kazadzis (2007), Optical and geometrical characteristics of cirrus clouds over a Southern European lidar station, *Atmospheric Chemistry and Physics*, *7* (21), 5519-5530.

Goldfarb, L., P. Keckhut, M. L. Chanin, and A. Hauchecome (2012), Cirrus climatological results from lidar measurements at OHP (44°N, 6°E), *Geophysical Research Letters*, *28* (9), 1687-1690.

Gordon, M. (2005), Arctic Climate: Past and Present, in *Arctic climate impact assessment report*, edited, p. 1042, Cambridge University Press.

Haag, W., B. Karcher, J. Strom, A. Minikin, U. Lohmann, J. Ovarlez, and A. Stohl (2003), Freezing thresholds and cirrus cloud formation mechanisms inferred from in situ measurements of relative humidity, *Atmospheric Chemistry and Physics*, *3*, 1791-1806.

Hagen, D. E., R. J. Anderson, and J. L. Kassner (1981), Homogeneous condensation - freezing nucleation rate measurements for small water droplets in an expansion cloud chamber, *Journal of the Atmospheric Sciences*, *38* (6), 1236-1243.

Hahn, C. J., S. G. Warren, J. London, R. M. Chervin, and R. Jenne (1982), Atlas of the simulatneous occurences of different cloud types over the ocean, *NACR Tech. Note*, 212.

Hahn, C. J., S. G. Warren, J. London, R. M. Chervin, and R. Jenne (1984), Atlas of simultaneous occurence of different cloud types over land *NACR Tech. Note*, 216.

Hallett, J., and S. C. Mossop (1974), Production of secondary ice particles during the riming process, *Nature 249*, 26-28.

Hartmann, D. L., and D. Doelling (1991), On the net radiative effectiveness of clouds, *Journal of Geophysical Research-Atmospheres*, *96* (D1), 869-891.

Hartmann, D. L., M. E. Ockertbell, and M. L. Michelsen (1992), The effect of cloud type on earths energy balance - Global analysis, *Journal of Climate*, *5* (11), 1281-1304.

Hawkins, D. M., M. W. Muller, and J. Krooden, A.T (1982), Cluster analysis, in *Topics in Applied multivariate analysis*, edited by D. M. Hawkins, pp. 303-353, Cambridge University Press, Great Britain.

Hoareau, C., P. Keckhut, V. Noel, H. Chepfer, and J. L. Baray (2013), A decadal cirrus clouds climatology from ground-based and spaceborne lidars above the south of France (43.9 degrees N-5.7 degrees E), *Atmospheric Chemistry and Physics*, *13* (14), 6951-6963.

Hobbs, P. V., and A. L. Rangno (1985), Ice particle concentrations in clouds, *Journal of the Atmospheric Sciences*, *42* (23), 2523-2549.

Hobbs, P. V., and A. L. Rangno (1998), Microstructures of low and middle-level clouds over the Beaufort Sea, *Quarterly Journal of the Royal Meteorological Society*, *124* (550), 2035-2071.

Hoff, R. M. (1988), Vertical structure of arctic haze observed by lidar, *Journal of Applied Meteorology*, *27* (2), 125-139.

Hogan, R. J., and A. J. Illingworth (2003), Parameterizing ice cloud inhomogeneity and the overlap of inhomogeneities using cloud radar data, *Journal of the Atmospheric Sciences*, *60* (5), 756-767.

Howard, L. (1803), On the modification of clouds and on the principles of their production, suspension and destruction, *Philisophical Magazine*, *16*, 97-107.

Intrieri, J. M., and M. D. Shupe (2004), Characteristics and radiative effects of diamond dust over the western Arctic Ocean region, *Journal of Climate*, *17* (15), 2953-2960.

Intrieri, J. M., C. W. Fairall, M. D. Shupe, P. O. G. Persson, E. L. Andreas, P. S. Guest, and R. E. Moritz (2002), An annual cycle of Arctic surface cloud forcing at SHEBA, *Journal of Geophysical Research-Oceans*, *107* (C10), SHE 13-01 - SHE 13-14.

Jeffery, C. A., and P. H. Austin (1997), Homogeneous nucleation of supercooled water: Results from a new equation of state, *Journal of Geophysical Research-Atmospheres*, *102* (D21), 25269-25279.

Jensen, E. J., O. B. Toon, S. A. Vay, J. Ovarlez, R. May, T. P. Bui, C. H. Twohy, B. W. Gandrud, R. F. Pueschel, and U. Schumann (2001), Prevalence of ice-supersaturated regions in the upper troposphere: Implications for optically thin ice cloud formation, *Journal of Geophysical Research-Atmospheres*, *106* (D15), 17253-17266.

Jin, Y., W. B. Rossow, and D. P. Wylie (1996), Comparison of the climatologies of high-level clouds from HIRS and ISCCP, *Journal of Climate*, *9* (11), 2850-2879.

Kalkstein, L. S., G. Tan, and J. A. Skindlov (1987), An evaluation of objective clustering procedures for use in synoptic climatological classification, *Journal of Climate and Applied Meteorology*, *26*, 717-730.

Kalkstein, L. S., M. C. Nichols, C. D. Barthel, and J. S. Greene (1996), A new spatial synoptic classification: application to air-mass analysis, *International Journal of Climatology*, *16* (9), 983-1004.

Kay, J. E., M. Baker, and D. Hegg (2007), Physical controls on orographic cirrus inhomogeneity, *Atmospheric Chemistry and Physics*, *7* (14), 3771-3781.

Keckhut, P., F. Borchi, S. Bekki, A. Hauchecorne, and M. Silaouina (2006), Cirrus classification at midlatitude from systematic lidar observations, *Journal of Applied Meteorology and Climatology*, *45* (2), 249-258.

Klett, J. D. (1981), Stable analytical inversion solution for processing lidar returns, *Applied Optics*, *20* (2), 211-220.

Korolev, A. (2007), Limitations of the Wegener-Bergeron-Findeisen mechanism in the evolution of mixed-phase clouds, *Journal of the Atmospheric Sciences*, *64* (9), 3372-3375.

Korolev, A., and G. Isaac (2003), Phase transformation of mixed-phase clouds, *Quarterly Journal of the Royal Meteorological Society*, *129* (587), 19-38.

Korolev, A., and P. R. Field (2008), The effect of dynamics on mixed-phase clouds: Theoretical considerations, *Journal of the Atmospheric Sciences*, *65* (1), 66-86.

Kruizinga, S. (1979), Objective classification of daily 500mb patterns in *Sixth Conference on Probability and Statistics in the Atmospheric Sciences*, edited, pp. 126-129, American Meteorological Society, Alberta, Canada.

Lampert, A., A. Ehrlich, A. Dornbrack, O. Jourdan, J. F. Gayet, G. Mioche, V. Shcherbakov, C. Ritter, and M. Wendisch (2009), Microphysical and radiative characterization of a subvisible midlevel Arctic ice cloud by airborne observations - a case study, *Atmospheric Chemistry and Physics*, *9* (8), 2647-2661.

Lanzante, J. (1996), Resistant, robust and non‐parametric techniques for the analysis of climate data: Theory and examples, including applications to historical radiosonde station data, *International Journal of Climatology*, *16* (11), 1197-1226.

Lhermitte, R. M. (1987), Small cumuli observed with a 3-mm wavelength doppler radar, *Geophysical Research Letters*, *14* (7), 707-710.

Lhermitte, R. M. (1989), Attenuation and scattering of millimeter wavelength radaition by clouds and precipitation, *Journal of Atmospheric and Oceanic Technology*, *7*, 464-479.

Li, Z. L., J. Li, W. P. Menzel, T. J. Schmit, and S. A. Ackerman (2007), Comparison between current and future environmental satellite imagers on cloud classification using MODIS, *Remote Sensing of Environment*, *108* (3), 311-326.

Liebe, H. J. (1985), An updated model for millimeter wave propagation in moist air, *Radio Science*, *20* (5), 1069-1089.

Liou, K. N. (1986), Influence of cirrus clouds on weather and climate processes - a global perspective, *Monthly Weather Review*, *114* (6), 1167-1199.

Liou, K. N., and R. M. Scotland (1971), Multiple backscattering and depolarization from water clouds for a pulsed lidar system, *Journal of Atmospheric Sciences*, *28*, 772-784.

Liu, Z. Y., M. Vaughan, D. Winker, C. Kittaka, B. Getzewich, R. Kuehn, A. Omar, K. Powell, C. Trepte, and C. Hostetler (2009), The CALIPSO lidar cloud and aerosol discrimination: Version 2 Algorithm and Initial Assessment of Performance, *Journal of Atmospheric and Oceanic Technology*, *26* (7), 1198-1213.

Lucchesi, R. (2012), File specification for MERRA products, *GMAO Office Note No.1 Version 2.3*, 82.

Ludlam, F. H. (1952), The production of showers by the growth of ice particles, *Quarterly Journal of the Royal Meteorological Society*, *78*, 543-553.

Mace, G. G., E. E. Clothiaux, and T. P. Ackerman (2001), The composite characteristics of cirrus clouds: Bulk properties revealed by one year of continuous cloud radar data, *Journal of Climate*, *14* (10), 2185-2203.

MacQueen, J. (1967), Some methods for classification and analysis of multivariate observations, *Proc. of the Fifth Berkely Symposium on Mathematical Statistics and Probability*, *Berkely, CA*, 281-297.

Mason, B. J. (1971), *The physics of clouds*, Second ed., Oxford University.

Matrosov, S. Y., A. V. Korolev, and A. J. Heymsfield (2002), Profiling cloud ice mass and particle characteristic size from Doppler radar measurements, *Journal of Atmospheric and Oceanic Technology*, *19* (7), 1003-1018.

Mauritsen, T., J. Sedlar, M. Tjernstrom, C. Leck, M. Martin, M. Shupe, S. Sjogren, B. Sierau, P. O. G. Persson, I. M. Brooks, and E. Swietlicki (2011), An Arctic CCN-limited cloud-aerosol regime, *Atmospheric Chemistry and Physics*, *11* (1), 165-173.

Menzel, W. P., D. P. Wylie, and K. I. Strabala (1992), Seasonal and diurnal changes in cirrus clouds as seen in 4 Years of observations with VAS, *Journal of Applied Meteorology*, *31* (4), 370-385.

Meyers, M. P., P. J. Demott, and W. R. Cotton (1992), New primary ice-nucleation parameterizations in an explicit cloud model, *Journal of Applied Meteorology*, *31* (7), 708-721.

Milligan, G. W. (1980), An examination of the effect of six types of error perturbation on fifteen clustering algorithms, *Psychometrika*, *45*, 325-342.

Minnis, P., D. F. Young, K. Sassen, J. M. Alvarez, and C. J. Grund (1990), The 27-28 October 1986 FIRE IFO cirrus case-study - cirrus parameter relationships derived from satellite and lidar data, *Monthly Weather Review*, *118* (11), 2402-2425.

Mock, C. J., P. J. Bartlein, and P. M. Anderson (1998), Atmospheric circulation patterns and spatial climatic variations in Beringia, *International Journal of Climatology*, *18* (10), 1085-1104.

Molders, N. (1987), Wolkenerkennung in AVHRR-Daten mit besonderer Beriicksichtigung der Gebiete tiber der Arktis, 80 pp, University of Cologne, West Germany.

Morris, T. R., and Braham (1968), The occurence of ice particles in Minnesota cumuli, paper presented at Proceedings of Weather Modification, American Meterological Society, Albany, NY.

Morrison, H., G. de Boer, G. Feingold, J. Harrington, M. D. Shupe, and K. Sulia (2012), Resilience of persistent Arctic mixed-phase clouds, *Nature Geoscience*, *5* (1), 11-17.

Mulmenstadt, J., D. Lubin, L. M. Russell, and A. M. Vogelmann (2012), Cloud properties over the North Slope of Alaska: Identifying the prevailing meteorological regimes, *Journal of Climate*, *25* (23), 8238-8258.

Murphy, D. M., and T. Koop (2005), Review of the vapour pressures of ice and supercooled water for atmospheric applications, *Quarterly Journal of the Royal Meteorological Society*, *131* (608), 1539-1565.

Noel, V., and M. Haeffelin (2007), Midlatitude cirrus clouds and multiple tropopauses from a 2002-2006 climatology over the SIRTA observatory, *Journal of Geophysical Research-Atmospheres*, *112* (D13206), 1-11.

Noh, Y. J., C. J. Seaman, T. H. Vonder Haar, D. R. Hudak, and P. Rodriguez (2011), Comparisons and analyses of aircraft and satellite observations for wintertime mixed-phase clouds, *Journal of Geophysical Research-Atmospheres*, *116* (D18207), 1-23.

Ogi, M., and J. M. Wallace (2007), Summer minimum Arctic sea ice extent and the associated summer atmospheric circulation, *Geophysical Research Letters*, *34* (L12705), 1-4.

Okamoto, H., K. Sato, and Y. Hagihara (2010), Global analysis of ice microphysics from CloudSat and CALIPSO: Incorporation of specular reflection in lidar signals, *Journal of Geophysical Research-Atmospheres*, *115* (D22209), 1-20.

Ovarlez, J., J. F. Gayet, K. Gierens, J. Strom, H. Ovarlez, F. Auriol, R. Busen, and U. Schumann (2002), Water vapour measurements inside cirrus clouds in Northern and Southern hemispheres during INCA, *Geophysical Research Letters*, *29* (16), 60-01 - 60-04.

Overland, J. E., and P. S. Guest (1991), The Arctic snow and air-temperature budget over sea ice during winter, *Journal of Geophysical Research-Oceans*, *96* (C3), 4651-4662.

Pappalardo, G., et al. (2010), EARLINET correlative measurements for CALIPSO: First intercomparison results, *Journal of Geophysical Research-Atmospheres*, *115* (D00H19), 1-21.

Pinto, J. O. (1998), Autumnal mixed-phase cloudy boundary layers in the Arctic, *Journal of the Atmospheric Sciences*, *55* (11), 2016-2038.

Pinto, J. O., J. A. Curry, and J. M. Intrieri (2001), Cloud-aerosol interactions during autumn over Beaufort Sea, *Journal of Geophysical Research-Atmospheres*, *106* (D14), 15077-15097.

Plana-Fattori, A., G. Brogniez, P. Chervet, M. Heaeffelin, O. Lado-Bordowsky, Y. Morille, F. Parol, J. Pelon, A. Roblin, G. Seze, and C. Stubenrauch (2008), Comparison of high-cloud characteristics as estimated by selected spaceborne observations and ground-based lidar datasets, *Journal of Applied Meteorology and Climatology*, *48*, 1142-1160.

Powell, K. A., C. A. Hostetler, Z. Y. Liu, M. A. Vaughan, R. E. Kuehn, W. H. Hunt, K. P. Lee, C. R. Trepte, R. R. Rogers, S. A. Young, and D. M. Winker (2009), CALIPSO lidar calibration algorithms. Part I: nighttime 532-nm parallel channel and 532-nm perpendicular channel, *Journal of Atmospheric and Oceanic Technology*, *26* (10), 2015-2033.

Protat, A., J. Delanoe, E. J. O'Connor, and T. S. L'Ecuyer (2010), The evaluation of CloudSat and CALIPSO ice microphysical products using ground-based cloud radar and lidar observations, *Journal of Atmospheric and Oceanic Technology*, *27* (5), 793-810.

Pruppacher, H. R., and J. D. Klett (1997), *Microphysics of clouds and precipitation*, Second ed., 954 pp., Springer, New york.

Randall, D. A., B. Albrecht, S. Cox, D. Johnson, P. Minnis, W. Rossow, and D. O. Starr (1996), On FIRE at ten, *Advances in Geophysics, Vol 38*, *38*, 37-177.

Rangno, A. L., and P. V. Hobbs (1991), Ice particle concentrations and precipitation development in small polar maritime cumuliform clouds, *Quarterly Journal of the Royal Meteorological Society*, *117* (497), 207-241.

Rasmussen, E. (1979), The polar low as an extratropical CISK disturbance, *Quarterly Journal of the Royal Meteorological Society*, *105*, 531-549.

Rauber, R. M., and A. Tokay (1991), An explanation for the existence of supercooled water at the top of cold clouds, *Journal of the Atmospheric Sciences*, *48* (8), 1005-1023.

Reuss, J. H. (1967), Wolken-stereomessbildreichen, II:grossraumige cirrus bandes als merkale von luftmassengrenzen der hohes troposphare and ihrer eigenshaften, *Beitr. Phys. Atmos.*, *36*, 7-15.

Richman, M. B. (1981), The retrieval of meteorological patterns via rotated principal components, *Bulletin of the American Meteorological Society*, *62* (6), 879-879.

Rogers, D. C., P. J. DeMott, S. M. Kreidenweis, and Y. L. Chen (1998), Measurements of ice nucleating aerosols during SUCCESS, *Geophysical Research Letters*, *25* (9), 1383-1386.

Rogers, R. R., and M. K. Yau (1988), *A Short Course in Cloud Physics*, 290 pp., Pergamon Press.

Rossow, W. B., and R. A. Schiffer (1999), Advances in understanding clouds from ISCCP, *Bulletin of the American Meteorological Society*, *80* (11), 2261-2287.

Sassen, K. (1977), Ice crystal habit discrimination with the optical backscatter depolarization technique, *Journal of Applied Meteorology*, *16*, 425-431.

Sassen, K. (1987), Ice-cloud content from radar reflectivity, *Journal of Climate and Applied Meteorology*, *26* (8), 1050-1053.

Sassen, K. (1991), The polarization lidar technique for cloud research - a review and current assessment, *Bulletin of the American Meteorological Society*, *72* (12), 1848-1866.

Sassen, K. (2002a), Cirrus clouds: a modern perspective, in *Cirrus*, edited by D. K. Lynch, K. Sassen, D. O. Starr and G. L. Stephens, pp. 11-40, Oxford University Press, New York.

Sassen, K. (2002b), Indirect climate forcing over the western US from Asian dust storms, *Geophysical Research Letters*, *29* (10), 103-001- 103-004.

Sassen, K. (2005), Dusty ice clouds over Alaska, *Nature*, *434* (7032), 456-456.

Sassen, K., and B. S. Cho (1992), Subvisual thin cirrus lidar dataset for satellite verification and climatological research, *Journal of Applied Meteorology*, *31* (11), 1275-1285.

Sassen, K., and J. R. Campbell (2001), A midlatitude cirrus cloud climatology from the facility for atmospheric remote sensing. Part I: Macrophysical and synoptic properties, *Journal of the Atmospheric Sciences*, *58* (5), 481-496.

Sassen, K., and J. M. Comstock (2001), A midlatitude cirrus cloud climatology from the facility for atmospheric remote sensing. Part III: Radiative properties, *Journal of the Atmospheric Sciences*, *58* (15), 2113-2127.

Sassen, K., and V. I. Khvorostyanov (2007), Microphysical and radiative properties of mixed-phase altocumulus: A model evaluation of glaciation effects, *Atmospheric Research*, *84* (4), 390-398.

Sassen, K., and V. I. Khvorostyanov (2008), Cloud effects from boreal forest fire smoke: evidence for ice nucleation from polarization lidar data and cloud model simulations, *Environmental Research Letters*, *3* (025006), 1-12.

Sassen, K., and Z. Wang (2012), The clouds of the middle troposphere: Composition, radiative impact, and global distribution, *Surveys in Geophysics*, *33* (3-4), 677-691.

Sassen, K., J. M. Comstock, and Z. Wang (2001), Parameterization of the radiative properties of midlatitude high and middle level clouds, *Geophysical Research Letters*, *28* (4), 729-732.

Sassen, K., J. Zhu, and S. Benson (2003a), Midlatitude cirrus cloud climatology from the facility for atmospheric remote sensing. IV. Optical displays, *Applied Optics*, *42* (3), 332-341.

Sassen, K., Z. Wang, and D. Liu (2008), Global distribution of cirrus clouds from CloudSat/Cloud-Aerosol Lidar and Infrared Pathfinder Satellite Observations (CALIPSO) measurements, *Journal of Geophysical Research-Atmospheres*, *113* (D00A12), 1-12.

Sassen, K., G. G. Mace, J. Hallett, and M. R. Poellot (1998), Corona-producing ice clouds: a case study of a cold mid-latitude cirrus layer, *Applied Optics*, *37* (9), 1477-1485.

Sassen, K., P. J. DeMott, J. M. Prospero, and M. R. Poellot (2003b), Saharan dust storms and indirect aerosol effects on clouds: CRYSTAL-FACE results, *Geophysical Research Letters*, *30* (12).

Scotland, R. M., K. Sassen, and R. Stone (1971), Observations by Lidar of linear depolarization ratios for hydrometeors, *Journal of Applied Meteorology*, *10*, 1011-1017.

Seifert, P., A. Ansmann, I. Mattis, U. Wandinger, M. Tesche, R. Engelmann, D. Muller, C. Perez, and K. Haustein (2010), Saharan dust and heterogeneous ice formation: Eleven

years of cloud observations at a central European EARLINET site, *Journal of Geophysical Research-Atmospheres*, *115* (D20201), 1-13.

Senior, C. A., and J. F. B. Mitchell (1993), Carbon-dioxide and climate - the impact of cloud parameterization, *Journal of Climate*, *6* (3), 393-418.

Serreze, M. C. (1995), Climatological aspects of cyclone development and decay in the Arctic, *Atmosphere-Ocean*, *33* (1), 1-23.

Serreze, M. C., and R. G. Barry (2005), *The Arctic climate system*, 404 pp., Cambridge University, New York.

Serreze, M. C., and A. P. Barrett (2008), The summer cyclone maximum over the central Arctic Ocean, *Journal of Climate*, *21* (5), 1048-1065.

Shulski, M., and G. Wendler (2007), *The climate of Alaska*, 202 pp., University of Alaska Press.

Shupe, M. D., and J. M. Intrieri (2004), Cloud radiative forcing of the Arctic surface: The influence of cloud properties, surface albedo, and solar zenith angle, *Journal of Climate*, *17* (3), 616-628.

Shupe, M. D., S. Y. Matrosov, and T. Uttal (2006), Arctic mixed-phase cloud properties derived from surface-based sensors at SHEBA, *Journal of the Atmospheric Sciences*, *63* (2), 697-711.

Shupe, M. D., P. Kollias, P. O. G. Persson, and G. M. McFarquhar (2008a), Vertical motions in Arctic mixed-phase stratiform clouds, *Journal of the Atmospheric Sciences*, *65* (4), 1304-1322.

Shupe, M. D., J. S. Daniel, G. de Boer, E. W. Eloranta, P. Kollias, C. N. Long, E. P. Luke, D. D. Turner, and J. Verlinde (2008b), A focus on mixed-phase clouds: the status of ground-based observational methods, *Bulletin of the American Meteorological Society*, *89* (10), 1549-1562.

Smith, A. J., V. E. Larson, J. G. Niu, J. A. Kankiewicz, and L. D. Carey (2009), Processes that generate and deplete liquid water and snow in thin midlevel mixed-phase clouds, *Journal of Geophysical Research-Atmospheres*, *114* (D12203), 1-18.

Smith, G. (1995), Mid-tropospheric dry layers and their relationship to precipitation type in a sub-freezing troposphere, *National Weather Digest*, *20* (2), 34-39.

Soden, B. J., and S. R. Schroeder (2000), Decadal variations in tropical water vapor: A comparison of observations and a model simulation, *Journal of Climate*, *13* (19), 3337-3341.

Solomon, S., D. Qin, M. Manning, Z. Chen, M. Marquis, K. B. Averyt, M. Tignor, and H. L. Miller (2007), Contribution of working group-I: fourth assessment report of the IPCC, edited, Cambridge University Press, United Kingdom and New York, NY, USA.

Stainforth, D. A., T. Aina, C. Christensen, M. Collins, N. Faull, D. J. Frame, J. A. Kettleborough, S. Knight, A. Martin, J. M. Murphy, C. Piani, D. Sexton, L. A. Smith, R. A. Spicer, A. J. Thorpe, and M. R. Allen (2005), Uncertainty in predictions of the climate response to rising levels of greenhouse gases, *Nature*, *433* (7024), 403-406.

Starr, D. O., and D. P. Wylie (1990), The 27-28 October 1986 FIRE cirrus case-study - meteorology and clouds, *Monthly Weather Review*, *118* (11), 2259-2287.

Stephens, G. L., D. G. Vane, R. J. Boain, G. G. Mace, K. Sassen, Z. E. Wang, A. J. Illingworth, E. J. O'Connor, W. B. Rossow, S. L. Durden, S. D. Miller, R. T. Austin, A. Benedetti, C. Mitrescu, and C. S. Team (2002), The cloudsat mission and the A-train - a new dimension of space-based observations of clouds and precipitation, *Bulletin of the American Meteorological Society*, *83* (12), 1771-1790.

Stith, J. L., J. E. Dye, A. Bansemer, A. J. Heymsfield, C. A. Grainger, W. A. Petersen, and R. Cifelli (2002), Microphysical observations of tropical clouds, *Journal of Applied Meteorology*, *41* (2), 97-117.

Stone, R. G. (1957), A compendium on cirrus and cirrus forecasting, *Air Force Weather Service Technical Report*, *AWS TR 105-130* (AWS).

Strom, J., M. Seifert, B. Karcher, J. Ovarlez, A. Minikin, J. F. Gayet, R. Krejci, A. Petzold, F. Auriol, W. Haag, R. Busen, U. Schumann, and H. C. Hansson (2003), Cirrus cloud occurrence as function of ambient relative humidity: a comparison of observations obtained during the INCA experiment, *Atmospheric Chemistry and Physics*, *3*, 1807-1816.

Stubenrauch, C. J., W. B. Rossow, F. Cheruy, A. Chedin, and N. A. Scott (1999), Clouds as seen by satellite sounders (3I) and imagers (ISCCP). Part I: Evaluation of cloud parameters, *Journal of Climate*, *12* (8), 2189-2213.

Thorsen, T. J., Q. Fu, and J. Comstock (2011), Comparison of the CALIPSO satellite and ground-based observations of cirrus clouds at the ARM TWP sites, *Journal of Geophysical Research-Atmospheres*, *116* (D21203), 1-27.

Turner, D. D. (2005), Arctic mixed-phase cloud properties from AERI lidar observations: Algorithm and results from SHEBA, *Journal of Applied Meteorology*, *44* (4), 427-444.

Vaughan, M. A., K. A. Powell, R. E. Kuehn, S. A. Young, D. M. Winker, C. A. Hostetler, W. H. Hunt, Z. Y. Liu, M. J. McGill, and B. J. Getzewich (2009), Fully

automated detection of cloud and aerosol layers in the CALIPSO lidar measurements, *Journal of Atmospheric and Oceanic Technology*, *26* (10), 2034-2050.

Verlinde, J., J. Y. Harrington, G. M. McFarquhar, V. T. Yannuzzi, A. Avramov, S. Greenberg, N. Johnson, G. Zhang, M. R. Poellot, J. H. Mather, D. D. Turner, E. W. Eloranta, B. D. Zak, A. J. Prenni, J. S. Daniel, G. L. Kok, D. C. Tobin, R. Holz, K. Sassen, D. Spangenberg, P. Minnis, T. P. Tooman, M. D. Ivey, S. J. Richardson, C. P. Bahrmann, M. Shupe, P. J. DeMott, A. J. Heymsfield, and R. Schofield (2007), The mixed-phase Arctic cloud experiment, *Bulletin of the American Meteorological Society*, *88* (2), 205-221.

Wang, P. H., P. Minnis, M. P. McCormick, G. S. Kent, and K. M. Skeens (1996), A 6-year climatology of cloud occurrence frequency from stratospheric aerosol and gas experiment II observations (1985-1990), *Journal of Geophysical Research-Atmospheres*, *101* (D23), 29407-29429.

Wang, Z. (2011), Level 2 Combined radar and lidar cloud scenario classification product process description and interface control document, *JPL Document*, *Version 1.0* (http://www.cloudsat.cira.colostate.edu/dataICDlist.php).

Wang, Z., and K. Sassen (2001), Cloud type and macrophysical property retrieval using multiple remote sensors, *Journal of Applied Meteorology*, *40* (10), 1665-1682.

Warren, S. G., C. J. Hahn, J. London, R. M. Chervin, and R. Jeene (1986), Global distribution of total cloud cover and cloud type amounts over the land, *NACR Tech Note*, *29*.

Warren, S. G., C. J. Hahn, J. London, R. M. Chervin, and R. Jeene (1988), Global distribution of total cloud cover and cloud type amounts over the ocean, *NACR Tech. Note*, *41*.

Wegener, A. (1911), *Thermodynamik der atmosphäre*, Leipzig.

Welch, R. M., S. K. Sengupta, A. K. Goroch, P. Rabindra, N. Rangaraj, and M. S. Navar (1992), Polar cloud and surface classification using AVHRR imagery - an intercomparison of methods, *Journal of Applied Meteorology*, *31* (5), 405-420.

Winker, D. M., M. A. Vaughan, A. Omar, Y. X. Hu, K. A. Powell, Z. Y. Liu, W. H. Hunt, and S. A. Young (2009), Overview of the CALIPSO mission and CALIOP data processing algorithms, *Journal of Atmospheric and Oceanic Technology*, *26* (11), 2310-2323.

WMO (1987), *International Cloud Atlas*, *I and II* (Geneva: World Meteorological Organization).

Wu, D. L., R. T. Austin, M. Deng, S. L. Durden, A. J. Heymsfield, J. H. Jiang, A. Lambert, J. L. Li, N. J. Livesey, G. M. McFarquhar, J. V. Pittman, G. L. Stephens, S. Tanelli, D. G. Vane, and D. E. Waliser (2009), Comparisons of global cloud ice from MLS, CloudSat, and correlative data sets, *Journal of Geophysical Research-Atmospheres*, *114* (D00A24), 1-20.

Wylie, D. (2002), Cirrus and weather: a satellite prespective, in *Cirrus*, edited by D. Lynch, K. Sassen, D. O. Starr and G. Stephens, pp. 136-146, Oxford University Press, New York.

Wylie, D. P., and W. P. Menzel (1999), Eight years of high cloud statistics using HIRS, *Journal of Climate*, *12* (1), 170-184.

Wylie, D. P., W. P. Menzel, H. M. Woolf, and K. I. Strabala (1994), 4 Years of global cirrus cloud statistics using HIRS, *Journal of Climate*, *7* (12), 1972-1986.

Yasunaga, K., K. Yoneyama, H. Kubota, H. Okamoto, A. Shimizu, H. Kumagai, M. Katsumata, N. Sugimoto, and I. Matsui (2006), Melting layer cloud observed during R/V Mirai cruise MR01-K05, *Journal of the Atmospheric Sciences*, *63* (11), 3020-3032.

Zahn, M., and H. von Storch (2010), Decreased frequency of North Atlantic polar lows associated with future climate warming, *Nature*, *467* (7313), 309-312.

Zhang, D. M., Z. Wang, and D. Liu (2010), A global view of midlevel liquid-layer topped stratiform cloud distribution and phase partition from CALIPSO and CloudSat measurements, *Journal of Geophysical Research-Atmospheres*, *115* (D00H13), 1-10.

Zhang, M. H., W. Y. Lin, S. A. Klein, J. T. Bacmeister, S. Bony, R. T. Cederwall, A. D. Del Genio, J. J. Hack, N. G. Loeb, U. Lohmann, P. Minnis, I. Musat, R. Pincus, P. Stier, M. J. Suarez, M. J. Webb, J. B. Wu, S. C. Xie, M. S. Yao, and J. H. Zhang (2005), Comparing clouds and their seasonal variations in 10 atmospheric general circulation models with satellite measurements, *Journal of Geophysical Research-Atmospheres*, *110* (D15S02), 1-18.

Zhang, X. D., J. E. Walsh, J. Zhang, U. S. Bhatt, and M. Ikeda (2004), Climatology and interannual variability of arctic cyclone activity: 1948-2002, *Journal of Climate*, *17* (12), 2300-2317.

Zuidema, P., B. Baker, Y. Han, J. Intrieri, J. Key, P. Lawson, S. Matrosov, M. Shupe, R. Stone, and T. Uttal (2005), An Arctic springtime mixed-phase cloudy boundary layer observed during SHEBA, *Journal of the Atmospheric Sciences*, *62* (1), 160-176.